Helsinki University of Technology Publications in Machine Design 3/2005
Teknillisen korkeakoulun Koneensuunnittelun julkaisuja 3/2005
Espoo 2005

MECHANICAL RELIABILITY OF OPTICAL FIBER IN COMBINED CONTINUOUS DRAW AND PROOF TESTING PROCESS

Harri Turunen

TEKNILLINEN KORKEAKOULU
TEKNISKA HÖGSKOLAN
HELSINKI UNIVERSITY OF TECHNOLOGY
TECHNISCHE UNIVERSITÄT HELSINKI
UNIVERSITE DE TECHNOLOGIE D'HELSINKI

Helsinki University of Technology Publications in Machine Design 3/2005
Teknillisen korkeakoulun Koneensuunnittelun julkaisuja 3/2005
Espoo 2005

MECHANICAL RELIABILITY OF OPTICAL FIBER IN COMBINED CONTINUOUS DRAW AND PROOF TESTING PROCESS

Harri Turunen

Dissertation for the degree of Doctor of Science (Technology) to be presented with due permission for public examination and debate in Auditorium E at Helsinki University of Technology (Espoo, Finland) on the 20th of May, 2005, at 12 o'clock noon.

Helsinki University of Technology
Department of Mechanical Engineering
Machine Design

Teknillinen korkeakoulu
Konetekniikan osasto
Koneensuunnittelu

Distribution:
Helsinki University of Technology
Machine Design
P.O. Box 4100
FI-02015 TKK
Tel. +358 9 451 3555
Fax +359 9 451 3549
E-mail: tiina.nikander@tkk.fi

ISBN 951-22-7607-0
ISSN 1456-4955

Otamedia Oy
Espoo 2005

ABSTRACT

The fiber manufacturing has traditionally had three different process phases: Preform Manufacturing, Fiber Draw and Proof Testing. This thesis focuses on combining draw process and proof testing, which requires catching the fiber end after break at full production speed without disturbing the draw process.

Proof testing means applying a specified tensile load to continuous lengths of optical fiber. The tensile load is applied for as short time as possible, yet sufficiently long to ensure the glass experiences the proof stress. The proof test cycle is divided into three steps: load, dwell and unload. Nowadays the industry commonly accepts that the dwell time has minor effect on the final minimum strength of fiber, but the strength decreases during the proof testing cycle. The unload time is considered to be a machine property by capstan design, but new approach is suggested in this thesis, where the unload time is a material property.

The two-region crack growth theory states that depending on the unload rate the crack growth may happen in two region. The effect of the coating was also studied. It was found that at high load rates the coating carries a substantially higher part of the load. Additionally theories suggest that the strength of the fiber is significantly higher just after draw than approx. 1 hour later, because of water penetration.

An approach for modeling tension behavior in combined draw and proof testing process mathematically was introduced and a universal simulating tool was generated. Experiments were carried out to verify the theory. The first was the draw tension experiment. The second part was the comparison of the conventional proof tension measurement and the new method needed for the combined processes. After this the effect of the different process elements were evaluated. Two different methods to survive proof testing break were introduced and tested. A combination of tubes and belts turned to be the most reliable.

Since the winding quality is important, a new winding algorithm was developed. Several trials focused on preventing whipping phenomenon. An optimal whipping guard and auxiliary blade minimized the whipping. The transfer reliability was tested with a separate take-up module. The result was that the transfer reliability is at satisfactory level at the existing production speeds. The future work will include more experimental testing, which will combine the critical components into one machine. The overall reliability depends on how well these critical components are integrated to each other.

Keywords: optical fiber, reliability, fiber draw, proof testing, winding, break recovery, tension control, simulation, measuring, fiber machinery, automatic transfer, dual take-up

PREFACE

First I would like to thank Nextrom and especially the Fiber Optics Group and all its personnel for giving me the opportunity to carry out this research. Special thanks go to Dr. Tommi Vainio about instructing the thesis. I also wish to thank the Post Draw team of Nextrom, and all the members for their specialist comments and help when making the trials, without which this study could not have been completed.

My special thanks go to all the customers and partners with whom the trials were done.

I would further like to extend thanks to Professor Mauri Airila of the Helsinki University of Technology for his important advice and suggestions on the contents, structure and language of this research work.

Finally I thank my family: my wife Jaana for her patience and support at all times, my sons Tommi and Saku for being an enormous source of inspiration, without which I could not have been able to carry out this effort, and my parents Seppo and Pirkko for supporting and showing interest in my research from the beginning.

Dacula GA, USA, March 2005 Harri Turunen

TABLE OF CONTENTS

ABSTRACT

PREFACE

SYMBOLS

1 INTRODUCTION 11

1.1 BACKGROUND 11

1.2 RESEARCH PROBLEM 12

1.3 AIM OF THE RESEARCH 12

1.4 SCOPE OF THE RESEARCH 13

1.5 RESEARCH METHODS 13

1.6 CONTRIBUTION 14

2 LITERATURE REVIEW 14

2.1 FIBER DRAWING PROCESS 14

2.2 PROOF TESTING PROCESS 16

2.3 DEVELOPMENT NEEDS 17

2.4 PROOF TESTING STANDARDS AND THEORY 18

3 THEORETICAL ANALYSIS 32

3.1 THEORETICAL MODELS OF PROCESS ELEMENTS 32

3.1.1 Payoff 33

3.1.2 Idle Wheel 35

3.1.3 Dancer 35

3.1.4 Capstan 38

3.1.5 Take-up 40

3.2 CHALLENGES IN COMBINED FIBER DRAW PROCESS AND PROOF TESTING 41

3.2.1 Limits of the Analysis 41

3.2.2 Proof Testing Region and Proof Tension Measurement 42

3.2.3 Automatic Break Recovery and Threading System 42

3.2.4 Dual Take-up and Transfer Reliability 44

3.2.5 Whipping Prevention during Winding and after Transfer 46
3.2.6 Winding and Traversing Turning Control 47
3.3 PROCESS TENSION SIMULATION MODEL FOR COMBINED PROCESS 53
3.3.1 Mathematics for Dynamic Model 53
3.3.2 Fourier Transform 56
3.3.3 Fiber Stress Analysis 57
4 EXPERIMENTS 60
4.1 TENSION BEHAVIOR TESTS 60
4.1.1 Draw Tension Measurement 60
4.1.2 Proof Tension: Conventional Method vs. New Method 61
4.1.3 Turning Wheel Effect on Tension 64
4.1.4 Capstan Effect on Tension 65
4.1.5 Take-up Effect on Tension 66
4.1.6 Dancer Movement in Turning Point 67
4.2 BREAK RECOVERY SYSTEM TESTS 68
4.2.1 Two Different Approaches 68
4.2.2 Testing of Tube System 69
4.2.3 Testing of Belt System 71
4.3 WINDING TESTS 72
4.3.1 Turning Point Control Optimization 72
4.3.2 Whipping Protection 73
4.3.3 Transfer Reliability 77
5 RESULTS 82
5.1 TENSION BEHAVIOR RESULTS 82
5.1.1 Draw Tension Data 82
5.1.2 Proof Tension Measurement results 83
5.1.3 Process Elements Affecting Tension 86
5.1.4 Complete Tension Simulation Results 91
5.2 BREAK RECOVERY RELIABILITY 93
5.2.1 Tube System Results 94

5.2.2 Belt System Results 96

5.3 WINDING QUALITY 98

5.3.1 Winding Control Algorithm Test Results 98

5.3.2 Whipping Guard Testing Result 99

5.3.3 In-Side End Whipping Investigation Results 100

5.3.4 Auxiliary Blade Test Results 102

5.3.5 Transfer Reliability of the Original Design 103

5.3.6 Transfer Reliability of the Improved Design 104

6 DISCUSSION 107

7 SUMMARY 110

REFERENCES

α_δ	angular acceleration of the dancer arm
α_n	non-linearity constant of fiber in bending
β	Weibull beta-value
δ	dancer angle measured from horizontal plane
ΔD	diameter change per turn
ΔL	excess fiber length in build-up
ΔV	average circumferential speed of the dancer arm
ε	relative strain of fiber
ε_b	additional uniform strain caused by bending
ε_i	relative strain of fiber in previous span
ε_o	relative strain of fiber in current span
ϕ_o	initial angular position of rotating part
θ_i	angle of incoming fiber
θ_o	angle of outgoing fiber
ν_o	cinematic viscosity of oil in grease
ρ	density of silica glass
σ	applied tensile stress
σ_a	applied service stress
σ_f	final strength
σ_{fmin}	strength of flaw just failing during unload
σ_l	loading stress
σ_p	proof stress
σ_u	unloading stress
σ^*	stress at failure during unloading
ω	angular rotating speed
ω_δ	average angular speed of the dancer arm
ξ	distance from center line of fiber
a	crack depth
A	area of glass cross section
A_i	area of inner primary coating cross section
A_o	area of outer primary coating cross section
A_{RW}	area of the reference area, worst case
A_{FB}	area of fiber cross sections in reference area, best case
A_{RB}	area of the reference area, best case
B	crack strength preservation parameter
C_m	auxiliary motor constant for back-EMF
d_m	mean diameter of bearing
d_f	fiber coating diameter
D_g	nominal diameter of uncoated fiber
D_i	nominal diameter of the inner primary coating
D_o	nominal diameter of the outer primary coating
E	Young's modulus of fiber
E_g	Young's modulus of uncoated fiber
E_i	Young's modulus of the inner primary coating
E_o	Young's modulus of the outer primary coating
f_k	vibration frequency
f_l	constant for deep groove ball bearing
f_s	sampling frequency
f_v	constant for speed dependent friction moment

F	load in fiber or failure probability
$F\%$	load share carried by coating
$F1, F2, F3$	actual loads in fiber spans
$F4, F5, F6$	actual loads in fiber spans
F_E	external force
F_i	tension of input fiber
F_o	tension of output fiber
F_{pset}	set proof tension
F_r	radial load to bearing
F_{wset}	set winding tension
F_{WB}	winding tension in build-up
g	gravitational constant
i_T	ratio between capstan wheel radius and belt pulley radius
j	number of dancer loops
J	total mass moment of inertia of the rotating parts
J_p	polar mass moment of inertia
k	spring constant
k_f	operator for Fourier transform
K_I	stress intensity factor
K_{IC}	critical stress intensity factor
K_a	constant for air resistance
K_{ap}	constant for dancer arm's air resistance
K_{bl}, K_{bv}	constants for bearing friction moment
K_{LB}	packing efficiency factor for the best case
K_{LW}	packing efficiency factor for the worst case
K_m	auxiliary motor constant
K_{pl}, K_{pv}	friction constants of dancer joint
K_v	auxiliary constant for speed dependent friction moment
l_e	external force distance from pivoting joint
l_i	input fiber distance from pivoting joint
l_o	output fiber distance from pivoting joint
L	length of fiber
L_b	length of fiber in buildup
L_i	length of incoming fiber
L_o	length of outgoing fiber
m, m_t	total mass of rotating part
m_d, m_s	Weibull m-values, dynamic and static
m_f	mass of fiber
M	motor torque
M_B	torque needed for bearing friction
M_l	load friction torque for deep groove ball bearing
M_W	torque needed for bending fiber
n, n_1, n_2	corrosion susceptibility factor
n_f	number of samples
n_p	number of belt pulleys
N	number of turns in buildup
p	traversing pitch
P	survival probability
q	acceleration operator (-1, 0, 1)
r	actual radius measured from rotating part center to fiber
r_f	glass fiber radius

r_{p}	radius of belt pulley
R	bending radius of fiber
$S_{1\mathrm{min}}$	pre-proof test strength
$S_{2\mathrm{min}}$	strength after surviving flaw growth during unload
S_{pmin}	strength after dwell zone
S_{f}	final strength of stress history
S_{i}	initial inert strength at t = 0
t	time
t_{b}	time on the buildup
t_{d}	dwell time
t_{f}	life time
t_{l}	load time
t_{p}	effective proof time
t_{u}	unload time
t_{*}	failure time during dwell time
T	cycle time of harmonic vibration
$\mathrm{T_u}$	unload time
u_{m}	anchor voltage
v_{i}	velocity of input fiber span end
v_{l}	line speed
v_{o}	velocity of output fiber span end
v_{set}	set line speed
V	crack growth velocity
W	bending resistance of fiber
x	deviation from 0-position
x_{b}	buildup size in x-direction
x_{c}	mass center x-coordinate
x_{f}	height of two layers in the best case
y_{b}	buildup size in y-direction
y_{c}	mass center y-coordinate

1 INTRODUCTION

1.1 Background

The use of optical telecommunication fiber has steadily increased over the past two decades. The driving force has been the data transfer capacity. One clear reason for higher data transfer rate has been the huge growth of Internet. The fiber optics industry has, however, reached the mature age and behind are the days of easy profit. The prices have come down and there is a lot of new competition in this market. All this leads to the fact that the manufacturing of the fiber must be more economical and efficient than in the past. To achieve this goal there are several things one might do. It is obvious that increasing the speeds and automation degree is helping in this job. Optical fiber manufacturing is done in several process steps nowadays. A clear saving potential is thus combining processes wherever technically possible, since this creates clear cost savings allowing the manufacturers to survive even with lower margins. The profitability calculations are presented in Appendix 1, which shows the arguments that support combining fiber manufacturing processes. More detailed view in fiber optics markets is presented in Appendix 2.

The fiber manufacturing has traditionally had three different process phases: Preform Manufacturing, Fiber Draw and Proof Testing. Proof testing does not add any value to the fiber, but it must be done for quality assurance. There have been some manufacturers who have tried to eliminate separate proof testing by combining it with fiber draw process. With existing technical solutions, random fiber break causes too much trouble to the fiber draw process that it has not been economically profitable in the long run.

Combining these two processes requires research and development efforts for investigating the problems and testing the solutions in practice. It is important to be able to simulate the tension behavior of the fiber in combined process and also confirm it experimentally. Proof testing and fiber handling mustn't oppress unnecessarily the fiber, since it affects the strength of fiber and therefore the lifetime.

The nature of proof testing is that the fiber breaks randomly on a weak spot. If proof testing is combined to the fiber draw the ultimate goal is to be able to catch the fiber end after the break and be able to thread it through proof test zone all the way to the take-up spool. All this should be done at full production speed without disturbing the draw process. There is no previous public information about conveying the free fiber end at high speeds, which requires experimental testing with prototypes.

1.2 Research Problem

The research problem is to ensure the mechanical reliability of optical fiber in different phases of the combined process. This is further explained below.

The tension behavior needs to be investigated to ensure that the fiber is not damaged during on-line proof testing. Combining these two processes requires giving up some principles commonly used in off-line proof testing. The proof tension has been possible to measure with an additional tension measurement wheel or wheels, since the threading is often done manually and always at low speed. The combined continuous process requires that the threading is automatic and possible at high speed. The proposed way is to measure the tension indirectly, which requires experiments to prove the quality of the measurement. Another thing to consider is the proof test length. The short test length gives benefits for automatic threading, but on the other hand affect the proof tension variation, because of the resolution of the servo drives.

Another part of the research problem is the fiber behavior after the break. The design should be such that it does not matter if the break is a random or planned. A device need to be designed and tested which can convey the fiber form the break point on to the take-up spool. It needs to be investigated what kind of possibilities there are to convey the fiber and what are the phenomena affecting the conveying.

Finally it needs to be proven that the overall reliability of the system is worth of the effort. The reliability includes the tension behavior and reliability of break recovery and additionally the transfer reliability, including whipping protection, of the necessary dual take-up and also winding quality.

1.3 Aim of the Research

The aim of the research is to develop a dynamic model to describe tension behavior of optical fiber generally in any of post draw processes. The thinking is that these processes have identical process elements, for which it is possible to find mathematical models. By combining these process elements it is possible to model complete processes.

As a special case combined continuous fiber draw and proof testing process will be modelled. The modelling is done in a form of an interactive computer simulation with commercial inexpensive office software. The user feeds the needed parameters; line speed, spool dimensions, etc. The simulation calculates fiber tension and tension variation along the fiber path. The results are given numerically and graphically.

An essential part of mechanical behavior of fiber in the combined process is to investigate fiber conveying after fiber break. This thesis

clears up and optimises the phenomena affecting conveying the loose fiber end. The fiber end needs to be conveyed through proof test zone on to take-up spool at low initial threading speed and also at full production speed. Two different approaches are investigated and experimentally tested. Since the materials around fiber path affect the static electricity and therefore to the conveying reliability, material selection was one target of the study.

Finally the challenges are listed as follows: Fiber tension control, proof tension measurement, break recovery, transfer reliability, whipping prevention and winding quality.

1.4 Scope of the Research

Although this thesis is closely related to fiber draw process and proof testing process, neither of them is handled very deeply. Fiber draw is a complex process, but already known technology. Fiber draw process is only described to show the state of the art. Proof testing is also a well-known process, but this is analysed more to find the boundaries for the combined process.

Fiber tension behavior and simulation as well as mechanical behavior after fiber break focus on fiber draw process only after the coater. The plan includes a fiber cutter and vacuum system, but also they are limited out of the scope of this thesis. The coater of the draw tower was now limited outside and all the parts above the coater. On the other hand all parts after break recovery system and dual fiber take-up were limited outside.

1.5 Research Methods

Fiber tension behavior before fiber break was studied theoretically, which enabled the modelling of the process elements and dynamic simulation. Theoretical study uses literature in form of articles, standards and patents. The models were tested experimentally and adjusted.

The mechanical behavior of the fiber end, whipping protection, transfer reliability and winding quality included empirical testing. The research methods included a high-speed camera, load cells, a high-speed data recorder, a scopemeter, proximity sensors, static control devices, an optical time domain reflectometer and various fiber post draw machines. All pieces of equipment are described detailed in Appendix 19. The testing of reliabilities required statistical data, which was gathered from test runs in laboratory conditions and partly from production conditions when it was possible.

1.6 Contribution

There is not much public information available about mechanical behavior of optical fiber or fiber tension behavior in manufacturing processes. The tension simulation model developed as part of this thesis can be used to study fiber tension behavior when designing the machinery.

The standards and literature were studied critically. Especially the unload rate has been a concern lately in standardization. In this study it is suggested a different approach to evaluate the unload rate based on the material properties not machinery properties.

The combined continuous fiber draw process and proof testing process is possible using the principles presented in this thesis. Earlier this has not been possible, since there were no technical solution to continue the proof testing and winding process automatically after proof test break without disturbing the fiber draw process.

The mechanical behavior of the loose fiber end after the break was clarified. This information was not available before. The new information includes; break recovery reliability, transfer reliability, whipping protection principle and winding quality optimisation at higher speeds than earlier with optical fiber. Additionally static electricity together with optical fibers was investigated and the information was used when optimising the materials.

The principles and critical functions presented in this thesis were tested by using several prototypes.

2 LITERATURE REVIEW

2.1 Fiber Drawing Process

The finished preform is drawn to optical fiber in a drawing tower (Figure 1). The preform turns to fiber in a furnace where the temperature is about 2,000 - 2,200 °C. Typically the preform diameter is 60-100 mm and length 1,5 – 3,0 m, but on-going development focuses on diameters around 150 mm. The fiber is drawn by a capstan located in the lower part of the tower. Above the capstan a coating unit is needed where the bare glass is coated with two coatings; primary acrylate and secondary acrylate. Nowadays the acrylates are UV curable, which allows fast curing and thus high speeds. The purpose of these coatings is to give the fiber better mechanical properties. The inner coating is typically softer than the outer to avoid damage to the glass fiber when bending the fiber. The outer and harder surface gives better mechanical protection to the fiber.

The fiber passes thorough the capstan after coating and UV-curing. The fiber is then wound on a reel by a take-up. The take-up spool

Figure 1. Draw tower

size is normally between 100 – 1,000 km and a dual take-up starts to be more common than a single take-up. Normal fiber production speed is nowadays in range between 1,000 and 1,500 m/min. The limiting factor seems to be the coating technology. Otherwise the quite recently developed drawing towers could support speeds in excess of 2,000 m/min.

There are several references in which the fiber drawing process is described. The essential components of the whole process are as follows: preform feeding, furnace, fiber diameter monitor, coating applicator, curing device, capstan (Figure 2) and take-up (Figure 3). All these components, excluding the capstan and take-up, have to be enclosed to provide a clean environment. The components are arranged in a vertical position to take advantage of the gravitational force.

One drawing nowadays produces 200-1,000 km fiber from one preform, but on-going development targets lengths even over 3,000 km from one preform. The height of the tower is usually between 20 and 30 m depending on the desired drawing speed.

The commonly used heat sources to melt the preform are a graphite resistance furnace, a zircon induction furnace or a graphite induction furnace.

Figure 2. Capstan

Figure 3. Take-up

During past 5 years PMD (Polarization Mode Dispersion) has played bigger role in fiber draw. The quality of the optical fibers has been improved by improvement of various fiber parameters. Quite recently the PMD started to be the limiting factor. The PMD can be lowered during fiber draw by introducing a twist to the fiber inside the furnace, when it is still melt. There are several techniques to get the twist. It is possible to rotate the preform or coating unit to twist the fiber core, but the most practical way is to apply an alternating twist to the fiber just after the curing device.

2.2 Proof Testing Process

The purpose of the proof test is to ensure that the tensile strength of the fiber is good enough. The fibers are loaded with a certain force, depending on the desired final strength, to test for tensile strength and cracks or other mechanical faults. The faults can be caused by impurities on the fiber surface or in the preform or possibly by too high drawing tension. The most commonly used minimum strength is 0.70 GPa (or 100 kpsi).

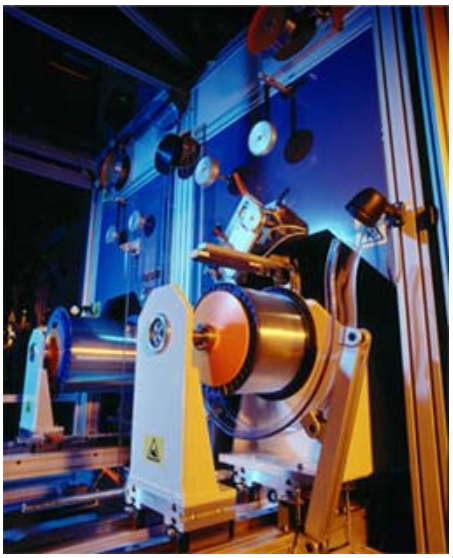

Figure 4. Proof testing system

The proof testing line (Figure 4) consists of a payoff and a take-up with the proof testing unit in between. Nowadays there are still two different methods in use for creating the proof tension. First is a braked-capstan type. The desired tension on the fiber is caused by two capstans, which have a small speed difference. The second is a dead-weight type, where the load is applied by using and additional dead-weight pulley between capstans. During testing the fiber undergoes stretching. The strain of a 10 N force is approximately 1%.

The fiber is tested over its entire length. Usually, one to twelve meters of fiber are set under stress at a given instant. The typical testing speed is between 1,200 and 2,100 m/min, but the state of the art machines can run even over 3,000 m/min.

If the fiber breaks, this occurs at its weakest points, where the fiber strength is under the testing stress. Proof testing ascertains that the fiber is strong enough throughout its lifetime.

Proof testing is divided into three phases. The first phase is loading during which the stress increases to the proof testing level. Then the fiber goes to the proof testing region where it is subjected to the proof testing tension, during the dwell time. After that the stress is unloaded during the unloading time. The fiber can break in every phase of proof testing. (Glaesemann 1991).

The speed of the take-up is controlled by a dancer so that it is possible to wind the fiber with controlled tension. A good winding result is extremely important, because poor winding may affect the fiber, causing a local increase in attenuation. The result may be same if the proof test tension varies too much. A quick line ramp-down is also required after a fiber break so that further damage to the fiber can be avoided. The proof tester needs to fulfill the guidelines for the safe handling of optical fiber. The practical guidelines are explained e.g. by Jacobs (Jacobs 2001). The proof tester is normally a stand-alone unit having all the needed controls and interface to the factory level information system.

2.3 Development Needs

The overall market situation in fiber optics can be characterized as a large negative correction after three to five years of overspending in the late-1990s and 2000. This correction affects both network operators and the suppliers of fiber and equipment. The correction began in late 2001 and continued into 2003.

The result has been a drop in the amount of fiber installed per year by 40% from 2001 to 2002, and no positive growth in fiber installations in 2003. About 20 fiber-making facilities have permanently or temporarily discontinued fiber manufacturing since 2001.

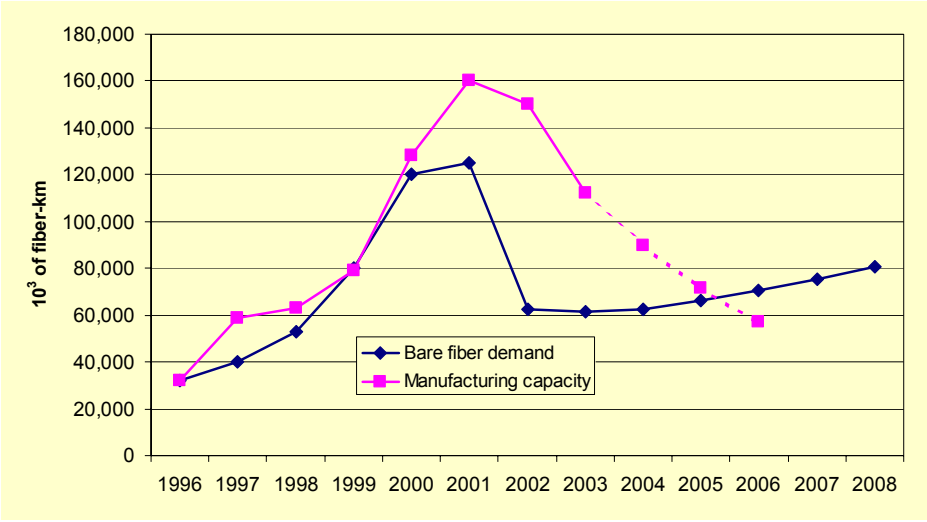

Figure 5. Fiber required vs. fiber capacity, 1996 – 2008 (000s of fiber-km)(KMI 2003)

It's estimated that the amount of fiber installed worldwide will increase from 55 million fiber-km in 2003 to 73 million fiber-km in 2008 (See Appendix 2 for details). This level of growth will not be enough to change the situation of excess fiber-manufacturing capacity, which has affected the world since 2001. Estimated worldwide capacity was approx. 100 million fiber-km in 2003. This means there is likely to be significant excess capacity and continued

competition on the basis of price and fiber performance features among the fiber suppliers.

The present situation is one of excess manufacturing capacity worldwide. The fiber demand and manufacturing capacity are compared in Figure 5. The figure shows that the capacity has started to vanish at the same time when the demand is decreasing. This is due to several companies going out of business, when the earlier capacity is not anymore easily available. It was assumed a 20% reduction in capacity after 2003, which would mean that more capacity to satisfy the demand is needed latest 2006.

The main sources of information for this short market review were KMI's report (KMI 2003) and interviews of several people in fiber optics industry. The Appendix 2 includes more information about the markets of different fiber types and the price comparisons. The following references were used as supporting material: (Mack 2003), (CRU 2003a), (CRU 2003b), (CRU 2003c).

2.4 Proof Testing Standards and Theory

Proof testing is a well-known procedure used in ceramics industry. Proof testing of optical fiber is a special application, which uses the same basic theory of fracture mechanics. There have been significant developments in the general understanding of fiber reliability, and especially the role of proof testing, over the last two decades. New models have been introduced that provide a better understanding of the reliability of fiber in the long run. The long-term physical data (Baker 1999) seems to support the two-region power law model best. The definition and requirements for proof testing have been developed to respond better to the requirements of these new models. The leading standards with respect to proof testing requirements have also changed during the past decade. The latest theory and standards, which the industry follows, highlight the following aspects:

- The dwell time of the proof testing cycle has minor effect on the final minimum strength of proof tested fiber.

- There is always a decrease in strength during the proof testing cycle in a non-ideal environment. This is a concern because the fiber might not break even though its strength decreases below the proof stress.

- The operation of the proof tester must be designed to minimize the decrease in strength. This can be achieved by arranging a high unloading rate in a proof test cycle.

- Since a decrease in strength does in fact occur, it must be monitored and reported. The proof test level itself is not pertinent, whereas the minimum strength after the proof testing cycle is of far more importance.

The next section gives more detailed description of the relevant standards. In the following theory section the commonly accepted principles have been explained. There are also mentioned newest results that have not been implemented in standards. Glaesemann gives a good review of recent advancements in the area of mechanical reliability of optical fiber, building upon previously published reviews in this area (Glaesemann 1999). The same reference has a wide list of the publications in this area as well. The background for the standards and the proof testing theory is the well-known Power Law Theory (IEC 2002).

Proof Testing Standards

The standards about mechanical reliability of fiber have been revised during past few years. The fiber is manufactured in large scale in North America, Europe and Asia. There are three different standardization organizations, which have relevant standards in this field.

Regardless the recent updates the standards have a tendency to follow behind the research results and practices in industry. Optical fiber manufacturing is still young developing industry compared to many other branches of industry, which requires continuous standardization work.

ITU - T Recommendation. G.650.1 (06/2002)

This standard is (ITU = International Telecommunication Union) the oldest standard regarding proof testing. It was revised last time in 2002. This standard defines methods for many different tests including proof testing.

General requirements for proof testing:

- Test conditions: Ambient temperature 23 ± 5 °C and ambient humidity 50 ± 20 %.
- The dwell time can be as short as possible supposing that tension is applied to the fiber.
- The fiber is tested along the whole length excluding 50 m from both ends.
- The failure must occur as full break.
- The fiber is inspected visually and/or measuring with an OTDR.
- Test documentation: Description of equipment, fiber identification, average proof tension, longest unloading time, dwell time and proof tested length passed the test.

Definitions for proof testing equipment:

- Tension in payoff and take-up can be max. 10% of proof tension.

- Unloading time must be controlled to be below limits agreed between machine supplier and user.

- Capstans and pulleys must be designed to minimize the strength decrease. Slipping in capstans is not accepted.

TIA/EIA-455-31C Proof Testing Optical Fibers by Tension

This standard is North American and published by TIA (Telecommunications Industry Association) and it was last time audited in 1999 by TIA and ANSI (American National Standards Institute). This standard is the most thorough describing the proof testing in details. Regardless the recent audit the proof testing principles have been unchanged since 1994.

In addition to ITU this standard defines the equipment as follows:

- Tensile load variations of payoff and take-up shall be isolated from the proof test region so as not to cause variations in proof tension.

- Ensure that the minimum fiber strength after proof testing is not decreased by too small bending radius in pulleys.

- The entire fiber length is tested, except 25 m in both ends.

- Test documentation: Date and title of the test, fiber identification, specified minimum strength and test results. Additionally more detailed description for US military applications.

- If a fiber does fail, evidence of failure shall be readily apparent: complete separation, automatic shut down, etc.

IEC 60793-1-30 Measurement methods and test procedures – Fibre proof test

This is the newest standard (IEC International Electrotechnical Commission) of proof testing published in 2001. The structure of this standard follows TIA/EIA-455-31C including references to ITU G.650.

The applicable standards do not restrict combining the proof testing to be a part of draw process.

Proof Testing Theory

The decrease in the strength of optical fiber for a given stress history can be expressed by the damage equation for sub-critical crack growth in brittle materials (Fuller et. al. 1980).

$$S_f^{n-2} - S_i^{n-2} = -\frac{1}{B}\int \sigma(t)^n dt \qquad \textit{Equation 1}$$

where σ is the stress applied to fiber, static or dynamic, S_i is the initial strength at the beginning of the test, S_f is the final strength for the stress history, t is time and set to 0 when the test begins and B and n are crack growth parameters for the fiber. This equation can be applied to components of the proof testing cycle by integration over the corresponding times.

Failure during Loading

Loading is similar to dynamic fatigue testing. The stress during loading is given by $\dot{\sigma}_l t$ and the upper limit of the integral is $t=\sigma_f / \dot{\sigma}_l$, where $\dot{\sigma}_l$ is the loading rate. This integration gives the equation for final strength of $S_f = \sigma_f$. (Glaesemann 1991).

$$\sigma_f^{n-2} = S_i^{n-2} - \frac{\sigma_f^{n+1}}{B(n+1)\dot{\sigma}_1} \qquad \textit{Equation 2}$$

It can be seen from Equation 2 that the decrease in strength during loading can be limited by a faster loading rate. When the loading rate increases, the upper limit of the integral decreases, and consequently the last term of Equation 2, which describes the decrease in strength, also diminishes.

Failure during Dwell

In this case, the fiber passes the loading portion, but fails at the proof stress $S_f = \sigma_p$. The upper limit of integration is now $t=\sigma_p / \dot{\sigma}_l + t_*$ when failure occurs at moment t_*, starting when dwell commences. Integration gives the following equation. (Glaesemann 1991).

$$\sigma_p^{n-2} = S_i^{n-2} - \frac{1}{B}\left[\frac{\sigma_p^{n+1}}{(n+1)\dot{\sigma}_1} + \sigma_p^n t_*\right] \qquad \textit{Equation 3}$$

Failure during Unloading

Unloading cannot be ignored in proof testing since it is an opportunity for crack growth. The strength at failure is a culmination of crack growth during loading, dwell and unloading. The upper limit of the integral is now $t=\sigma_p / \dot{\sigma}_l + t_d + (\sigma_p - \sigma_*)/\dot{\sigma}_u$, where σ_* is the failure strength during unloading. Integration over time t gives an equation describing the failure strength during unloading. (Glaesemann 1991).

$$\sigma_*^{n-2} - \frac{\sigma_*^{n+1}}{B(n+1)\dot{\sigma}_u} = S_i^{n-2} - \frac{1}{B}\left[\frac{\sigma_p^{n+1}}{(n+1)\dot{\sigma}_1} + \sigma_p^n t_d + \frac{\sigma_p^{n+1}}{(n+1)\dot{\sigma}_u}\right] \qquad \textit{Equation 4}$$

Passing the Test

The flaws that pass the proof test have a final strength, which is affected by all three components of the proof test cycle. The upper

limit of integration is now $t=\sigma_p/\dot{\sigma}_l + t_d + \sigma_p/\dot{\sigma}_u$. Integration over the entire proof test cycle gives the final strength of fibers surviving the test. (Glaesemann 1991).

$$S_f^{n-2} = S_i^{n-2} - \frac{1}{B}\left[\frac{\sigma_p^{n+1}}{(n+1)\dot{\sigma}_1} + \sigma_p^n t_d + \frac{\sigma_p^{n+1}}{(n+1)\dot{\sigma}_u}\right] \qquad \textit{Equation 5}$$

The dotted lines in Figure 6 describe the strength of the fiber during a proof testing cycle. The continuous line describes the proof stress during the cycle. Failure occurs when the two lines cross each other.

With respect to loading, failures occur in stress below the proof stress (curve A). During dwell time, those flaws with an initial strength greater than proof stress grow and subsequently fail. Note that flaws do not grow to a final strength below the proof stress during dwell time and that the minimum final strength is exactly equal to the proof stress. The dwell time has no effect on the minimum strength after the test. The minimum strength is independent of exactly when the failure occurred in dwell time.

The dwell time does, however, cause crack growth. Therefore a higher initial strength S_i is needed to survive a longer dwell time (curve B). Failures during unloading are of special interest because the strength at failure is at that point below the proof stress. The strength at failure is a culmination of crack growth during loading, dwell and unloading (curve C). The flaws that pass the proof test have a final strength that is affected by all three components of the proof test cycle. The most concerning fact is that these flaws can grow during unloading to below the proof stress and still pass the test (curve D).

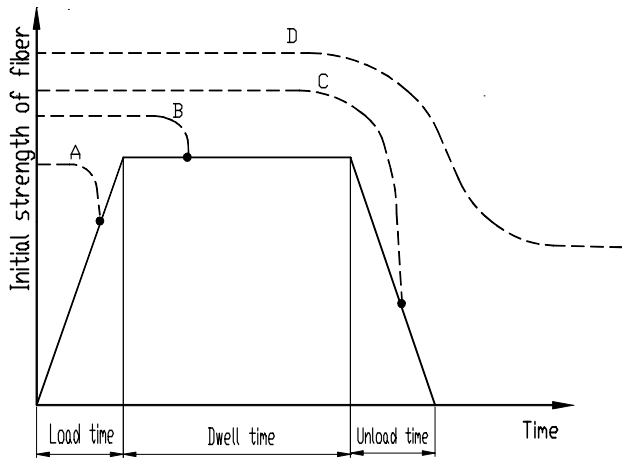

Figure 6. Strength decrease during proof testing (Glaesemann 1991)

Longer dwell time, does not produce stronger fiber, but affects to the lifetime prediction as discussed later. This is an important finding for the on-line proof-testing concept. It is also interesting to note that the requirement for a high unloading rate can be met in the on-

line proof tester concept. In an optimized proof tester, the proof test level and the minimum strength after the test do not differ significantly.

Unload time considerations

The current standards emphasize the importance of the unload rate. In the literature (Glaesemann 1991) can be found that recommended unload rate should be even as high as 70,000 MPa/s. The standards (TIA/EIA 1999) seem to be much more less demanding showing values approx. 3,500 MPa/s – 23,000 MPa/s at proof stresses 0.35 GPa – 1.05 GPa respectively. Never the less the calculation of the unload rate assumes that the unload time is known. The standard (TIA/EIA 1999) suggests that the unload time is the time the fiber travels under the capstan belt. Up till now, it has not been possible to measure the unload phenomenon and this has been safe, but conservative assumption.

In practice the unloading cannot be evenly distributed under the capstan belt, since in this case there should be slippage between belt and fiber surface. On the other hand the glass portion of the fiber cannot move in respect of the coating, since otherwise the loading of the glass by pulling from the outer surface wouldn't be possible.

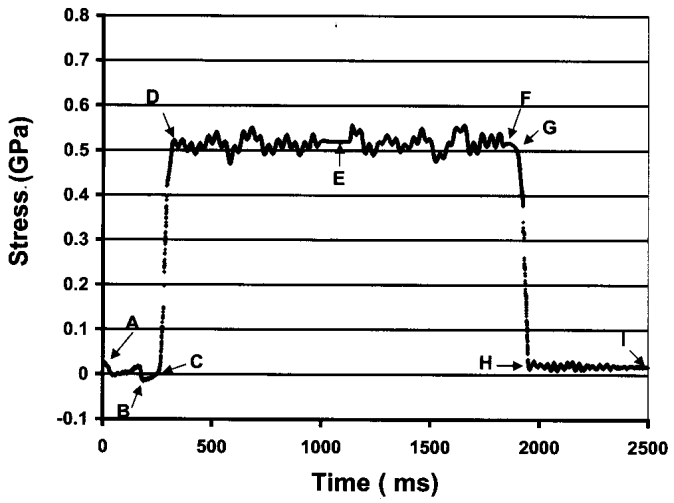

Figure 7. Measurement of proof testing cycle (Capouilliet et. al. 2001)

In the recent research the stress in the fiber has been possible to measure using Bragg gratings (Capouilliet et. al. 2001), (Baker et. al. 1999). This method allows the measurement of the stress while the fiber travels through different parts of the proof testing process. Earlier the measuring of the stress during loading and unloading has not been possible. One of the measurements is illustrated in Figure 7. In the reference it is explained that distances between B-C and F-G are under capstan belts. It is immediately seen that the loading is mostly happening just after entry capstan i.e. in the beginning of dwell region. Similarly the unloading really starts after exit capstan. It can also be seen that there is a slope after point G, but it is

possible that it is caused by slipping, since according to the test setup description in the same study, the fiber seems to touch the capstan wheel still after coming out from between the wheel and the belt. Therefore it is suggested that the unloading does not depend entirely on the capstan design like is suggested in standards.

In this thesis it is suggested that the unloading rate is more depending on the material characteristics than equipment design. The test length, however, is important, since it affects the parameters as described below.

It is assumed that the loaded fiber can be considered to be a spring, which has a deviation x from the zero-position without load. The relationship between the load F and the deviation x can be expressed as

$$F = kx \qquad \textit{Equation 6}$$

where k is the spring constant. The value of spring constant depends on the absolute strain (deviation x) and therefore the test length. Now it is assumed that the test length is L. The specified proof stress 0.729 GPa (TIA/EIA 1999) is used and the deviation x is calculated by using well-known Hooke's law. First the relative strain is given

$$\varepsilon = \frac{\sigma}{E} \qquad \textit{Equation 7}$$

The deviation x is then

$$x = \varepsilon L \qquad \textit{Equation 8}$$

By knowing now the relationship

$$\sigma = \frac{F}{A} \qquad \textit{Equation 9}$$

It can be written

$$F = \varepsilon EA \qquad \textit{Equation 10}$$

A is now the area of glass cross-section, if it is assumed that the glass carries the load completely. Using the standard fiber diameter d = 0.125 mm and E = 72 GPa (Griffioen 1994) the spring constant can be calculated with given test length

$$k = \frac{EA}{L} \qquad \textit{Equation 11}$$

It is assumed now that the loading and unloading is a simple non-suspended harmonic vibration, where loading and unloading together form one cycle. The cycle time is expressed

$$T = 2\pi\sqrt{\frac{m_f}{k}} \qquad \textit{Equation 12}$$

The unload time would be a half of that

$$T_u = \pi\sqrt{\frac{m_f}{k}} \qquad \textit{Equation 13}$$

where m_f is the mass of the fiber in dwell region

$$m_f = (L - x)A\rho \qquad \textit{Equation 14}$$

Figure 8 presents the spring constant and unload time as function of the test length. The unload rate as function of the test length is shown in Figure 9. The graphs show that the unload time is shorter and unload rate greater than suggested in literature at all lengths below 11.78 meters. The unload rate is much faster than required by standards. Unlike the standards suggest the unload rate is independent on line speed and capstan geometry, if slippage is not assumed.

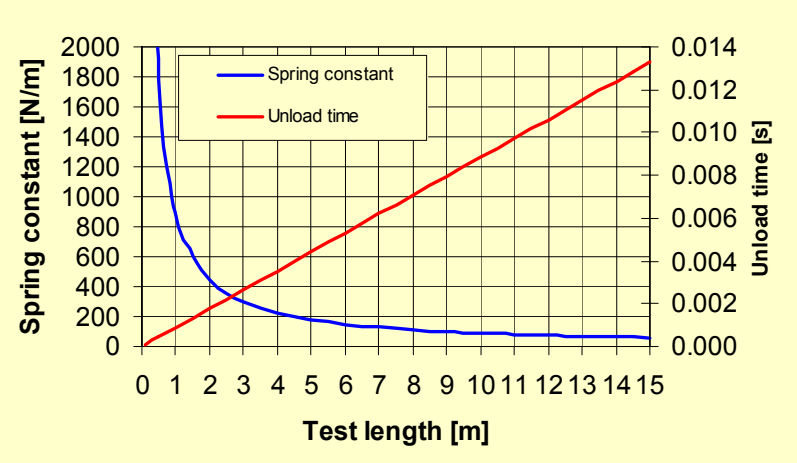

Figure 8. Effect of spring constant to unload time

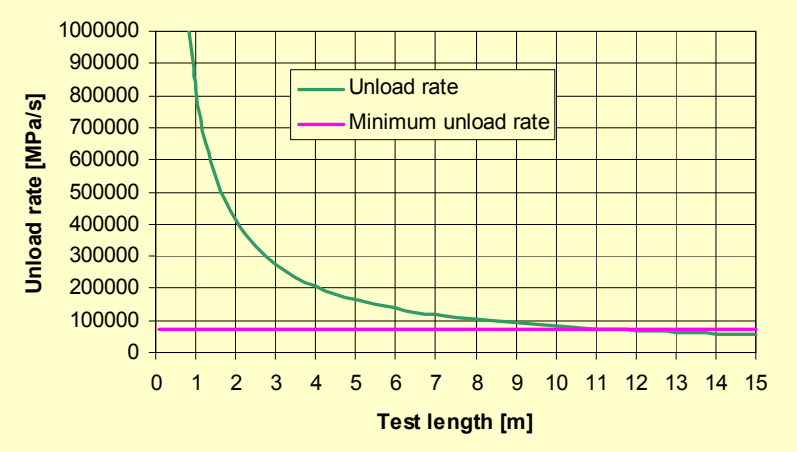

Figure 9. Unload rate as function of test length

Two-region crack growth

Most mechanical reliability models for optical fiber assume the same crack growth parameters *(n* and *B)* for both proof testing and in-service life. However, this assumption leads to inconsistencies in understanding of how the fiber behaves in the laboratory and in the field. Recent high-speed strength tests of abraded optical fibers indicate that crack-growth parameters change as a function of time under the same environmental conditions. It was suggested that at high processing speeds, the presence of crack growth in Region II of the *K-V* relationship should be entertained. Hanson and Glaesemann (Hanson and Glaesemann 1997) explored, the impact of Region II crack growth during proof testing and evaluated the effect on mechanical reliability predictions.

The power law has long been used as a model of flaw growth and as a basis of computing the reliability of fused silica-clad optical fiber. Most fibers are proof tested at a nominal proof stress of 0.69 GPa (100 kpsi) during manufacturing to remove large flaws from the population. Hanson and Glaesemann demonstrated that the standard Region I power law is insufficient for completing the analysis of the reliability of proof-tested fiber and that incorporating the effect of Region II should be considered.

Fuller et. al. (Fuller et. al. 1980) showed that, with the single-region power law, the minimum surviving strength depends on the proof stress and unloading time in a relationship with the stress corrosion parameter, *n,* and the *B* parameter according to a complex arrangement. The relationship depends on whether unloading is fast, or slow. Fast corresponds to conditions in which unloading is sufficiently fast for no unloading failures to occur. In slow unloading, the minimum surviving strength is only a function of the unloading rate, and can approach zero as *B* approaches zero. Hence the value of *B* has direct relevance to the reliability derived from conducting a proof test for both fast and slow conditions.

Various values of *B* have been reported in the literature (from 5×10^{-9} to 0.5 GPa^2s). Glaesemann and Helfinstine (Glaesemann and Helfinstine 1993) conducted inert testing on weak fibers and concluded that *B* is around $5.8 \times 10^{-4} GPa^2s$ by comparing strength measured at -120°C to room-temperature dynamic fatigue measurements at 4% min^{-1}. This low value of *B* would suggest that most proof-test unloading rates may not be fast enough to preclude proof-test unloading failures.

Consequently, the minimum surviving strength could be significantly less than the proof stress. This result is not consistent with historical field data. Tens of millions of kilometers of fiber have been installed with bend stress ranging from 20%-30% of the proof stress. At most, only a handful of fatigue related failures have been reported.

A dynamic fatigue experiment was conducted (Glaesemann 1995) to explore the phenomena of high-speed fracture in more detail. These results have led the authors to conclude the Region II, as described

by Lawn (Lawn 1993), plays an important role in high-speed events such as proof testing dynamics.

Two-region power-law mathematics is discussed in literature earlier. It is well known that sub critical crack growth in many glasses follows the classic schematic curve in Figure 10, where crack velocity, *da/dt,* is plotted as a function of the stress intensity factor, K_I. Three regions of crack growth have been identified and thoroughly discussed in the literature (Lawn 1993). Hanson and Glaesemann (1997) primarily concerned with incorporating the effects of Region II type crack growth into conventional models for sub-critical crack growth in Region I. To do this, they modeled these regions as two power laws, each having different slopes, which they called n_1 for the usual Region I, and n_2, describing Region II. This is shown schematically in Figure 11. There are corresponding *B1* and *B2* values as well.

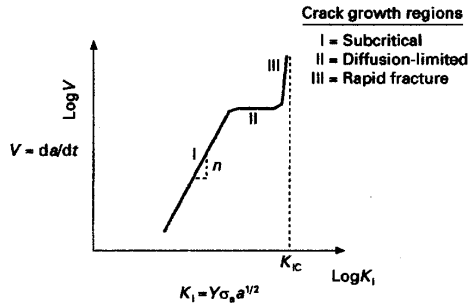

Figure 10. Classic K-V curve (Hanson and Glaesemann 1997)

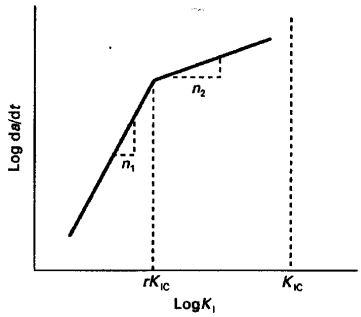

Figure 11. Two-region power law model (Hanson and Glaesemann 1997)

Dwell Time Effect on Lifetime Estimations

Proof testing standards require that a specified tension or proof stress is applied sequentially along the full length of the fiber. Because the starting of the drawing process is slow, all possible interruptions during the draw have to be minimized. The on-line proof tester requires an automatic break recovery system, which limits the design alternatives. It is not easy to design a system where there is a wheel or wheels in test zone. Ideally the distance between capstans should be as short as possible and clear from any obstacles. Therefore, the proof test time t_d becomes short, approximately 0.01 s to 0.04 s depending on the line speed. As an example; line speed 3,000 m/min and 1 m test length gives 0.02 s. Kapron shows (Kapron 1999) that increasing the proof stress level increases fiber reliability. In addition, increasing the dwell time has a similar effect.

For example, if a crack of initial strength S_i before proof testing survives the proof test, it is reduced to the strength S_f after proof testing as given by (Kapron 1999)

$$S_f^{n-2} = S_i^{n-2} - \frac{\sigma_p^n t_p}{B} \qquad \textit{Equation 15}$$

Here B is the crack strength preservation parameter or B-value; fibers with a higher value of this parameter will experience relative less weakening. The Equation 15 is another form of the Equation 5. In the Equation 15 the effective proof time is given by (Kapron 1999)

$$t_p = t_d + \frac{t_l + t_u}{n+1} \qquad \textit{Equation 16}$$

where n is the stress corrosion susceptibility parameter or n-value. Note in Equation 16 that the dwell time is the biggest contributor to the proof time. By Equation 15 the weakening of a crack clearly increases with the dwell time (Kapron 1999). If the dwell time is shortened, the lifetime estimations decrease.

Reliability in service is characterized by a lifetime or by a failure rate. For survival probability P, the fiber lifetime to failure is

$$t_f = \left[\left[\frac{\beta^{m_s}}{L} \ln \frac{1}{P} + \left(\sigma_p^n t_p\right)^{m_s} \right]^{\frac{1}{m_s}} - \sigma_p^n t_p \right] \sigma_a^{-n} \qquad \textit{Equation 17}$$

Note that when the applied stress increases, the lifetime will decrease quite rapidly (Kapron 1999). Figure 12 shows results from lifetime calculations, which were made with 0.69 GPa proof stress with following parameters: L = 1,000 km, $\ln\beta$ = 25.499, m_d = 2.359, t_l = 0.015 s, t_u = 0.015 s and $\sigma_a = 0.15\sigma_p$. Figure 13 shows that when proof stress is doubled and the dwell time is shortened, the lifetime remains on a similar level.

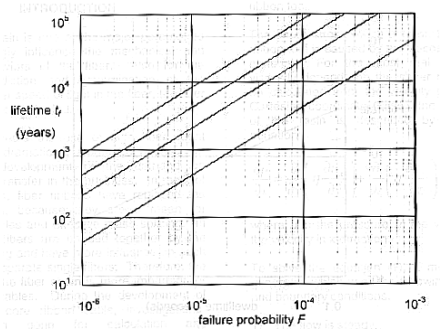

Figure 12. Life time at 0.69 GPa (Kapron 1999)

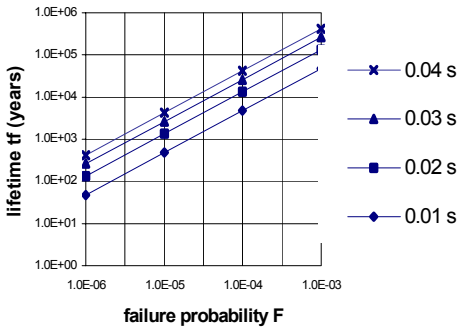

Figure 13. Life time at 1.38 GPa (Lipponen 2001)

The Effect of the Coating Material on Mechanical Properties of Optical Fiber

Earlier the theory determined the strength of fiber almost entirely based on the strength of the glass. Due to changes in dynamic fatigue test results, the behavior of the coating material in different strain rates has been studied. It has to be noted that 75 percent of the volume of fiber is coating material and only 25 percent is glass.

Standards (IEC 2001), (TIA/EIA 1999) state that proof stress shall be applied uniformly through the cross-sectional area of the test sample. When the results of dynamic fatigue tests are examined, it is seen that contribution of the coating can significantly affect the dynamic fatigue measurement of optical fiber (Overton et. al. 1995). Test was performed using six different stress rates: 0.005 %, 0.025 %, 0.25 %, 2,5 %, 25 % and 100 % per minute of gage length.

The problem has been the so-called S-shape existence within the log-stress rate/log-break stress curve of the dynamic fatigue test. It has been proven that the strength of the fiber coating is strain rate dependent, and that the contribution of the coating can significantly affect the dynamic fatigue measurement of optical fiber. The thicker the coating, the more load is exerted on the coating. The effect is also similar when using high strain speeds; the faster the strain rate, the more load the coating carries. (Overton et. al. 1995).

Optical fiber manufactures commonly use the minimum strength of 0.69 GPa, which correlates to elongation of 1 %. The loading rate of the proof test can be extremely high, 150-250 GPa/s or even more. In such a case the coating can carry a substantial part of the proof tension during the proof test and the risk of inadequate stress exertion to glass fiber could be possible. Therefore it is recommend that higher proof tension is used with an on-line proof tester than with a conventional proof tester to overcome coating effects.

Another remarkable issue is the temperature dependence of the viscoelastic properties of the coating (Apone et. al 1995). When glass fiber is coated, it goes to the UV-curing unit, where the coating material is cured. The temperature of the coating can be over the T_g-temperature, and therefore the microstructure is relatively soft. When proof testing fiber immediately after curing, it may be possible to damage the fiber unless it is properly cooled after the UV-lamps.

The Effect of Water on the Strength

When drawing fiber, the preform has to be heated to approximately 2,000°C. The fiber cools rapidly during the draw and remains dry. If the fracture strain of the fiber is measured immediately after the draw (Griffioen 1994), an obvious decrease in strain during the time after draw is seen. The value of the fiber strength decreases in a similar way.

This phenomenon is caused by stress corrosion, the effect of which begins immediately after stress is applied on the fiber, and moisture is diffused through the coating material to the surface of the glass. The water entry into a glass can promote structural relaxation, and this leads to strength reduction. Figure 14 shows fracture strain for dynamic fatigue measurements of fiber as a function of time after drawing from the preform. Fracture strain balances in 50 minutes after the draw. This value is dependent on the coating material's permeability for water. The coating material's main functions are to protect the fiber from mechanical abrasion and to reduce

microbending; however, it also works as a diffusion barrier against water.

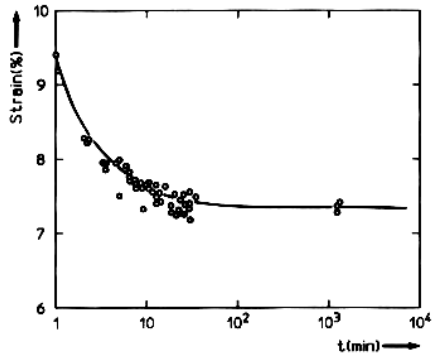

Figure 14. Fracture strain for dynamic fatigue (Griffioen 1994)

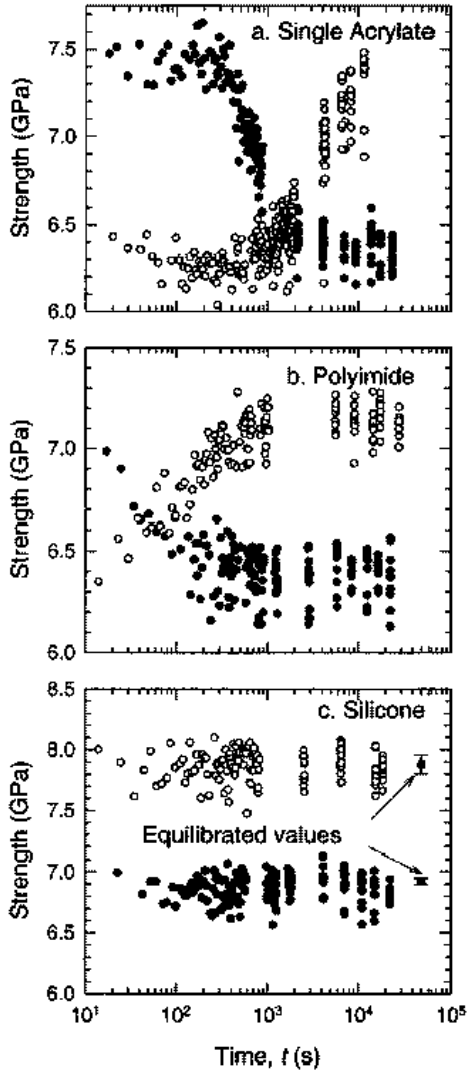

Figure 15. Strength as a function of time after changing the humidity (Mrotek et. al 2001)

Figure 15 shows the raw data for strength as a function of time after changing the ambient environment for the acrylate, polyamide, and silicone-coated fibers (Mrotek et. al. 2001). A two-point bend apparatus was used to measure the strength of fiber and it was

operated with a constant faceplate velocity of 5,000 μm/s. Twenty samples were broken at each humidity level. For all the coatings, moisture penetrates on a time scale of ~10^2 – 10^3 s (Mrotek et. al. 2001). It is seen in Figure 14 that fracture strain balances simultaneously.

When considering proof testing fiber immediately after the draw, it has to be taken into account the fact that fiber is considerably dry (as in an inert environment), and the strength balances only after several minutes from the draw. In that case the proof test tension would need to be multiple compared to a conventional proof tester. Therefore, the chances of damaging the warm and soft coating are higher.

Higher proof tension creates a need for next generation coatings, which could survive the higher tensile stress. Increasing the proof tension significantly is not necessarily the only alternative. If the existing proof tension level and coatings are used, moistening the fiber or accelerating the water penetration could be possible. Also a mechanical accumulator with exceptional capacity might be feasible in future, when the preform lengths are long enough. These are already clearly out of scope of this thesis, but a new interesting field of study. A couple of alternatives are introduced below (Lipponen and Turunen 2002) for future reference:

- Development of new coating materials to be used with high proof test tension, which is needed to compensate loading rate, coating effects and dryness of the glass fiber.

- The moistening of the fiber immediately after the fiber comes out of the furnace.

- After UV-curing the fiber must be effectively cooled to room temperature, and after that the proof test can be executed. Similar cooling techniques than used for bare fiber might be possible.

- Accelerating the water diffusion before on-line proof test. It may be possible to accelerate the penetration of the water through the coating by utilizing equipment that adjusts the pressure, temperature and moisture. In addition, possibly some chemicals could be used to activate the process.

- Preventing the water diffusion. It is possible to prevent water diffusion to the glass by exposing the fiber to deuterium. This technique is used when making Low-Water-Peak-Fibers. When the fiber is exposed to deuterium gas at elevated temperature and pressure deuterium atoms migrate into the glass matrix filling the “holes”.

- Using a high capacity accumulator between the drawing tower and the proof tester. This machine holds the fiber in ambient air for approximately 20-30 minutes regardless of the line speed. During this relaxation time the humidity and temperature of the

fiber balances, and the proof test can be executed immediately afterwards.

3 THEORETICAL ANALYSIS

3.1 Theoretical Models of Process Elements

In this chapter an approach for modeling tension behavior in combined draw and proof testing process mathematically is introduced. The models are general and can be used to model all fiber finishing processes. The basis for the idea comes from research dealing with the tension control of paper manufacturing machinery. The models generated later in this chapter can then be used for the static and dynamic tension analysis of the paper and fiber processes and also processes where other monofilaments are handled i.e. textile fibers and various plastic or composite fibers.

The problem of modeling whole fiber finishing processes is solved by the assumption that the processes can be divided into several primitive elements (Reid et al. 1989). During the process, these elements may then dynamically interact with each other.

Each primitive element has to be modeled individually. Different manufacturing systems can then be formed by combining the necessary primitive elements (Lin & Campbell 1994). The possible outputs of the aggregate models are tension levels and the tension variation of the fiber, the velocity variations of the rollers and the position changes of the dancers.

Some assumptions have been made to facilitate the derivation of the mathematical models. This means that the models are idealized based on the fact that the effect of the assumptions is minor. The assumptions are listed below:

- No slippage between fiber and rollers
- No tension variation in contact region between fiber and roller
- No temperature or humidity changes within free fiber span
- No change in density or modulus of elasticity within free fiber span
- No change in cross-sectional area within free fiber span
- Small fiber strain
- Uniform strain within free fiber span

The modeling of free fiber between elements is based on the observation that the tension in a fiber span depends on its past value, the tension in the next span, and the velocity difference

between the two ends of the free span (Shelton 1994). The elements that affect tension during a normal run in combined continuous draw process are the capstans, dancer, idle wheels and take-ups. Evaluation begins with the payoff model since it is useful, when modeling the other finishing processes more generally. The detailed mathematics behind the process element models is described in previous work supporting this thesis (Turunen 1997a, Turunen 1997b).

3.1.1 Payoff

Payoff modeling is based on the phenomena that affect the rotational movement of the payoff reel and thus also the tensile load of the fiber to be unwound. The phenomena considered necessary for evaluation are included in the following Equation 18 in the order motor torque, reel inertia, bearing friction, fiber tension, fiber bending, air resistance and reel geometry. See also Figure 16.

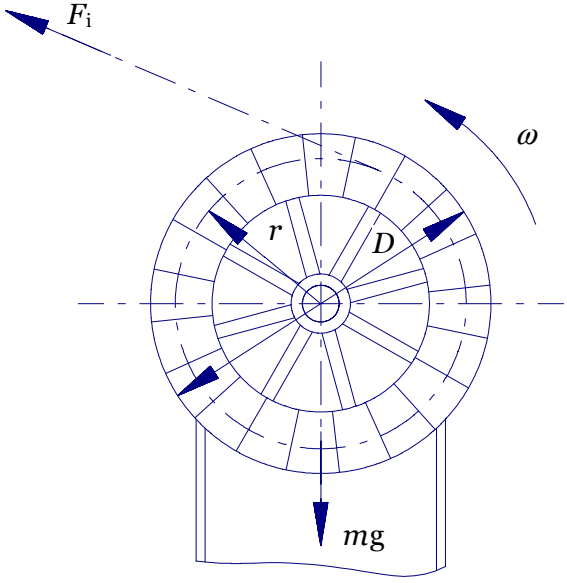

Figure 16. Payoff model

The torque equilibrium of payoff is given as

$$\left(\mathrm{K_m}u_\mathrm{m} - \mathrm{C_m}\omega\right) - J\frac{d\omega}{dt} - \left(\mathrm{K_{bl}} + \mathrm{K_{bv}}\omega^{\frac{2}{3}}\right) + F_\mathrm{o}r + \sigma\left(r_\mathrm{f}\right)W \qquad \textit{Equation 18}$$
$$-\mathrm{K_a}\omega^2 + \sqrt{x_\mathrm{c}^2 + y_\mathrm{c}^2}\,mg\sin\left(\omega t + \phi_0\right) = 0$$

where $\mathrm{K_m}$ and $\mathrm{C_m}$ are motor constants, u_m anchor voltage, $\mathrm{K_{bl}}$ and $\mathrm{K_{bv}}$ bearing constants and x_c, y_c and ϕ_o parameters denoting the eccentricity of the reel, J mass moment of inertia, m reel mass, W bending resistance and σ fiber stress. Each of the terms is derived in details in earlier work (Turunen 1997b). Only the derivation of the bearing friction is introduced, since it is a special interest in experimental section. The accurate model in simulation instead the simplified presented in earlier work was decided to be used.

When evaluating the bearing friction torque, two phenomena have to be taken into consideration, i.e. the friction caused by the radial load on the bearing and the speed dependent torque induced e.g. by the viscosity of the lubricating grease.

The load friction torque for a deep groove ball bearing is given by (Harris 1984)

$$M_{\mathrm{l}} = \mathrm{f_l} F_{\mathrm{r}} d_{\mathrm{m}} \qquad \textit{Equation 19}$$

and the torque needed for speed dependent friction is expressed as (Harris 1984)

$$M_{\mathrm{v}} = \mathrm{K_v f_v} \left(\nu_{\mathrm{o}} \frac{60}{2\pi} \right)^{\frac{2}{3}} d_{\mathrm{m}}^3 \omega^{\frac{2}{3}} \qquad \textit{Equation 20}$$

The total moment of friction is the sum of the load friction torque and viscosity friction torque. More generally the same approach is usable for belt-pulley system

$$M_{\mathrm{B}} = n_{\mathrm{p}} \mathrm{f_l} F_{\mathrm{r}} d_{\mathrm{m}} + n_{\mathrm{p}} \mathrm{K_v f_v} \left(\nu_{\mathrm{o}} \frac{60}{2\pi} \right)^{\frac{2}{3}} d_{\mathrm{m}}^3 \left(i_{\mathrm{T}} \omega \right)^{\frac{2}{3}} \qquad \textit{Equation 21}$$

where n_{p} is the number of belt pulleys and i_{T} the ratio between the drive wheel radius and belt pulley radius

$$i_{\mathrm{T}} = \frac{r}{r_{\mathrm{p}}} \qquad \textit{Equation 22}$$

where $\mathrm{r_p}$ is the radius of the belt pulley.

However, since it is not possible to accurately estimate the coefficients using literature, the experimental derivation of factors is necessary. Because all the factors except speed can be regarded as constants for a specific capstan, the equation can be simplified by denoting

$$\mathrm{K_{bl}} = n_{\mathrm{p}} \mathrm{f_l} F_{\mathrm{r}} d_{\mathrm{m}} \qquad \textit{Equation 23}$$

and similarly to the speed dependent part of bearing friction

$$\mathrm{K_{bv}} \omega^{\frac{2}{3}} = n_{\mathrm{p}} \mathrm{K_v f_v} \left(\nu_{\mathrm{o}} \frac{60}{2\pi} \right)^{\frac{2}{3}} d_{\mathrm{m}}^3 \left(i_{\mathrm{T}} \omega \right)^{\frac{2}{3}} \qquad \textit{Equation 24}$$

The desired form for bearing friction is thus

$$M_{\mathrm{B}} = \mathrm{K_{bl}} + \mathrm{K_{bv}} \omega^{\frac{2}{3}} \qquad \textit{Equation 25}$$

3.1.2 Idle Wheel

The phenomena that affect the rotational movement of the idle wheel and the tensile load of fiber are included in Equation 26 in the order idle wheel inertia, bearing friction, out-coming fiber tension, in-going fiber tension, air resistance and idle wheel geometry. See Figure 17. The torque equilibrium of the idle wheel is given as

$$-J\frac{d\omega}{dt}-\left(\mathrm{K_{bl}}+\mathrm{K_{bv}}\omega^{\frac{2}{3}}\right)+\left(F_{\mathrm{o}}-F_{\mathrm{i}}\right)r$$
$$-\mathrm{K_a}\omega^2+\sqrt{x_{\mathrm{c}}^2+y_{\mathrm{c}}^2}\,mg\sin\left(\omega t+\phi_0\right)=0 \qquad \text{Equation 26}$$

It is now easy to establish that all the sub-models of the idle wheel model were already derived when evaluating the payoff model. It must, however, be noted in this case that the inertia J is a constant, for idle wheels.

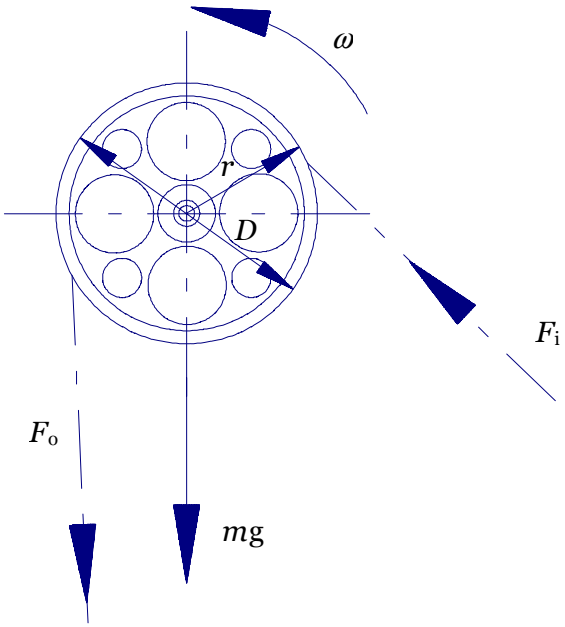

Figure 17. Idle wheel model

The payoff model was expanded to include the tension F_{i} of the in-going fiber. The equations for bearing friction and air resistance are exactly the same, but the bearing constants $\mathrm{K_{bl}}$ and $\mathrm{K_{bv}}$, and shape constant $\mathrm{K_a}$ have to be evaluated individually for different types of bearings and idle wheels. For an idle wheel in connection with a reel, the normal geometry irregularity is eccentricity rather than non-roundness. There are examples in which idle wheels are dealt with in the experimental part of this study.

3.1.3 Dancer

The dancer modeled here is a pivot-type dancer. A pivot joint and dancer wheel are modeled separately. The phenomena that affect the

dancer wheels and have to be evaluated are included in Equation 27 in the order wheel inertia, bearing friction, out-coming fiber tension, in-going fiber tension, air resistance and dancer wheel geometry. See Figure 17. The torque equilibrium of the dancer wheel is given as

$$-J\frac{d\omega}{dt}-\left(\mathrm{K_{bl}}+\mathrm{K_{bv}}\omega^{\frac{2}{3}}\right)+\left(F_{\mathrm{o}}-F_{\mathrm{i}}\right)r$$
$$-\mathrm{K_a}\omega^2+\sqrt{x_{\mathrm{c}}^2+y_{\mathrm{c}}^2}\,mg\sin\left(\omega t+\phi_0\right)=0 \qquad \textit{Equation 27}$$

This model is obviously identical with fixed idle wheel model. This is of course trivial considering that the dancer wheel is fixed in relation to the dancer arm.

The model presented here is only valid and accurate for one dancer wheel, i.e. only one dancer loop is used. The model can also be used when the dancer has more than one wheel, but then the air resistance shape factor is likely to deviate from the one wheel model.

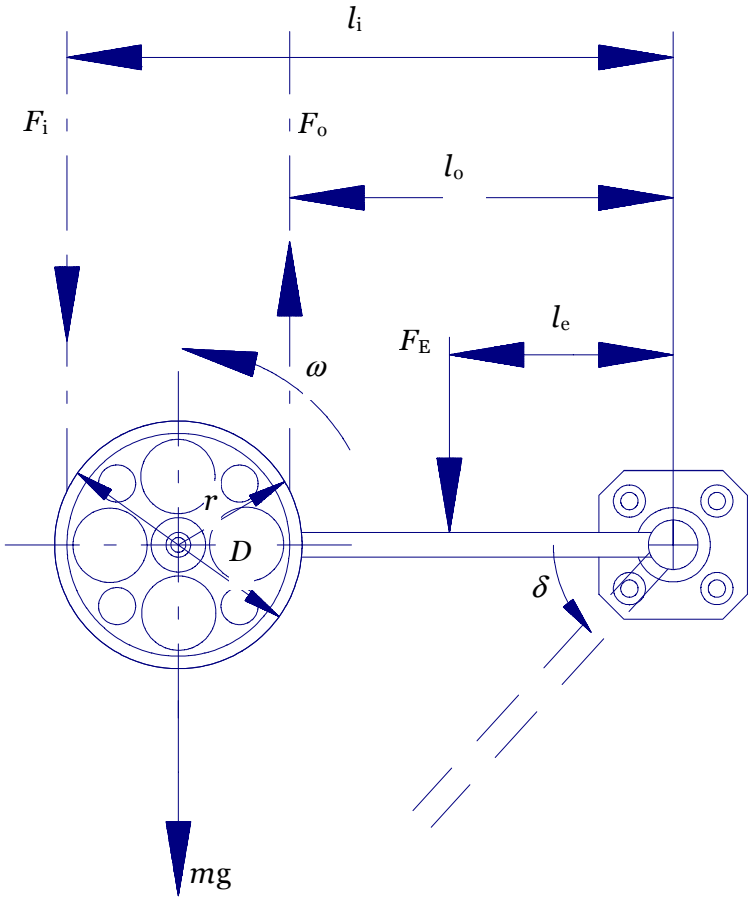

Figure 18. Dancer model

The pivot joint model is in Equation 28. The model incorporates the idle wheel inertia, pivot joint friction, air resistance, external force, out-coming fiber tension and in-going fiber tension. See Figure 18. The following assumptions facilitate the derivation of the pivoting dancer model:

- The displacement of the dancer wheel is small in comparison with the length of the adjacent fiber spans
- The change in the wrap angle of the fiber around the dancer wheel due the displacement of the wheel is negligible

$$J_{\mathrm{p}}\frac{d\dot{\delta}}{dt}+\left(\mathrm{K}_{\mathrm{pl}}+\mathrm{K}_{\mathrm{pv}}\dot{\delta}^{\frac{2}{3}}\right)+K_{ap}\omega^{2}-F_{\mathrm{E}}l_{\mathrm{e}}+F_{\mathrm{o}}l_{\mathrm{o}}+F_{\mathrm{i}}l_{\mathrm{i}}=0 \quad \textit{Equation 28}$$

where J_{p} is the polar mass moment of inertia, and $\mathrm{K_{pl}}$ and $\mathrm{K_{pv}}$ are the friction constants of the joint. With these equations it is possible to evaluate the fiber tensions F_{o} and F_{i}. The polar moment of inertia is defined as

$$J_{\mathrm{p}}=J+ml_{\mathrm{p}}^{2} \qquad \textit{Equation 29}$$

where l_{p} is the length of the arm and J is the inertia of wheel. The angular velocity of the pivoting arm in torque balance Equation 28 is defined as

$$\dot{\delta}=\frac{d\delta}{dt} \qquad \textit{Equation 30}$$

The relation between the strain and velocity of the fiber in the dancer can be derived in the same way as the free span, taking into account that the idle wheel now has vertical and horizontal displacement. The dynamic continuity equation is (Lin & Campbell 1994)

$$\begin{aligned}&\frac{d}{dt}\left[L_{\mathrm{o}}\left(1-\varepsilon_{\mathrm{o}}\right)\right]-v_{\mathrm{i}}\left(1-\varepsilon_{\mathrm{i}}+\frac{\delta l_{\mathrm{p}}}{L_{\mathrm{i}}}\sin\theta_{\mathrm{i}}\right)\\&+v_{\mathrm{o}}\left(1-\varepsilon_{\mathrm{o}}+\frac{\delta l_{\mathrm{p}}}{L_{\mathrm{o}}}\sin\theta_{\mathrm{o}}\right)+\dot{\delta}l_{\mathrm{p}}\sin\theta_{\mathrm{o}}=0\end{aligned} \qquad \textit{Equation 31}$$

where θ_{i} and θ_{o} are the angles of the incoming and outgoing fibers as shown in Figure 19. The relation between the strain and velocity is based on the geometry described in Figure 19. The second and third terms in the torque balance equation are derived as follows. The change of fiber length when the dancer is moving is

$$dL_{\mathrm{o}}=\delta l_{\mathrm{p}}\sin\theta_{\mathrm{o}} \qquad \textit{Equation 32}$$

and

$$dL_{\mathrm{i}}=\delta l_{\mathrm{p}}\sin\theta_{\mathrm{i}} \qquad \textit{Equation 33}$$

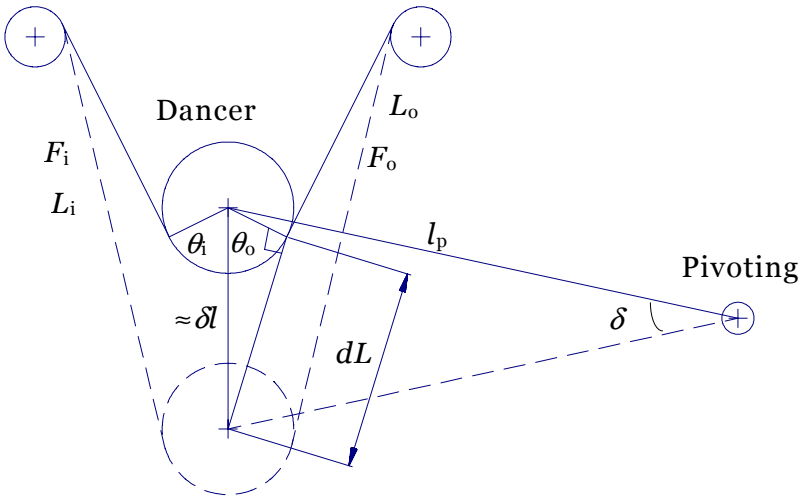

Figure 19. Dancer geometry

The relative changes in the lengths of fiber spans can thus be expressed in the same form as in the equilibrium equation

$$\frac{dL_o}{L_o} = \frac{\delta l_p \sin\theta_o}{L_o} \qquad \textit{Equation 34}$$

and

$$\frac{dL_i}{L_i} = \frac{\delta l_p \sin\theta_i}{L_i} \qquad \textit{Equation 35}$$

The last term in the equation denotes the speed at which the length is changing. The pivot-type dancer is now modeled. In principle, the dancer could also be of the linear moving type, but the pivoting type is normally preferred in fiber draw and finishing processes. Linear moving dancers are not included in this report. It is only pointed out that the evaluation of linear dancers is based on same methods as for pivoting dancers, but the angular movement is replaced by linear movement.

3.1.4 Capstan

The modeling of the capstan is based on the phenomena that affect the rotational movement of the capstan and thus also the tensile load of the fiber going through it. These are included in Equation 36 in the order motor torque, capstan wheel inertia, bearing friction, out-coming fiber tension, in-going fiber tension, belt pulley bearing friction and capstan wheel geometry. See Figure 20.

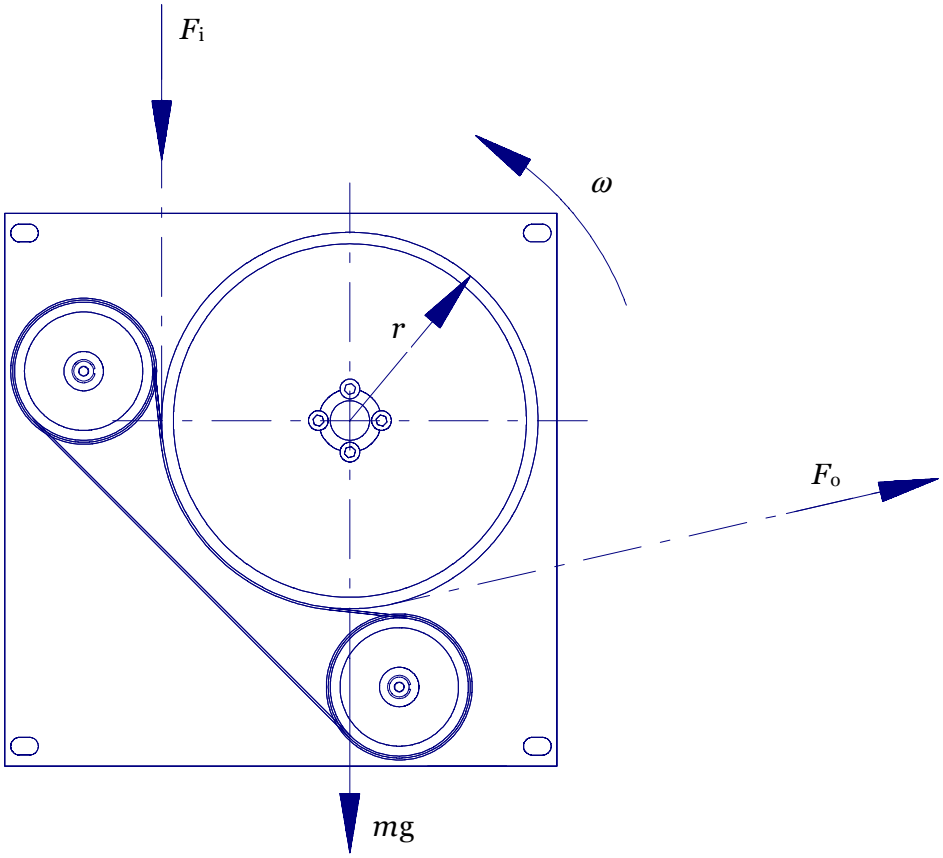

Figure 20. Capstan model

The torque equilibrium of the capstan is given as

$$\left(\mathrm{K_m}u_\mathrm{m} - \mathrm{C_m}\omega\right) - J\frac{d\omega}{dt} - \left(\mathrm{K_{bl}} + \mathrm{K_{bv}}\omega^{\frac{2}{3}}\right) + \left(F_\mathrm{o} - F_\mathrm{i}\right)r$$
$$- \mathrm{K_a}\omega^2 - \left(\mathrm{K_{tl}} + \mathrm{K_{tv}}\omega^{\frac{2}{3}}\right) + \sqrt{x_\mathrm{c}^2 + y_\mathrm{c}^2}\,mg\sin\left(\omega t + \phi_0\right) = 0 \qquad \textit{Equation 36}$$

where $\mathrm{K_{tl}}$ and $\mathrm{K_{tv}}$ are the friction constants of the capstan belt pulleys. It is clear that the capstan model is a combination of the payoff model and idle wheel model. This is naturally the case since this kind of capstan is basically a wheel rotated by a motor. The pulling force is transmitted to the fiber by belt friction. The motor of the capstan modeled here is on the same axis as the capstan wheel. What is different compared to earlier models is that the belt friction is included. Belt friction, which is in fact the bearing friction of the belt pulleys, on the other hand has a great effect on the torque balance of the capstan. Belt tightness affects the friction, because it causes loading on the bearings. Because belt friction is now regarded as bearing friction, there is good reason to assume that this model will have the same form as normal bearing friction.

3.1.5 Take-up

The tension is affected by a take-up rotating according to Equation 37 which includes the terms for the motor torque, reel inertia, bearing friction, winding tension, fiber bending, air resistance and reel geometry. See Figure 21.

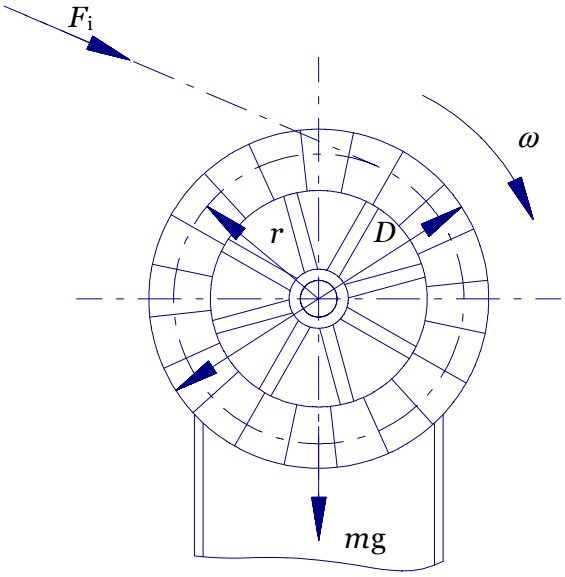

Figure 21. Take-up model

The torque equilibrium of the take-up is given as

$$\left(\mathrm{K_m}u_\mathrm{m} - \mathrm{C_m}\omega\right) - J\frac{d\omega}{dt} - \left(\mathrm{K_{bl}} + \mathrm{K_{bv}}\omega^{\frac{2}{3}}\right) - F_\mathrm{o}r - \sigma(r_\mathrm{f})W \\ -\mathrm{K_a}\omega^2 + \sqrt{x_\mathrm{c}^2 + y_\mathrm{c}^2}\,mg\sin(\omega t + \phi_0) = 0 \qquad \text{Equation 37}$$

The winding tension F_i can be determined from this equation. When comparing the payoff model derived earlier and the take-up model, it is noticed that they are almost identical. As far as structure is concerned the models are exactly the same. This is only natural since the payoff winder and take-up winder can be, and they often are, the same mechanical construction. There are, however, a few differences, which is why the take-up must have a model of its own. The only differences between the models are the effects of the fiber tension and fiber bending. In the take-up model, both of these have the opposite signs compared with the payoff model. This is because the fiber tension now causes torque in the opposite direction to that in the motor model. In the case of the payoff, the motor torque and fiber tension have an effect in the same direction. The situation is the same with the fiber bending torque.

3.2 Challenges in Combined Fiber Draw Process and Proof Testing

3.2.1 Limits of the Analysis

Methods to realize continuous proof testing combined to fiber draw are introduced. The mechanical solutions to proof test the fiber according to the standards are included and at the same time it is shown that surviving from a random proof testing break at full speed without disturbing the draw process is possible.

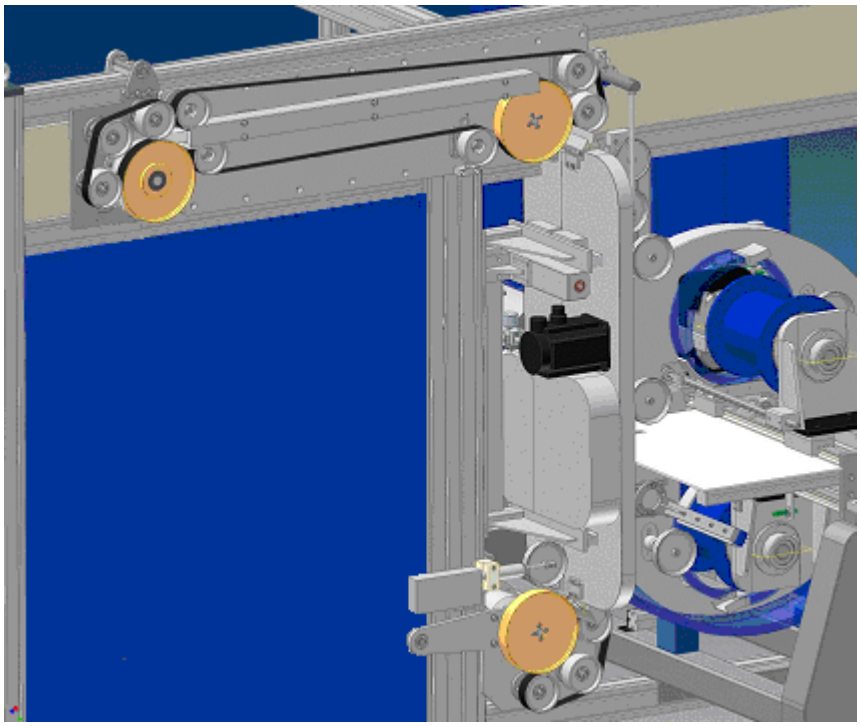

Figure 22. Schematic view of on-line proof testing unit

Also a universal simulating tool was generated to predict the tension behavior of the fiber. Tension behavior and simulation downstream from the draw tower coater but upstream from the auxiliary capstan were focused on. This eliminated the draw coater and all parts upstream as well as the fiber cutter and the suction fan downstream from the auxiliary capstan.

The following descriptions are based on the patent granted in Finland (Turunen and Mäkelä 2002a), an international patent application (Turunen and Mäkelä 2002b) and US patent application (Turunen and Mäkelä 2003). The same idea was briefly introduced first time publicly in International Cable & Wire Symposium 2000 (Turunen et. al. 2000) after filing the patent application in Finland. The descriptions are only a general overview allowing different approaches for realization in many parts. Figure 22 shows a schematic view of the entire on-line proof testing unit with break recovery system and take-up.

3.2.2 Proof Testing Region and Proof Tension Measurement

The proof testing is performed by addressing the speed difference between two servo-driven capstans; the entry and exit capstans. In proof testing zone the tension is loaded to the fiber right after the entry capstan. The tension is maintained inside the tolerances indicated in standards in all situations. The dwell zone length in this machine is only about 1 m to minimize the free length fiber needs to travel after fiber break. On the other hand the length is long enough to keep the tension control simple and the tension variation inside the tolerances. If the test length is too short the resolution of the digital servo drives is not enough to maintain the tension variation in the limits. According to the earlier experiences 1 m shouldn't be a problem, but it needs to be confirmed by testing as explained later.

The entry capstan includes a load cell for proof tension measurement. Between these capstans the fiber runs through a channel that guides the fiber during threading and after a fiber break. The channel needs to be possible to open for cleaning. This is now different from the existing proof testers where normally the tension is measured directly inside the dwell region by using a load cell and turning pulley. This is an accurate measurement method and easy to calibrate, when the pulley and bearing design is right. The requirement for break recovery, which is explained in details later, makes it difficult to use measurement pulley in test region. The proposed method is now indirect measurement, where the force objected to the entry capstan is measured. If the fiber entering angle and exiting angle in respect of load cell measurement direction are selected correctly, the force acting to capstan is caused entirely by the fiber under proof stress. Another alternative would be measuring the force from exit capstan, but since similar measurement method is required after exit capstan, it is better to keep the measurement in entry capstan. The measurement from entry capstan was tested and the arrangement and results are reported in experiments and results sections respectively.

After exit capstan the fiber goes through a small gap between splittable channel and capstan belt wheel continuing to the take-up servo dancer.

Normally all the needed running parameters are down loaded from the line control. These are e.g. line speed, run length and reel recipes. Some of them like reel recipes may be controlled by the local control panel. The machine calculates the needed proof testing tension during ramp up according to the standards, ensuring that the entire length is proof tested properly.

3.2.3 Automatic Break Recovery and Threading System

Threading and break recovery are realized using both proof testing capstans and a channel between them. After the exit capstan there is an additional splittable channel, which guides the fiber to a third auxiliary capstan. Static electricity needs to be discharged from both

capstans to prevent static problems during threading or break recovery. A fiber cutter and a suction fan are needed to waste the fiber lost during fiber break after the auxiliary capstan. For fixing the fiber end to empty reel the revolving system, gripping flange and cutting blade are used. Additionally an auxiliary horizontally moving wheel is needed to push the fiber deep enough between gripping flanges.

The initial threading during line start-up is planned to be automatic. The operator needs to thread the fiber end between the entry capstan belt and capstan wheel. The entry capstan pulls the fiber from the tower and the fiber end goes through the channel between capstans. After the channel the fiber goes between exit capstan's belt and wheel, which bends the fiber to go downwards. The exit capstan rotates slightly faster than entry capstan. The fiber is kept tight between capstans by using the tension measurement located in entry capstan.

Now the fiber travels in the splittable channel between the exit capstan and an auxiliary capstan located in the bottom of the machine. The auxiliary capstan rotates slightly faster than the exit capstan. Also the auxiliary capstan has tension measurement, which is now used to detect that the fiber is through this capstan. Now the fiber is tight before entry capstan, between entry capstan and exit capstan and between entry capstan and auxiliary capstan. At the same time the fiber is run to the waste chamber.

Then the splittable channel opens and the take-up dancer moves between the splittable channel halves on the other side of the fiber. Before this the dancer has moved slightly outside from the fiber line that the dancer wheel can go between the fiber and the other channel half. The dancer moves the fiber from between the channel halves and with the help of the auxiliary horizontally moving wheel the fiber will be between the gripping flanges of the take-up finally. During this operation the draw tower is feeding the fiber through entry and exit capstans as well as auxiliary capstan keeping the tension constant in all fiber spans.

When the fiber is between the gripping flanges (Figure 23) the flanges are pressed together by a pneumatic cylinder, before which the take-up accelerates to the line speed. The fiber-cutting blade cuts the fiber end when the flanges are closed. Then auxiliary capstan pulls the scrap piece to the scrap vessel. The revolving mechanism rotates the take-up just enough that the fiber touches the traversing guide wheel. Now the machine is proof testing and winding the fiber on the scrap flange outside the spool and then on the measurement flange after which the traversing movement moves the fiber onto the spool through a slot on the flange. See Figure 24.

The machine can recover automatically from proof test break using the same system as for threading described above. The fiber breaks either under the entry capstan's belt or inside the channel between the capstans. The fiber break is detected primarily with the proof tension load cell, but also separate break detector can be used. In the

event of fiber break, the full spool brakes at maximum moment to stop the spool fast. The whipping guard on the full reel side is on the fiber path and protects the fiber package from damaging.

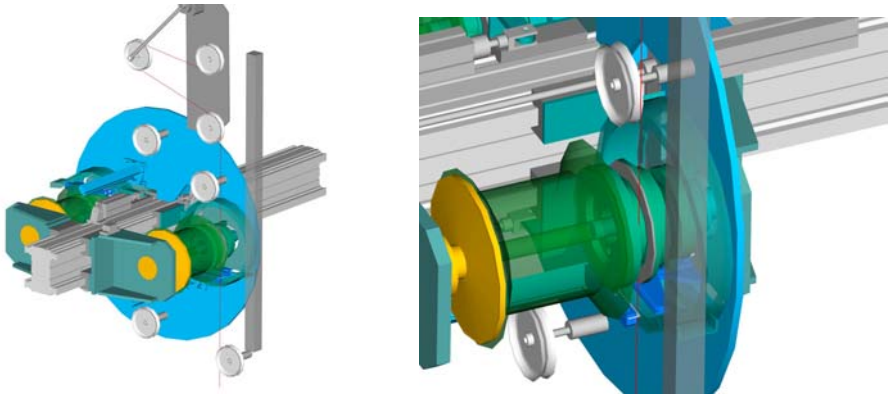

Figure 23. Fiber between gripping flanges

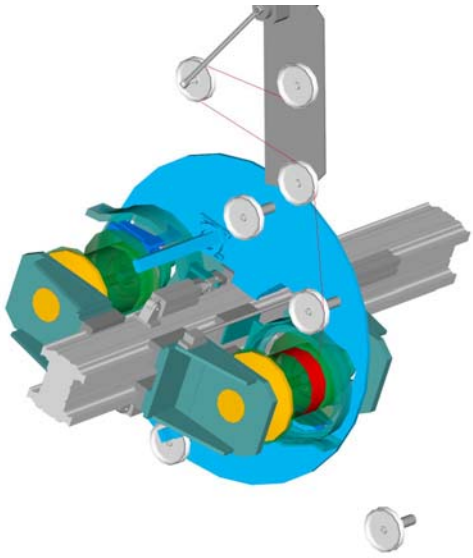

Figure 24. Revolver in winding position

Now, if the empty spool was assembled to the other take-up, the revolver rotates to fiber picking position. If the empty spool is not waiting on start position, the machine stops all the functions in a controlled manner. The reliability of the break recovery system is essential for the whole concept. The reliability percent effects on the draw tower yield. Therefore this function was tested first before entering into detailed engineering. The results are presented in tests and results sections.

3.2.4 Dual Take-up and Transfer Reliability

When the preset length is achieved or the operator chooses to make the change-over the sequence starts, if the empty reel is ready on the other take-up. This is called a planned change-over.

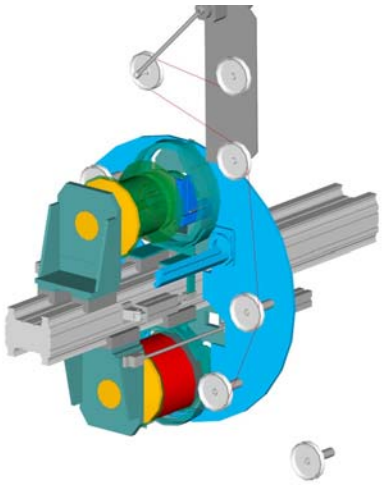

Figure 25. Take-up revolving

First the take-ups revolve to move the empty spool near the fiber path. When the revolver rotates further, another turning wheel starts to guide fiber (Figure 25). When the revolver rotates still further the fiber goes between gripping flanges and the blades. The whipping guard on the empty spool side must go inside from the fiber path before that (Figure 26). A new reel is accelerated to process speed and the gripping flange is closed, simultaneously cutting the fiber with an integrated cutting blade.

The full spool brakes at maximum moment to stop the spool fast. The whipping guard on the full reel side is on the fiber path and protects the fiber package from damaging. Then the revolving mechanism rotates the take-up just enough that the fiber touches the traversing guide wheel. See Figure 27.

Since the plan is to wind relatively short delivery spools the number of planned change-overs will be remarkable. The reliability of change-over has a great impact on fiber draw yield like has the break recovery reliability as well. The reliability was tested in various ways both is laboratory conditions and on the field by customers to get full confident on the principle, before introducing it in combined process.

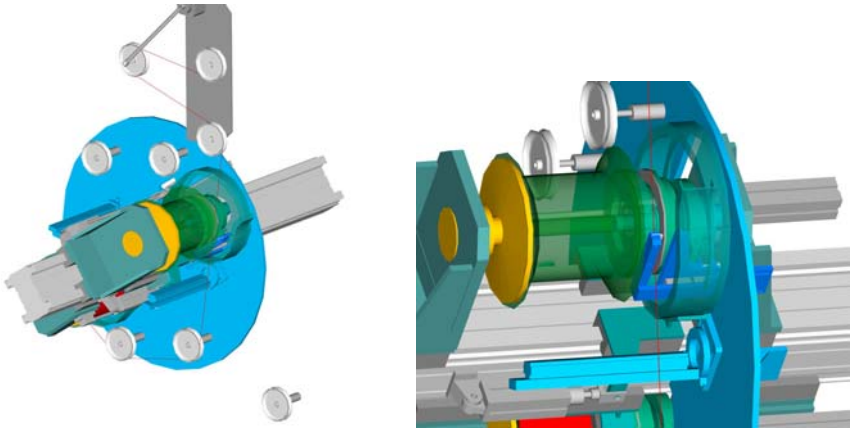

Figure 26. Fiber between gripping flanges after planned change-over

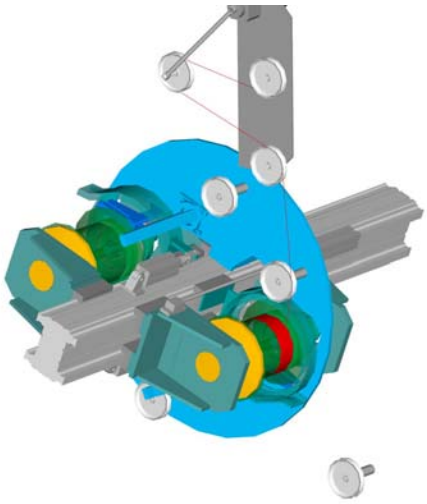

Figure 27. Take-up in winding position after change-over

3.2.5 Whipping Prevention during Winding and after Transfer

As mentioned in earlier chapters the take-up is equipped with means to prevent whipping. There are a couple of different kinds of whipping phenomena that can damage the fiber package either during winding or after transfer.

The whipping after transfer is caused by the fiber end, which achieves the full spool before the take-up stops. The motor and drive are sized to decelerate the spool fast but without harming the fiber. In this case, when the fiber is cut near the spool in planned change-over, it is not possible to stop the spool before the fiber end reaches the spool, without damaging the fiber package (Mattila 1997). It would be desirable to remove all the obstacles from the fiber path and eliminate the source of the back swing, which damages the package surface. In practice this is not possible, since there are always some machine elements near the fiber path to ensure good winding. These are e.g. static control devices and guiding wheels.

An effective solution to prevent whipping damages after fiber break or planned change-over at high speed is a properly designed whipping guard. Typically this kind of guard can catch the fiber end and guide it without creating back-swing to the fiber. The fiber end has a change to rotate inside the guard while the spool has time to stop.

Another phenomenon causing whipping damages is the loose in side end. First it is essential to ensure that the fiber is gripped properly. Secondly the inside end needs to be wound with bigger pitch outside the spool to minimize the scrap length. At high rotating speeds it is essential to prevent the fiber from moving sideways outside the spool, since otherwise loose loops are forming causing whipping. The scrap flange needs to be designed to prevent this. Thirdly it is essential to protect the fiber wound outside the spool from damages,

since in case the fiber breaks, in-side-end whipping may destroy whole package and the draw tower needs to be stopped.

The effectiveness of whipping guard and other devices to prevent whipping damages were tested. The arrangements and the results are explained later in this work

3.2.6 Winding and Traversing Turning Control

The tension and speed controls are realized by servo-dancer and automatic tension control. The winding tension is measured continuously and kept constant by adjusting the moment of the dancer motor. The take-up is a “revolver” type dual take-up. The operating principle is to revolve both take-ups during change-over, so that they change places. The revolver frame is partially steel structure to reduce machine vibration. See Figure 28.

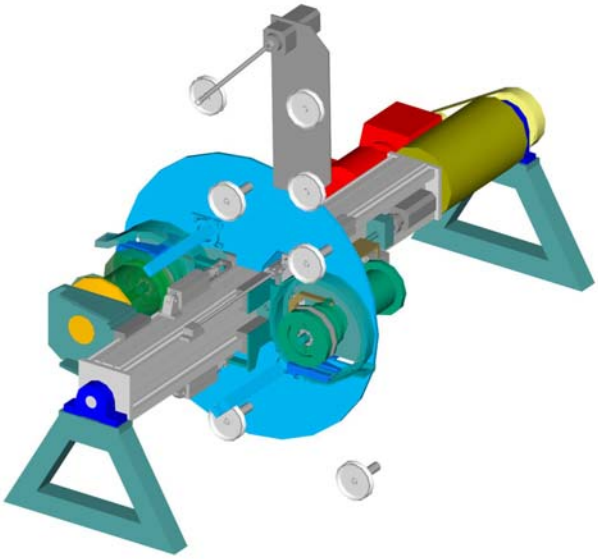

Figure 28. Principle of take-up

The unloading of the full reel and loading of the empty reel are done manually. This can be automated at least partly, if interest occurs. All needed electrical parts, drives and PLC are assembled to the revolving part, so only electrical supply, minimum amount of signals and pneumatic air needs to go through rotating joint. The rotating movement of the active take-up is controlled by a servo dancer, which also keeps the winding tension constant. For tension control a feedback measurement is needed and it is located just after the dancer.

The rotating and synchronized traversing movement of the take-up spool is used to make the winding. The PLC and automatic turning correction algorithm adjust the winding parameters during filling the reel. Both straight and conical winding patterns can be adjusted automatically.

There are basically two phenomena to consider when modeling take-up's winding behavior. The first is the optimal traversing pitch and packing density. They affect the maximum amount of fiber that can be fitted on to a spool and on the other hand optical properties e.g. attenuation. The second is traversing turning control. The most difficult part of winding is to change the traversing direction in controlled manner. If the turning happens too early or too late, it will cause tension peaks and also loose winding, which can be seen as attenuation discontinuity point in OTDR (Optical Time Domain Reflectometer) measurement.

First the theoretical packing density needs to be evaluated. This is done by calculating minimum and maximum packing efficiency factors. It is simply calculated from the geometry of the fiber package cross section. This is naturally very simplified approach and does not take into account the fact that the fiber is always wound in an angle onto the spool. Figure 29 illustrates the worst and the best case. In both cases the pitch is exactly the same as fiber diameter. In reality it is no point to try to control exactly the laying, since the speed is too fast to do it in economical way. The packing density factor is always between these minimum and maximum regardless the pitch. The pitch is always bigger than the fiber diameter, because of the irregularities and their effect on the optical properties. This is outside of the scope of this study. The optimal pitch to find a good compromise between packing quality and optical characteristics has been studied in e.g. by Turunen (1998).

First a look into the worst case is taken. Area of the fiber cross sections in reference area is

$$A_{FW} = 4\pi\left(\frac{d_f}{2}\right)^2 = \pi d_f^2 \qquad \textit{Equation 38}$$

Area of the reference area is

$$A_{RW} = 2d_f \cdot 2d_f = 4d_f^2 \qquad \textit{Equation 39}$$

The packing efficiency factor in the worst case is

$$K_{LW} = \frac{A_{FW}}{A_{RW}} = \frac{\pi}{4} \qquad \textit{Equation 40}$$

The best case gives

$$A_{FB} = 4\pi\left(\frac{d_f}{2}\right)^2 = \pi d_f^2 \qquad \textit{Equation 41}$$

Area of the reference area is

$$A_{RB} = 2d_f \cdot x_f \qquad \textit{Equation 42}$$

where

$$x_f = \frac{d_f \sin(a)}{\sin(b)} \qquad \textit{Equation 43}$$

The packing efficiency factor in the best case is

$$K_{LB} = \frac{A_{FB}}{A_{RB}} = \frac{\pi \sin(b)}{2\sin(a)} \qquad \textit{Equation 44}$$

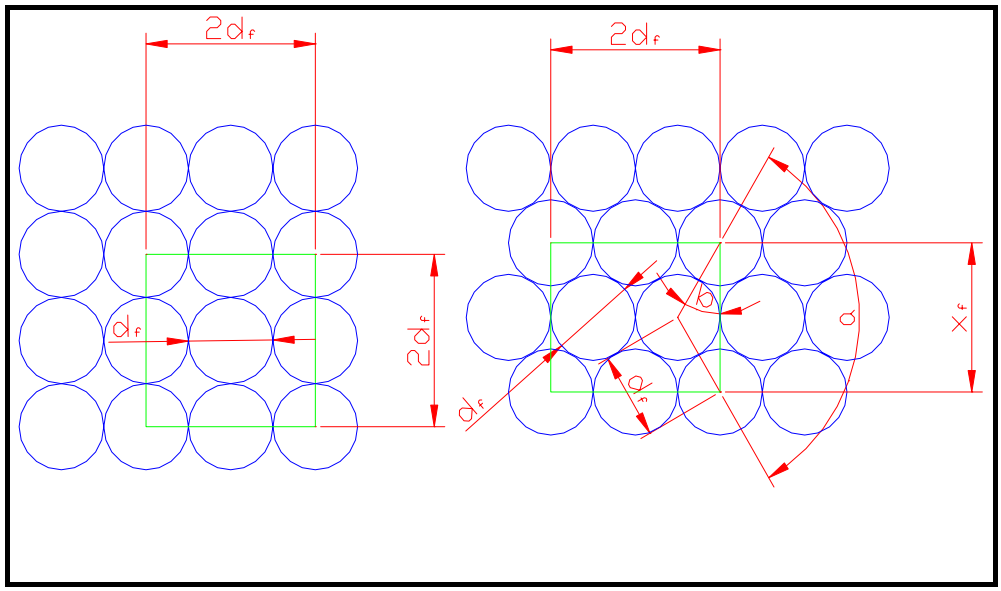

Figure 29. Minimum and maximum winding package density

The second phenomenon needed to be studied is the winding direction turning near flanges. The turning should be optimized so that no build-ups or roll offs occur near flanges. The challenge is the fact that the spools are somewhat flexible and therefore the actual turning position may change while the spool is filling up. There are also differences between spools, which means that constant parameters for all spools and on the other hand during filling up one spool are not possible.

The theoretical approach to model tension behavior near flanges is presented below. Figure 30 illustrates situation where there is a build-up near the flange. First the number of the turns in a build-up needs to be calculated

$$N = \frac{x_b}{p} \qquad \textit{Equation 45}$$

The diameter change per one turn can be expressed as

$$\Delta D = 2\frac{y_b}{N} \qquad \textit{Equation 46}$$

The total length of the fiber in the build-up can be integrated as

$$L_b = \pi \int_0^N (D + x_b \Delta D) dx_b \qquad \textit{Equation 47}$$

On the other hand the length, if no build-up occurs would be

$$L = \pi D N \qquad \textit{Equation 48}$$

Excess length because of the build-up is then

$$\Delta L = L_b - L \qquad \textit{Equation 49}$$

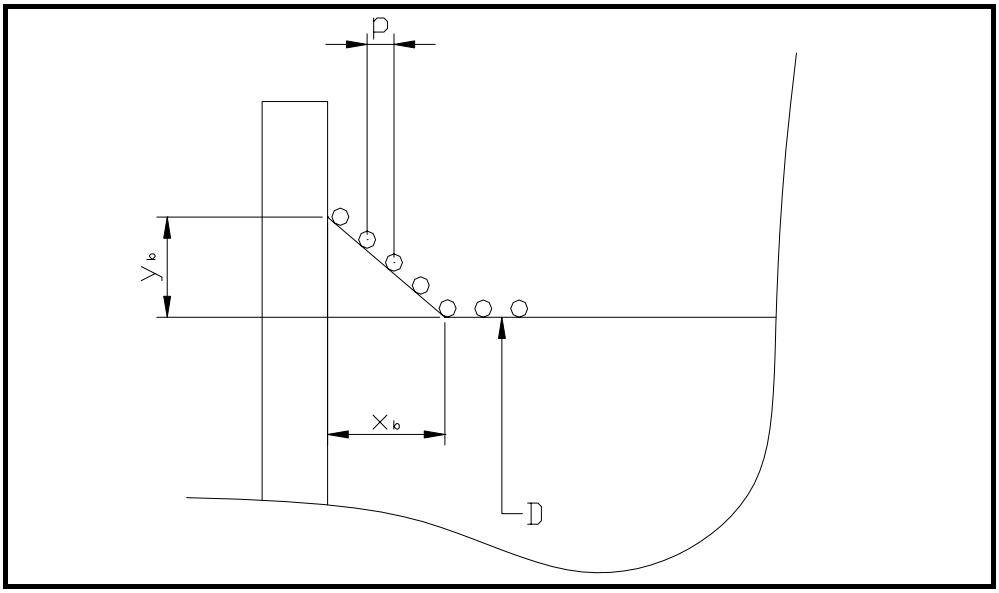

Figure 30. Fiber build-up geometry near spool flange

Time needed to wind on to the build-up is

$$t_b = \frac{L_b}{v_1} \qquad \textit{Equation 50}$$

The dancer's average circumferential speed is then approx.

$$\Delta v = \frac{\Delta L}{2 t_b j} \qquad \textit{Equation 51}$$

where j is the number of fiber loops. Now the average angular speed of the dancer arm is solved

$$\omega_\delta = \frac{\Delta v}{l_p} \qquad \textit{Equation 52}$$

In this case the acceleration is linear and the maximum speed is 2 x ω_δ, which gives for angular acceleration then

$$\alpha_\delta = \frac{2\omega_\delta}{t_b} \qquad \textit{Equation 53}$$

If a dancer position as it is shown in Figure 31 is assumed, some simplifying assumptions can be done. First it is assumed that the pivoting movement creates the same amount of tension change to both input and output fibers

$$2F_{WB} = F_i + F_o \qquad \textit{Equation 54}$$

The torque equilibrium is given according to Equation 28. The equation is further extended by adding the term for gravity effect.

$$J_p\alpha_\delta + \left(K_{pl} + K_{pv}\omega_\delta^{\frac{2}{3}} \right) + K_{ap}\omega^2 - F_E l_e + 2F_{WB} l_p + mg\sin(\delta + \phi_0) = 0$$

Equation 55

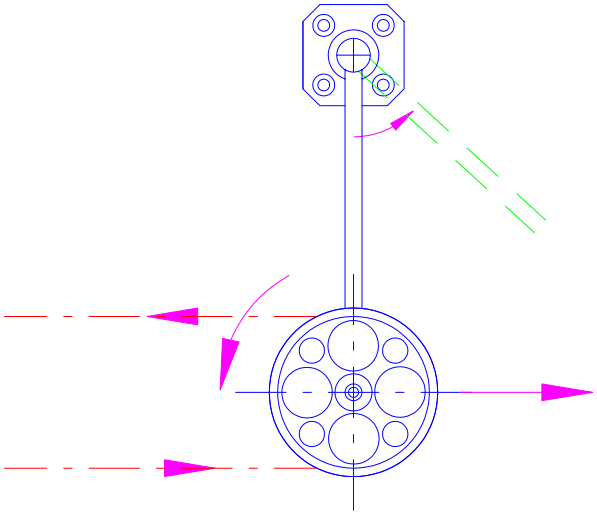

Figure 31. Vertically pivoting dancer

F_{WB} is the additional tension created by the dancer movement. The same equations apply in the case of roll off also.

The following is the description how one can overcome the above-mentioned problems. The surface of the fiber is normally UV curable acrylate. Depending on the manufacturing parameters the surface may be well cured and hard or on purpose slightly “sticky”. In this case fiber tends to stick to the flange during winding. On the other hand static electricity may cause the same effect, although the surface is hard and smooth.

The proposed approach is to use existing dancer signal to detect defects near flanges. This is known technique (Karppo 1974) from copper winding and also been used in some optical fiber proof

testers several years. This technique allows small errors to occur, which is the reason that the effect on the tension needs to be modeled. This alone, however, is not enough to prevent loose loops from forming with most difficult fiber surface materials. The software algorithm has an important role in efficiency of this technique. It has been found experimentally very effective way to use this already known method to prevent loose loops and attenuation discontinuing points (later steps).

When winding the fiber to the reel the flanges of the reel tend spread out somewhat during winding. To compensate the spreading the traversing needs to be widening by each layer. This spreading can be detected by the dancer movement caused by the gap. The simplest algorithm corrects this phenomenon filling the gap by spreading the traverse Figure 32.

This type of over-traversing causes the fiber to lean against the flange while the gap is filling. Two clear reasons can be found to cause the problems; firstly the amount of over-traverse in order to fill the gap and secondly the distance of the last guide pulley. The greater the distance the smaller the angle and force against the flange. On the other hand, if the guide pulley is too far from the reel it starts to affect the traversing of the fiber and thus creates problems, so a compromise has to be found. With current functioning principle and “sticky” fiber the distance intuitively has been between 20 to 30 mm from the flange. However, the surface of the fiber and its friction coefficient has an influence on this distance.

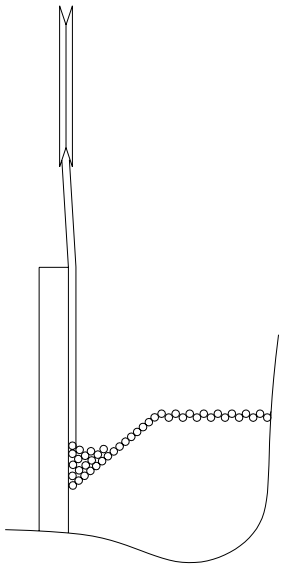

Figure 32. Flange correction principle

This then causes the fiber to stick to the flange due to the friction or static electricity. At the same time the fiber forms a small bump near flange. The gap starts to fill by the fiber turns falling to the gap from flange. These layers of fiber that fall from the lump bend under next layers of wound fiber and cause steps in attenuation measurements. This has been learned by experiments and as a result new software

algorithm was created. The new algorithm was tested experimentally and the results are reported later in this work.

3.3 Process Tension Simulation Model for Combined Process

In this case only the end part of the combined fiber draw and proof testing process were modeled. A computer simulation based on the modeling work was then generated. The input parameters for the simulation include line speed, reel dimensions, the eccentricity of rotating parts, etc.

The Appendix 3 shows the required inputs from the user. Some of the inputs are calculated separately as explained partly earlier in this section and partly later in experiments section. These are density of acrylate, Young's modulus of fiber, draw tension, bearing coefficients air resistance coefficient and laying factor. The screen includes a section for general parameters and a section for each process elements, which in this case are a take-up, guide wheel, dancer wheel, dancer arm, exit capstan, entry capstan and turning wheel. As intermediate results outputs for each of the elements and also some general outputs are calculated. These outputs can be seen in Appendix 4.

The results of the simulation are graphical and numerical presentations of fiber tension in different situations and also other mechanical behavior. Tension behavior and simulation downstream from the draw tower coater but upstream from the auxiliary capstan were focused on. This eliminated the draw coater and all parts upstream as well as the fiber cutter and the suction fan downstream from the auxiliary capstan.

The on-line proof testing process was modeled by using process elements. The simulation included disturbances traveling in both directions - i.e., from the coater to the take-up and from the take-up to the coater. The reflection from the coater and from the take-up was ignored. The speeds of the rotating parts formed an essential part of the simulation. The speed differences between rotating parts create elongation, which can be seen as tension.

It was assumed that the angular speed of the motor-driven shafts remains constant regardless of fiber tension. The eccentricity of the rotating parts then creates a variation in tension because the circumferential speed varies. The circumferential speed of the idle wheels varies with the tension because the tension is comparable to the speed difference between the wheels. In this case, the fiber is the driving force.

3.3.1 Mathematics for Dynamic Model

The equations used in dynamic modeling were evaluated. It was assumed that the angular speed of the motor-driven shafts remains constant regardless of fiber tension. The eccentricity of the rotating

parts then creates a variation in tension because the circumferential speed varies. The circumferential speed of the idle wheels varies with the tension because the tension is comparable to the speed difference between the wheels. In this case, the fiber is the driving force.

Using the symbols in Appendix 3 and Equation 37 the winding tension is

$$F1 = \frac{M_1 - J_1 q\alpha_1 - M_{W1} - K_{bl1} - K_{b1}\omega_1^{2/3} - K_{a1}\omega_1^2 + \sqrt{x_{c1}^2 + y_{c1}^2}\, m_{t1} g \sin(\omega_1 t + \phi_1)}{r_1}$$

Equation 56

From Equation 26 follows similarly for tension between dancer roller and guide roller

$$F2 = \frac{-J_2 q\alpha_2 - K_{bl2} - K_{b2}\omega_2^{2/3} - K_{a2}\omega_2^2 + \sqrt{x_{c2}^2 + y_{c2}^2}\, m_{t2} g \sin(\omega_2 t + \phi_2)}{r_2} + F1$$

Equation 57

Tension between exit capstan and dancer roller from Equation 27

$$F3 = \frac{-J_3 q\alpha_3 - K_{bl3} - K_{b3}\omega_3^{2/3} - K_{a3}\omega_3^2 + \sqrt{x_{c3}^2 + y_{c3}^2}\, m_{t3} g \sin(\omega_3 t + \phi_3)}{r_3} + F2$$

Equation 58

Proof testing tension from Equation 36, when capstan wheel bearing friction and belt pulley bearing friction are combined

$$F4 = \frac{M_4 - J_4 q\alpha_4 - K_{bl4} - K_{b4}\omega_4^{2/3} - K_{a4}\omega_4^2 + \sqrt{x_{c4}^2 + y_{c4}^2}\, m_{t4} g \sin(\omega_4 t + \phi_4)}{r_4} + F3$$

Equation 59

Tension between turning wheel and entry capstan using the same Equation 36

$$F5 = \frac{M_5 - J_5 q\alpha_5 - K_{bl5} - K_{b5}\omega_5^{2/3} - K_{a5}\omega_5^2 + \sqrt{x_{c5}^2 + y_{c5}^2}\, m_{t5} g \sin(\omega_5 t + \phi_5)}{r_5} + F4$$

Equation 60

Finally the draw tension using again Equation 26 is

$$F6 = \frac{-J_6 q\alpha_6 - K_{bl6} - K_{b6}\omega_6^{2/3} - K_{a6}\omega_6^2 + \sqrt{x_{c6}^2 + y_{c6}^2}\, m_{t6} g \sin(\omega_6 t + \phi_6)}{r_6} + F5$$

Equation 61

Using the similar approach and the same symbols the following formulas for tensions from the coater to the take-up can be written.

F6 = Measured data from draw tower experiment

$$F5 = \frac{J_6 q\alpha_6 + K_{bl6} + K_{b6}\omega_6^{2/3} + K_{a6}\omega_6^2 + \sqrt{x_{c6}^2 + y_{c6}^2}\, m_{t6} g \sin(\omega_6 t + \phi_6)}{r_6} + F6$$

Equation 62

$$F4 = \frac{-M_5 + J_5 q\alpha_5 + K_{bl5} + K_{b5}\omega_5^{2/3} + K_{a5}\omega_5^2 + \sqrt{x_{c5}^2 + y_{c5}^2}\, m_{t5} g \sin(\omega_5 t + \phi_5)}{r_5} + F5$$

Equation 63

$$F3 = \frac{-M_4 + J_4 q\alpha_4 + K_{bl4} + K_{b4}\omega_4^{2/3} + K_{a4}\omega_4^2 + \sqrt{x_{c4}^2 + y_{c4}^2}\, m_{t4} g \sin(\omega_4 t + \phi_4)}{r_4} + F4$$

Equation 64

$$F2 = \frac{J_3 q\alpha_3 + K_{bl3} + K_{b3}\omega_3^{2/3} + K_{a3}\omega_3^2 + \sqrt{x_{c3}^2 + y_{c3}^2}\, m_{t3} g \sin(\omega_3 t + \phi_3)}{r_3} + F3$$

Equation 65

$$F1 = \frac{J_2 q\alpha_2 + K_{bl2} + K_{b2}\omega_2^{2/3} + K_{a2}\omega_2^2 + \sqrt{x_{c2}^2 + y_{c2}^2}\, m_{t2} g \sin(\omega_2 t + \phi_2)}{r_2} + F2$$

Equation 66

For calculating the speeds the following equations in the simulation were used. The first is the angular speed for the take-up. To simplify the simulation it is assumed the angular speed to be constant at given moment

$$\omega_1 = \omega_5 \frac{r_5}{r_1}\left(\frac{F_{wset}}{EA} + 1\right) \qquad \textit{Equation 67}$$

The angular speed for the guide wheel is given as

$$\omega_2 = \omega_1 \frac{r_1}{r_2\left(\frac{F1}{EA} + 1\right)} \qquad \textit{Equation 68}$$

The angular speed of dancer wheel is given similarly

$$\omega_3 = \omega_2 \frac{r_2}{r_3\left(\frac{F2}{EA} + 1\right)} \qquad \textit{Equation 69}$$

The exit capstan angular speed is also assumed to be constant an depending on the proof tension and constant angular speed of entry capstan

$$\omega_4 = \omega_5 \frac{r_5}{r_4}\left(\frac{F_{pset}}{EA}+1\right) \qquad \textit{Equation 70}$$

For entry capstan, which is also the line speed capstan, getting the speed command from the main line control, angular speed is given as

$$\omega_5 = \frac{v_{set}}{r_5} \qquad \textit{Equation 71}$$

The angular speed of the turning wheel varies similarly to the guide wheel and dancer wheel.

$$\omega_6 = \omega_5 \frac{r_5}{r_6\left(\frac{F5}{EA_c}+1\right)} \qquad \textit{Equation 72}$$

Using the above equations the tensions are calculated once in each direction. The tensions are then combined by using superposition principle. The stable conditions where the vibration has had time to travel through the line in both directions are focused on. This is done by neglecting the first 0.5 s of the output of the simulation.

3.3.2 Fourier Transform

The time domain signals can be presented as function of the vibration frequency by using Fourier Transform. An efficient and fast way to calculate is Fast Fourier Transform (FFT). This analysis tool solves problems in linear systems and analyzes periodic data by using the Fast Fourier Transform (FFT) method to transform data. When the number of input range values is an even power of 2 the FFT is considerably faster. There are several different definitions for discrete Fourier Transforms. More information about Fourier Transforms is available e.g. in references (Bracewell 1999) and (Conte & de Boor 1988).

The existing Fourier analysis tool in the software package was used. The calculation based on the FFT described above. Table 1 shows the input and output data format. The frequency range was selected to be 0 – 1,000 Hz and the number of samples n_f was selected to be 2^{10} = 1,024. The time domain input data was the tension data combined by superposition principle calculated earlier. The data could be the real measurement data as well. The FFT gives results, which all corresponds to different frequency. The result is same size complex vector as the time domain source data. To be able to calculate the real frequency f_k one must know the original sampling frequency f_s of the time domain data.

Table 1. Input and output data of Fast Fourier Transform

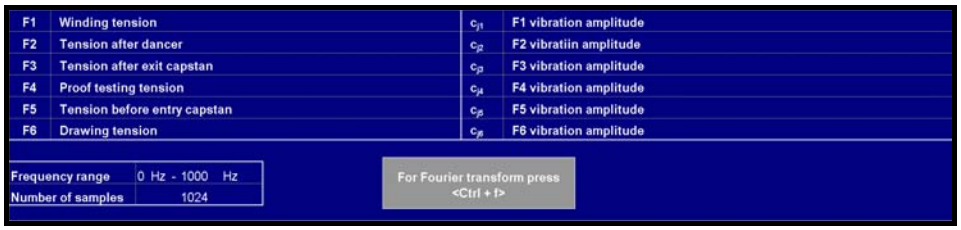

The frequency is calculated form the equation

$$f_k = \frac{k_f}{n_f} f_s \qquad \textit{Equation 73}$$

3.3.3 Fiber Stress Analysis

Ultimately the interest is in the actual stress, which is applied to the fiber. Knowing the tensile tension is not enough. The fiber needs to go around several pulleys and other machine elements while it is processed. The fiber bending is creating additional stress to the fiber, which is essential to know. The bending is not obviously applying the stress evenly, but the outermost part of the surface has the maximum stress. Additionally the coating is carrying a part of the tensile load. When all these 3 phenomena are taken in to account, the maximum stress through the entire path can be accurately calculated.

The mechanical behavior of optical fiber subjected to bending is the first object to study. The relation between stress and strain in silica is already known in the tensile region. However, the fiber is subjected to bending several times during manufacturing and once inside a cable. This can occur any time when the fiber passes an idle wheel or through a capstan. The fiber is naturally also bent when wound on a reel. When fiber is bent, a large part of it is subjected to compressive stress. In these cases it is also necessary to know the calculated stresses on the fiber surface due to non-linear elastic effects.

The stress-strain relation of optical fibers is examined in several references. It has been stated that the stress is non-linearly related to the strain in an optical fiber. The formula is given as

$$\sigma = E\varepsilon\left(1 + \frac{1}{2}\alpha_n\varepsilon\right) \qquad \textit{Equation 74}$$

where ε is the relative strain of the fiber and α_n is a non-linearity constant.

In the literature, values for Young's modulus E = 72 GPa and non-linearity constant α_n = 6 can be found. These values are valid for most commonly used optical fibers. These values are confirmed in later experiments, for example in (Griffioen 1994) E = 73 ± 2 GPa

and $\alpha_n = 5{,}5 \pm 1$. It must be mentioned that these values do not take the coating in to a consideration.

The above illustrated stress-strain relationship leads to the stresses in a bent fiber. When the fiber is bent, an additional uniform strain ε_b will be present. This strain profile can be written as $\varepsilon(\xi)=\xi/R+\varepsilon_b$ in which R is the bending radius of fiber and ξ is the distance from the center point of the fiber, see Figure 33. Since $\int\sigma(\xi)dA = 0$, and $A = \pi r_f^2$, on the basis of Equation 74

$$\varepsilon_b = \frac{1}{\alpha_n}\left[\sqrt{1-\frac{\alpha_n^2}{4}\left(\frac{r_f}{R}\right)^2}-1\right] \qquad \textit{Equation 75}$$

where r_f is the radius of glass fiber and R is the bending radius of the fiber.

The strain ε_b is always less than zero, which means that it is compressive. When the Equation 74 is used again and the higher-order terms are neglected, it emerges that

$$\sigma(\xi) = E\left[\frac{\xi}{R}+\frac{1}{2}\alpha_n\left(\frac{\xi}{R}\right)^2-\frac{1}{8}\alpha_n\left(\frac{r_f}{R}\right)^2\right] \qquad \textit{Equation 76}$$

where ξ is the distance from the center point of the fiber.

The stress is not uniformly distributed over the fiber surface and reaches its maximum when $\xi = r_f$. The above equations help to calculate the applied stress. The maximum allowed stress depends on the proof test tension and the application where fiber is used. Normally the maximum allowed stress is from 1/6 to 1/3 of the proof test tension (Glaesemann & Castilone 2002), (Castilone 2001), (Glaesemann 1997).

The coating carries a portion of the tensile load. The coating does not affect the bending stress directly. Indirectly the coating increases the bending radius, which has a small effect on the stress. The fraction the coating carries about the tensile load is determined by (IEC 2001), (TIA/EIA 1999)

$$F\% = \frac{\left[E_o\left(D_o^2-D_i^2\right)+E_i\left(D_i^2-D_g^2\right)\right]}{\left[E_o\left(D_o^2-D_i^2\right)+E_i\left(D_i^2-D_g^2\right)\right]+E_gD_g^2} \qquad \text{Equation 77}$$

Normally in proof testing the proof tension is corrected to be higher to compensate the load sharing by coating.

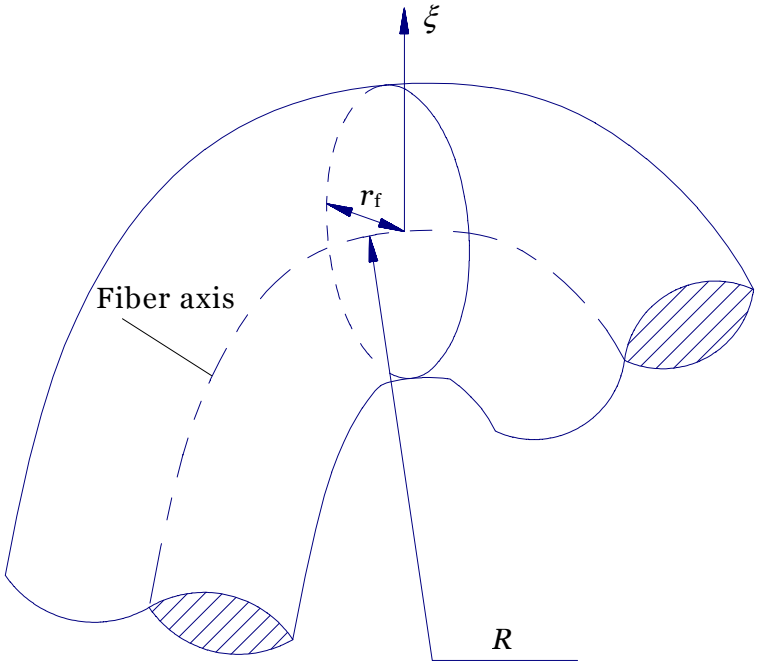

Figure 33. Bent fiber

For simulation purposes the Equation 77 is used to calculate the coating share, which is then used to calculate the over all Young's modulus for coated fiber. This corrected Young's modulus is then used in tension simulation. The Table 2 includes the material information used when calculating coating share. The corrected Young's modulus is then 73.2 GPa.

Table 2. Young's modulus of coated fiber

Parameters				
Young's modulus of the uncoated fiber	E_g	72,000	MPa	(Bouten 1987), (Griffoen 1994)
Young's modulus of the outer primary coating	E_o	750	MPa	(DSM 2001b)
Young's modulus of the inner primary coating	E_i	1.5	MPa	(DSM 2001a)
Nominal diameter of the uncoated fiber	D_g	0.125	mm	(Kouzmina et. Al. 2003), (Corning 2004)
Nominal diameter of the outer primary coating	D_o	0.245	mm	(Kouzmina et. Al. 2003), (Corning 2004)
Nominal diameter of the inner primary coating	D_i	0.190	mm	(Kouzmina et. Al. 2003)
Young's modulus of a coated fiber				
Load sharing by coating	F%	1.57%		
Young's modulus of a coated fiber	E	73.2	GPa	

The Young's modulus in the table was calculated as follows. Hooke's law gives

$$F = \left(\varepsilon E_i A_i + \varepsilon E_o A_o\right) + \varepsilon E_g A \qquad \textit{Equation 78}$$

Then the coating share calculated earlier is marked

$$\varepsilon E_i A_i + \varepsilon E_o A_o = F\% \cdot F \qquad \textit{Equation 79}$$

This leads to

$$F = \frac{\varepsilon E_g A}{1 - F\%} \Leftrightarrow \frac{E_g}{1 - F\%} = F\varepsilon A \qquad \textit{Equation 80}$$

By using the values given in Table 2 it is marked

$$E = \frac{E_g}{1 - F\%} = \frac{72 \cdot GPa}{1 - 0.0157} = 73.2 \cdot GPa \qquad \textit{Equation 81}$$

4 EXPERIMENTS

4.1 Tension Behavior Tests

Now the tension behavior is determined in theory. It is important to make necessary experiments to verify the theory and also to get a good overall view of the state of the art of the fiber optic machinery. This section discusses first about draw tension experiment. The second part is the comparison of the conventional proof tension measurement and the new method needed for the combined processes. After this the effect of the different process elements; turning wheel, capstan and dancer movement are evaluated.

4.1.1 Draw Tension Measurement

This study did not focus on the draw process as much as the combined processes. It is, however, important to know the draw tension, since in case of combined process it may have an impact to the proof testing. This data was then used as input data for the simulation model.

The experiment was run in a fiber draw laboratory, with a full size production draw tower. The tower height was 25 m and it had all the latest instrumentation commonly known in fiber industry. In this tower it is possible to measure the tension before coater from the bare fiber or just before draw capstan with a load cell. Since the region above the coater was not in the scope of the study, only the data measured from the draw capstan was used.

The tension was measured from trials, which were run to optimise the behavior of the new coating die design. The tension was recorded with draw tower's standard data logging system integrated to the line control system. Figure 34 shows the capstan and the load cell used to measure the tension. The actual measurements were carried out at speeds between 600 m/min and 1,500 m/min.

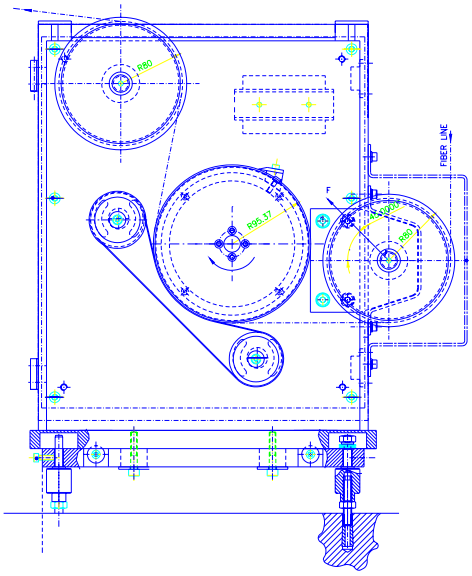

Figure 34. Draw capstan with tension measurement

4.1.2 Proof Tension: Conventional Method vs. New Method

The combined continuous draw and proof testing process requires a new approach to the proof tension measurement. Traditionally a load cell located in a turning pulley has measured the tension of fiber. This is a reliable and simple way to measure the tension and should be used whenever possible. In case of on-line proof testing this is not practically possible, since one of the requirements is to be able to thread the fiber through the line at full line speed in fiber break automatically. To overcome this problem a new approach to tension measurement was developed. This new method allows the fiber path to be straight between capstans, which makes the automatic threading and therefore automatic break recovery possible.

It is essential that the proof tension variation is small enough to be able to control the tension reliably. The practical maximum variation for existing off-line proof testers is ±5% of the proof tension. With proper design this is possible to achieve in production conditions at commonly used process speeds 1,200 – 2,100 m/min and proof tension range 5 – 20 N and test lengths 1.5 m – 12 m.

The test runs were run with the new method using various test lengths, proof tensions and speeds. The test machine was a commercial proof testing machine type OFC 35. These results were compared to the conventional turning pulley measurement.

For testing the new tension measurement principle two prototypes were built. The first was based on the linear bearing assembly and the second was a pivoting assembly where normal rotary bearings were used.

Figure 35. High-speed recorder and load cell

The first test was performed to confirm that it is possible to measure the force on the capstan caused by the fiber. This signal is then used as feedback for controlling proof tension. The first trial was arranged to evaluate the measurement signal quality. The purpose was to show that the signal is good enough for feedback purposes. In the first trial the capstan was run at different speeds without changing the proof tension. The test length was varied and two different spring alternatives were tested in capstan assembly. The results were recorded with a high-speed recorder (Figure 35). The test conditions are summarized in Table 3.

Table 3. Test conditions for measurement method trial

Proof tension [N]	8			
Test length [m]	2.5	9.5	No fiber	
Springs	2	4		
Line speed [m/min]	500	1000	1500	2100

The test rig for the second part of linear bearing test is shown in Figure 36 and a closer look in to linear bearing assembly in Figure 37. Load cell 1 measured the force on the capstan, which was installed on linear bearings. The fiber tension was simultaneously measured by load cell 2, which was mounted inside a wheel. The purpose was to demonstrate that the actual fiber tension was still within the specifications stipulated in the standards even though the capstan was installed on linear bearings. The trials were run at speeds 1,000 m/min and 1,500 m/min. See Table 4 for complete conditions.

Table 4. Test conditions for linear bearing effect measurement

Proof Tension [N]	5	8	10
Load Cell	1 (capstan)	2 (wheel)	
Speed [m/min]	1000	1500	

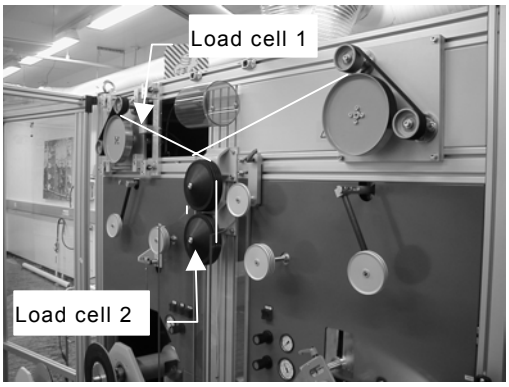

Figure 36. Test setup for comparison

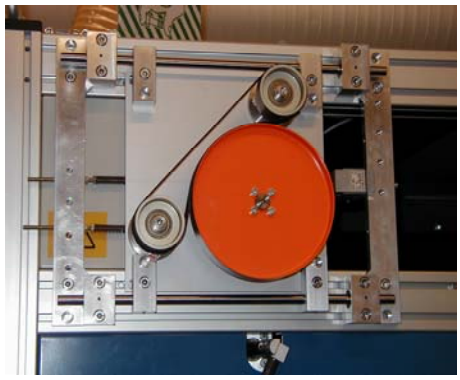

Figure 37. Linear bearing system

The next part of testing focused on pivoting design. This design was tested more thoroughly, since it was recognized to be the potential final design. The prototype design was done extra carefully to minimize all the errors and wrong conclusions. The design minimizes the capstan vibrations affecting the sensor. The following are the considerations for causes of the vibration; eccentricity of the capstan wheel and the mass center, belt non-homogeneity, servomotor speed variation and tension disturbances outside.

Based on earlier experience and information from the suppliers it is stated that the biggest contributor for vibrations is the eccentricity of the mass center and geometrical eccentricity. The load of the belts is small, since their role is only to keep the fiber tight. Therefore the belts are not a great source of vibration. Servomotors are nowadays very accurate mechanically and electrically and do not cause excess vibration when the parameters are right. The fiber vibration coming outside may cause vibration, but only significant source is take-up spool. If the winding control is good also this can be neglected. In reference (Lipponen 2001) the mathematics behind the proto design is explained in details.

The Figure 38 illustrates the rig for this experiment. The capstan is hanging with a fork. It can move in the direction of the load, because of the bearings in the fixing. The bearings are commercial standard components. The fiber causes a force to the capstan, which is guided to the load cell via a push bar.

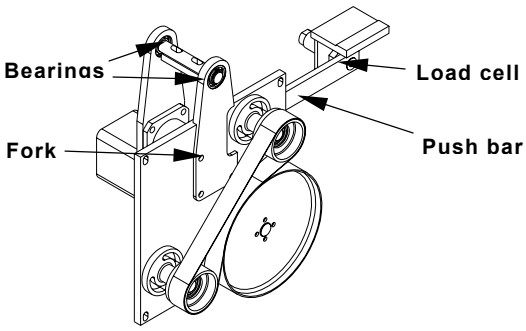

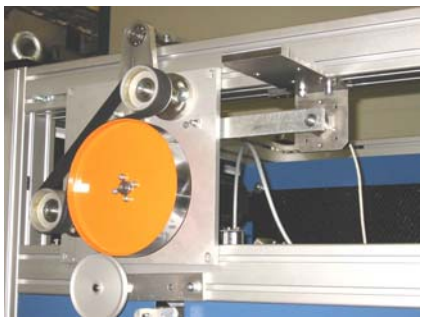

Figure 38. Pivoting capstan measurement system

The same proof tester type OFC 35 was used again. The design allows using rubber dampers or bearing between load cell and push bar. The setup is similar to the first one, where a second load cell was used as reference. The test started with long test length moving to the shorter lengths when the experiment proceeded. These trials were run at speeds 500 – 2,500 m/min. See Table 5 for rest of the test conditions.

Table 5. Test conditions for pivoting capstan measurement

Load Cell	1 (capstan)	2 (wheel)			
Speed [m/min]	500	1000	1500	2000	2500
Proof tension [N]	10	15			
Test length	9.5 m	1 m			

4.1.3 Turning Wheel Effect on Tension

A series of trials were conducted to evaluate the coefficients for bearing friction and air resistance for a fiber turning wheel. Typical fiber wheels with two low friction noise tested bearings were used in trials. The test machine was at this time a coloring system type OFC 53 in Figure 39.

The machine was run in rewinding mode thus simulating the normal proof testing process. The unwinding tension was measured after the payoff dancer and winding tension between take-up and the take-up dancer. The tension set on the payoff at 0-speed was 0.8 N. On take-up side 0.4 N and 0.5 N set tensions were used. The tension was then recorded at different speeds up to 3,000 m/min. The tension increase recorded was then a sum of all 5 wheels used in the dancer setup. The test conditions are summarized in Table 6.

The tensions were recorded by the machine's own PLC and displayed on the screen. The results are filtered average tensions, since the actual variation was not a special interest in this trial. As a result of the trials the load friction torque and bearing speed factor for the bearings were evaluated and also the air resistance factor, which were then used in simulation model.

Table 6. Test conditions for turning wheel effect

Speed [m/min]	500	1000	1500	2000	2500	3000
Winding Tension [N]	0.4	0.5				
Unwinding Tension [N]	0.8					

Figure 39. Coloring system used for turning wheel trial

4.1.4 Capstan Effect on Tension

Similarly to the turning wheel tests the bearing parameters and air friction characteristics were tested for the capstan. In these trials the OFC 35 proof testing machine was used again, since the capstan design was right. The entire capstan was handled as one unit, which have a certain load friction torque and bearing speed factor and also air friction factor. The individual belt pulleys, capstan wheel or the belt were not evaluated separately.

It should be noted that the setup does not represent fully the on-line process when the break recovery is realized by a combination of belts and tubes as described later. In reality in this case the effect of the belt is greater, since two long belts instead of one short are used. The results reported later are, however, useful for simulation purposes and gave good guidance for the final capstan design.

The OFC 35 has two identical capstans, which both were tested separately. The final results are the averages between these two capstans. The machine was adjusted to run faster than normal and speeds up to 3,200 m/min could be achieved. The capstans were rotated without fiber and the motor torque was measured at different speeds. The torque was measured directly from the servo drive's torque measurement output. The output gave the torque as percentage of the nominal torque, which was 2.45 N with this particular drive. Figure 40 shows the servo drive and Figure 41 presents the test machine. The test conditions are summarized in Table 7.

Figure 40. Servo drive with torque output Figure 41. Test machine

Table 7. Test conditions for capstan effect trial

Nominal torque	100% = 2.45 Nm														
Speed [m/min]	1	5	50	150	300	600	900	1200	1500	1800	2100	2400	2700	3000	3200
Capstan	1 (Entry)	2 (Exit)													

4.1.5 Take-up Effect on Tension

The effect of the take-up and the spool was also tested. The bearing friction characteristics and air resistance behavior were as special interest. To simplify the testing and the simulation model, it was assumed that the air resistance of the take-up parts is negligible comparing to the spool. This is probably true, since all the rotating parts of the take-up have very smooth surface and the area against the rotating direction is minimal. The spool on the other hand has reinforcements in flanges, which are at least partly against the rotating direction creating air resistance.

Table 8. Test conditions for take-up effect test

Nominal Torque	100% = 2.45 Nm									
Nominal Speed	32767 bit = 6000 rpm									
Spool Barrel Diameter [m]	0.18									
Spool Type	Sonoco-Crellin 50 km			No spool						
Speed command [Bit]	10	100	500	1000	5000	10000	15000	20000	25000	30000
Speed command [rpm]	1.8	18.3	91.6	183.1	915.6	1831.1	2746.7	3662.2	4577.8	5493.3
Calculated Line Speed [m/min]	1.0	10.4	51.8	103.5	517.7	1035.5	1553.2	2070.9	2588.7	3106.4

The test was done in similar way than with the capstans. The take-up was run with and without the spool and the motor torque at different speeds up to 3,100 m/min was recorded. The spool used was a widely used 50 km spool manufactured by Sonoco-Crellin and can be seen in Figure 42 as well as the test take-up. Unlike in the picture the spool was empty during the runs. The load friction torque and bearing speed factor for the bearings and also the air resistance factor were then evaluated. See Table 8 for test conditions.

Figure 42. Take-up tension effect trial setup

4.1.6 Dancer Movement in Turning Point

The traversing turning point is the most difficult part of fiber winding. If the turning point is not exactly correct a fiber build-up (bump) or roll off (gap) will occur, which gets worse when the spool fills up. The theoretical approach to the behavior near the flange was explained earlier. To test the theory in practice, the same machine OFC 35 than in the capstan and take-up tests was used.

The spool was modified to deliberately create a build-up on the flange. The bump was built to the spool barrel so that both the x and y dimensions were 5 mm during the turning. The bump was run over at different speeds up to 1,000 m/min to the flange and back. The bump caused a movement to the dancer arm, which created a disturbance to the tension. The tension was recorded simultaneously by an oscilloscope. In the results section the measured and the modeled tensions are compared.

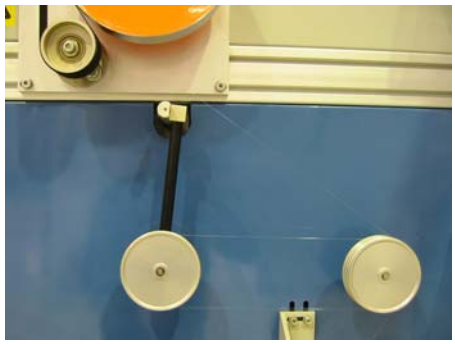

Figure 43. Modified spool *Figure 44. Test Dancer with two loops*

Figure 42 shows the take-up and Figure 43 and Figure 44 the modified spool and the test dancer. Table 9 shows the test conditions for the dancer behavior trial.

Table 9. Test conditions for dancer behavior trial

Spool Type	Modified Sonoco-Crellin 50 km		
Dancer arm length [m]	0.2		
Dancer wheel diameter [m]	0.09		
Number of loops	2		
Speed [m/min]	100	500	1000

4.2 Break Recovery System Tests

4.2.1 Two Different Approaches

Two different methods to survive proof testing break are introduced. The first method uses tubes to guide the fiber end. The second is a combination of tubes and belt conveying system. Either systems form a closed channel described earlier and in details in reference (Turunen & Mäkelä 2002a).

The tube system consists of closed tube between capstans. There are not any additional means to convey the fiber, but the first capstan keeps pushing the fiber in to the tube, where it goes forward with the help of its own inertia. Additionally it is possible to blow air inside the tube and also ionize the tube, air and the fiber. A similar arrangement is then needed between second and third capstans also.

The belt system has also tube like elements, but additionally there is a pair of belts inside the tubes moving to the same direction and at the same speed as fiber. This arrangement uses belts to convey air in the tube. The static is also possibly helping in this case, if fiber sticks on to the belts.

4.2.2 Testing of Tube System

When proof testing fiber, there are occasional breaks depending on the quality of the drawing process. These occur normally after a few tens or hundreds kilometers, depending on the preform manufacturing and fiber draw quality. In a conventional proof tester fiber break causes a stop, and the operator has to thread the fiber again to the machine to continue the proof test. This interruption is not acceptable with on-line proof testing because ramping down the drawing process is a slow process.

Public information of conveying fiber inside tube couldn't be found, but there are patents concerning the so-called air-blown fiber, e.g. Reeve and Cassidy (1987), Wells et. al. (2000) and Cain et. al. (1991). This is not actually a fiber but a fiber bundle with special coating, which helps the transportation of the bundle by air. The guiding duct can be made of an antistatic material. Some antistatic agents are also added to the airflow to minimize static electricity. The installation speed of air-blown fiber is remarkably lower than needed for on-line proof testing.

The tests focused on handling fiber breaks in the proof test region (test arrangement shown in Figure 45). Artificially weakened fiber was used in trials. This was done by cutting through the coating of the fiber on the payoff reel. This weakened the fiber enough to cause fiber breaks at proof testing tension. A guiding tube was located between the entry capstan and the exit capstan, and the proof tension was measured from the moving capstan with a load cell tested earlier.

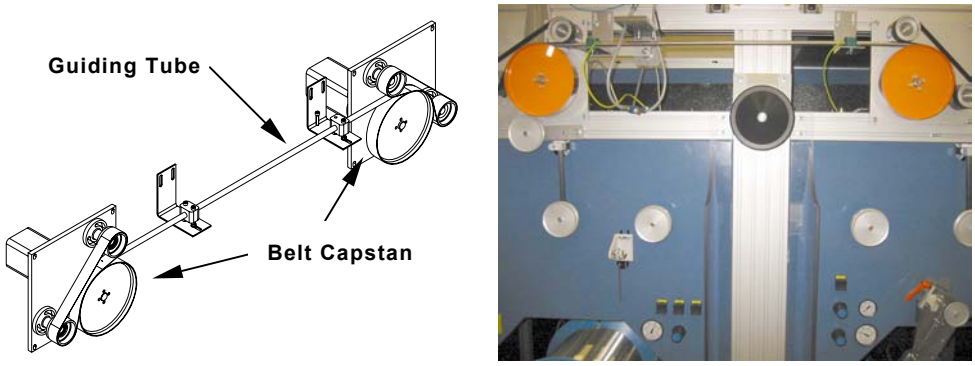

Figure 45. Test setup for tube system

In the first test series five different pipe materials were tested; acrylic, aluminum, inside polished steel, vinyl with carbon fiber and PTFE ("Teflon"). The line speed was set to values from 250 m/min to 1,750 m/min, and the break recovery success was calculated from ten breaks per measured speed for each tube material. The total amount of the breaks was then 350. Before the tests even wider range of tests were run to debug the design errors. Test conditions are in Table 10.

Table 10. Test conditions for tube material test

Test period	October 2001 - November 2001						
Number of breaks	5 (materials) x 7 (speeds) x 10 = 350						
Tube material	Acrylic	Steel	PTFE	Carbon fiber	Aluminum		
Speed [m/min]	250	500	750	1000	1250	1500	1750

The second test series focused on removing the negative effect of static electricity on conveying the fiber in the tube. Commercial static eliminators were used in the tests and also specially designed 2-layer tube. The tests were run at four different conditions according to Table 11.

Table 11. Test conditions for static elimination trial

Test period	November 2001 - December 2001					
Number of breaks	4 (static control) x 6 (speeds) x 10 = 240					
Static control	No control	Static bars	Bars + blower	Bars + blower +2 layer tube		
Speed [m/min]	250	500	750	1000	1250	1500

In this trial series the first setup consisted of a Teflon tube (diameter 8x14 mm and length 1 m). The proof tension in each run was 15 N to get clean breaks. No static control was used this time. The second setup was run otherwise in same conditions but 3 static bars; one on payoff, one on belt and one on entry capstan wheel were added. For the third setup an ionizing blower near entry capstan was added. The last setup was run including static bars and blower, but the tube was changed to two-layer-design, where ionized air at 0.8 bar was blown between layers. The inner tube was the same Teflon tube, but it had 1 mm holes to let the air enter. The outer tube was clear acrylic.

Total number of runs was 238 instead of planned 240, since only 8 breaks with first setup could be run.

After finding the most promising tube configuration with proper static elimination that structure was tested in more details. The best system occurred to be the 2-layer tube as explained in results section.

Now more tests were run also at higher speeds to see if the speed was a limiting or helping factor. It was decided not to change the construction, but only the pressure inside the 2-layer tube. The speeds between 250 m/min and 2,500 m/min and tube pressure 0.1 bar or 0.8 bar were used. See summary in Table 12.

Table 12. Test conditions for 2 layer tube

Test period	March 2002 - April 2002									
Number of breaks	277 (total)									
Pressure (bar)	0.1	0.8								
Speed [m/min]	250	500	750	1000	1250	1500	1750	2000	2250	2500

4.2.3 Testing of Belt System

After completing the trials with tubes, it was decided to investigate further the second alternative. The idea was to add belts to the system to help the conveying of the fiber and therefore increase the success rate. First a prototype for testing was designed and built. The prototype was designed without the tube-like channel. This was done to simplify and quicken the testing. It was believed that by introducing only the belts is the worst case, which only improves when closed channel is done. The Figure 46 shows the prototype, where two belts form a channel where the fiber moves. The belts move at least the same speed as the fiber. Both the belts are mechanically attached only to the exit capstan, which allows using of the same tension measurement system than earlier.

The testing was done in similar manner with the tube trials. Artificially weakened fiber was used and the proof testing was elevated to 15 N. The speed range was the same as earlier 250 – 2,500 m/min and 10 breaks at each speed were planned. The trial was repeated several times and number of recorded fiber breaks was 285. See test conditions in Table 13. The result of the tests can be seen in results section.

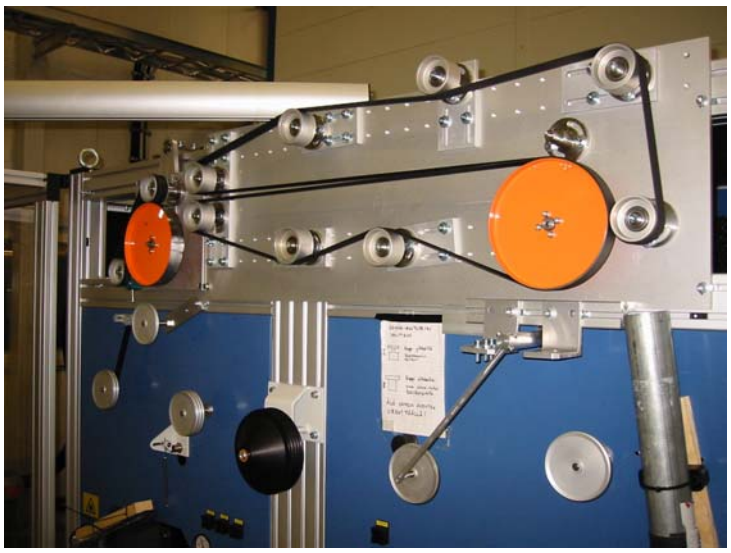

Figure 46. Belt system test setup

Table 13. Test conditions for belt system

Test period	April 2002 - July 2002									
Number of breaks	285 (total)									
Speed [m/min]	250	500	750	1000	1250	1500	1750	2000	2250	2500

4.3 Winding Tests

4.3.1 Turning Point Control Optimization

Winding package quality is essential in proof testing machines and even more challenging at future's high speeds with online proof testing machines. The take-up spool is always a delivery spool, which must have visually good winding and it must pass optical attenuation measurements. The measurement is done by an OTDR and the total attenuation increase must be under certain limit typically 0.01 dB/km. Additionally the attenuation discontinuity points, steps, are not allowed. Typical maximum allowed step size is between 0.02 and 0.05 dB.

The turning point control tests were carried out with special fiber having coating material with high friction coefficient against fiber spool material. The trials begun first in laboratory conditions, where the aim was to rewind same fibers several times. What was found during the trials was that the surface properties of the fiber changed, when it was rewound repeatedly. The fiber, which first was difficult changed to easy while the coating properties changed. Therefore the tests were continued at fiber factory where it was possible to proof test high amount of fiber in production conditions. The final tests were then carried out at customer's fiber production facility with seven OFC 35 proof testers.

The first trial was run to evaluate the failure percentage with the existing system, where the gap was filled with over-traversing explained earlier. If a spool had one or more steps or too high attenuation, it was considered to be one failure. The data was recorded by customer's process tracking system during 7 months long test period between January 2001 and August 2001. The exact number of the runs is not public information, but it is estimated based on the information about the production parameters. The Appendix 5 summarizes the production parameters and gives an estimation of the samples as result.

As a result of the first trials and to improve the winding performance in turning point the software algorithm was developed further. The main improvements were as follows

- The traversing movement is not allowed to go over the calculated flange position, but fill the gap by stopping the traversing movement for a controlled time at flange.

- If the gap filling has been going on for long, the pitch will be changed smaller in the turning point window. The filling will be faster in this way.

- To widen the traverse, if dancer has detected that a certain number turning points have been OK, the gap filling function will be started, although the gap has not detected. This way the gap was anticipated and prevented to form too large.

Pre-tests were run in July 2002 at laboratory conditions simulating the conditions used in the trials with original algorithm. Only 151 spools were run in this pre-test after which the testing was continued at the same customer location as earlier.

The testing of these new modifications started in September 2002 and lasted totally two months in the same conditions as the first trials. The fiber type was the same as used before. The production data is estimated in Appendix 6.

4.3.2 Whipping Protection

As mentioned in earlier chapters the take-up needs to be equipped with means to prevent whipping. There are few different kinds of whipping phenomena that can damage the fiber package either during winding or after transfer. These were already explained more detailed in the theory section.

The following explains in details the whipping guard trials, trials to investigate the in-side-end whipping and testing arrangements for invented auxiliary blade trials.

Whipping Guard Trials

The first test series was focused on the proper whipping guard design. The starting point was the existing design used at lower speed in off-line proof testing machine. It was known already in the beginning that the existing design used for the proof testers was not suitable for new combined process, because of the higher speed and the proximity of the cut point. The design used for the existing dual take-ups, however, had been working reliably with larger spools, when the fiber has been cut near the spool. The Figure 47 shows a typical whipping damage, when the whipping guard does not work properly.

Figure 47. Whipping damage

A prototype (called “spiral”), suitable for 25 km or 50 km standard delivery spools, was manufactured and it was tested in OFC 35 Proof Testing machine. The test procedure remained the same through out all whipping guard trials.

First almost the entire fiber length from payoff spool was run to the take-up spool in proof testing mode starting at 12 N proof tension. Just before the fiber ended, an artificial fiber break was made and it was observed visually, if the fiber end went inside the guard and remained in until the spool was stopped. Then the same spool was assembled back to the payoff and run again, but at 0.5 N lower proof test tension than the previous run. If the fiber broke at lower tension, it proved that the fiber was damaged due to the whipping in previous run. The same fiber was used until 5.0 N proof testing tension was achieved, after which the test continued with new fiber at 12 N again. The trials were run at speed 2,100 m/min. In Appendix 7 the spiral design is illustrated. The spiral design was also slightly modified during testing and the final design was tested in similar manner.

As the trials continued it came clear that the spiral design did not have optimal performance. A new prototype (called “round”) was designed and manufactured based on the “spiral” trial results. Two test series were run with “round” design as well; one with the prototype and one with improved design. There are more results regarding whipping protection in transfer reliability section, but they refer to the larger diameter guard. In Appendix 7 the “round” design is seen. The test conditions are summarized in Table 14.

Table 14. Test conditions for whipping guard trials.

Test Period	April 2002 - June 2002			
Whipping Guards	Spiral: Proto	Spiral: Improved	Round: Proto	Round: Improved
Proof Tension [N]	0.5 - 12.0 stepping down in 0.5 increments			
Speed [m/min]	2100			

Trials to Investigate Inside-end Whipping

The reason for these trials was information collected from several customers, which indicated that there were occasionally inside-end whippings during the run with existing gripping and cutting design of the dual take-up. These whippings occurred typically after several tens of kilometers were run after the transfer. Up to this point the winding is going well in normal manner. The whipping begun outside the spool on the scrap flange, but if it continued the fiber end eventually hit the fiber on spool and the result was severe whipping and multiple fiber ends. The difficult part here was that there seemed to be differences between machine individuals.

At least three possible causes for this phenomenon could be thought. First; improper cutting during change-over, second; failed gripping during change-over and third; fiber breaks in spool slot area.

a. Improper cutting during change-over. The theory is that the blade does not cut the fiber fast enough, but the fiber cuts partly by pulling. This leaves longer end than normal (normal is about 5 - 10 mm) on blade side. This end then whips in every round against blade support and hits back to scrap flange causing eventually fiber to break near gripping flange. When fiber is broken, it gets loose and starts to whip heavily hitting finally on spool side.

b. Failed gripping during change-over. If the gripping is only half successful the fiber may slip from between the gripping flanges during winding. Then the fiber starts to whip as described above. After stopping the machine there is no fiber between gripping flanges.

c. Fiber breaks in spool slot area. Now gripping and cutting are successful and it is managed to move from scrap flange on to spool through the slot on the flange. The fiber is tight when going through slot. Then 50 – 60 km or even more are wound at typical winding tension 0.5 to 0.7 N. The pressure increases in the fiber package and it starts to push the fiber in the slot against the slot edge. Finally the fiber breaks and starts to whip. In this case a piece of fiber should be found between gripping flanges.

The first priority was to find which of 3 alternatives was causing the problem, if any. The methods of the experiments were visual inspection and finally also high speed camera. When the spool stopped it was checked, if the fiber was still between gripping flanges. After this it was inspected, where the fiber broke; near by gripping area or near spool slot. Also the length of fiber end sticking out from between flanges was checked.

As it turned out the high-speed camera was needed to find the cause to this whipping phenomenon. The detailed results of high-speed camera investigation follow later in the results section. Four runs were photographed and recorded, where the in-side-end got loose causing whipping. The Table 15 shows test information.

Table 15. High-speed camera trials

	Run 1	Run 2	Run 3	Run 4
Number of frames	343	830	334	83
Film length [ms]	281.1	368.9	148.4	36.9
Frame interval [ms], Internal timing	0.8	0.4	0.4	0.4
Frame size	256x256	256x256	256x256	256x256
Take date	02-03-20	02-03-20	02-03-20	02-03-20
Take time	11:37:11	12:05:56	14:22:24	15:07:52
File name	KOE001.HSS	KOE002.HSS	KOE003.HSS	KOE004.HSS
Line speed [m/min]	2100	2100	2100	2100
Take-up	Right	Right	Right	Right

As a result of the tests a new construction was designed called auxiliary blade. The following trials were conducted to verify the functionality of this new construction and its efficiency in preventing inside-end whippings.

Testing arrangements for auxiliary blade trials

After confirming the cause of the in-side-end whipping a device called “auxiliary blade” was developed. The purpose of the tests was to compare the existing design without the auxiliary blade and this new design. OFC 35 proof testing machine was used as a payoff unit for dual take-up where this new blade was tested. Fiber was threaded between the machines so that the OFC 35 take-up unit was disabled and one guiding wheel was added. On the pay-off side a 50 km standard reel was used. No reels were used in dual take-up, because the only interesting thing was the behavior of the short fiber tail. In Figure 48 is the mechanism without the blade and Figure 49 with the blade.

Figure 48. Cutter without auxiliary blade

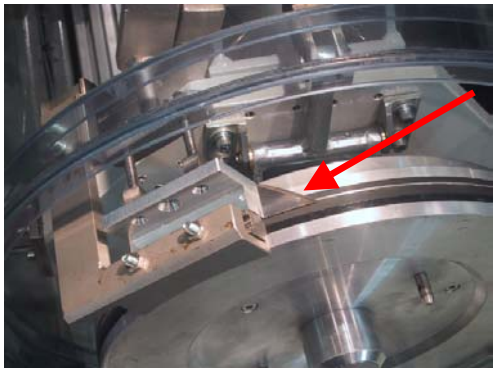

Figure 49. Cutter with auxiliary blade

The trial begun by threading the fiber at slow speed to the dual take-up. Then the take-up wound the fiber on the scrap flange still at low speed. Before the fiber moved out from the scrap flange the machine was stopped and the fiber was cut near the scrap flange edge and fixed by tape. Then the take-up was rotated 10 minutes or as long as the whipping started at speed corresponding to the line speed 2,100 m/min. In cases where noticeable whipping did not occur the fiber was visually inspected for whipping damages and also pulled manually to find possible weak spots. The trial was repeated 5 times without the blade after which 5 runs were run with the blade. The same was repeated until 20 trials had been run with and without the blade. See Table 16 summarizing the trials.

Table 16. Test conditions for auxiliary blade trial

Test Period	March 2002	
Cutter Design	Without Blade	With Blade
Run Time [min]	10	10
Line Speed [m/min]	2100	2100
Number of runs	20	20

4.3.3 Transfer Reliability

The transfer reliability was tested with a separate take-up module. The same principle only slightly modified is used in online proof testing needed for combined continuous process.

The following describes the test runs in laboratory conditions and wide test series run in production conditions with a customer. The first test period was realized at customer fiber plant, where normal production speed was 1,500 m/min. After this first test period the design was improved to achieve higher reliability. The new design was tested first in laboratory, after which the same was repeated at the same factory as before and additionally also in another fiber factory. All these tests were carried out at lower speeds than needed for online proof tester eventually. To simulate this requirement an additional test series was run at high speeds in laboratory conditions for future need.

Field tests with original design

The original gripping and cutting mechanism was first pre-tested in laboratory conditions, but soon after functionality testing the trials continued in production environment. The most important reason for that was the fiber consumption in this destructive test.

Figure 50. The original design

The mechanism was assembled in to 10 identical machines used in five dual draw towers. The mechanism is seen in Figure 50. The towers were operated in normal production and the transfer reliability was recorded five months from all 10 machines starting in October 2001. The production was not evenly distributed between the towers since they all were new towers and just ramping up in production. The production speed was 1,500 m/min and the operators were trained to use the machine and make observations and fill a transfer reliability log. To keep everything as simple as

possible the transfer failures and in-side end whipping failures were not separated, but the reliability percent describes the overall reliability.

This field test gave enough information to improve the design further. On the other hand new means to prevent in-side end whipping were developed and furthermore a new gripping and cutting construction was designed to solve all the issues rose during field test with the customer. The design and laboratory tests started parallel to the field tests, since already after one month good feedback was received from the customer.

Laboratory tests with improved design

OFC 35 proof testing machine was used as a pay off unit for dual take up, which had the transfer mechanism wanted to be tested. The setup was quite similar than in the trials with auxiliary blade. Fiber was threaded between the machines so that the take-up unit of the proof tester was disabled and one guiding wheel was added. The Figure 51 shows the setup, where the actual fiber line is highlighted.

Figure 51. Test setup for transfer reliability test

It had occurred earlier that at high speeds the fiber had tendency to get loose on the scrap flange during long runs. To overcome this problem a dual sided tape was added on top of the scrap flange. This was later in the final design replaced by a threaded flange. During these trials the gripping tape was originally changed only when necessary, but as the tests went on, changing period was once a day. When the tape was changed before problems occurred, it did not affect the result of the trial. The next Figure 52 shows how the double-sided tape was assembled to the gripping flange. If the tape is not changed as often as needed, the possibility for in-side end whipping will increase.

All the tests were run without the foams on the reels, see Figure 53. Running at high rotating speed with foams will cause problems, because foams usually are not glued all the way to the spool to allow easy replacement. Maximum safe speed running with existing foam was approx. 1,500 m/min, but with proper adhesives higher speeds

are achievable. Even 2,500 m/min was demonstrated in test runs later, but these trials are not described more detailed. The main parts of the improved gripping and cutting mechanism are shown in Figure 54.

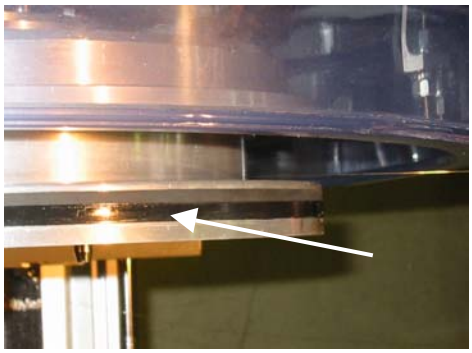

Figure 52. Dual sided tape

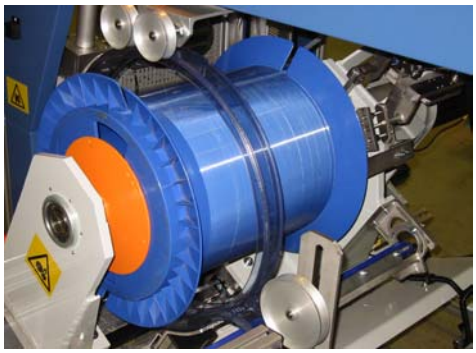

Figure 53. Test spool without foam

Alignment of the cutting knives and gripping flange were checked at least twice a day or more often, if there were problems. The machine was cleaned once a day from fiber debris and the free movement of the clamping fork was checked after every run. This was done because in the beginning of the test period there was a problem with left side fork. It caused whipping due to failed gripping. The first end of the fiber got out from the clamping area during the run and started whipping. The problem was solved by modifying the fork. This fork transfers the movement of the cylinder to the moving gripping flange.

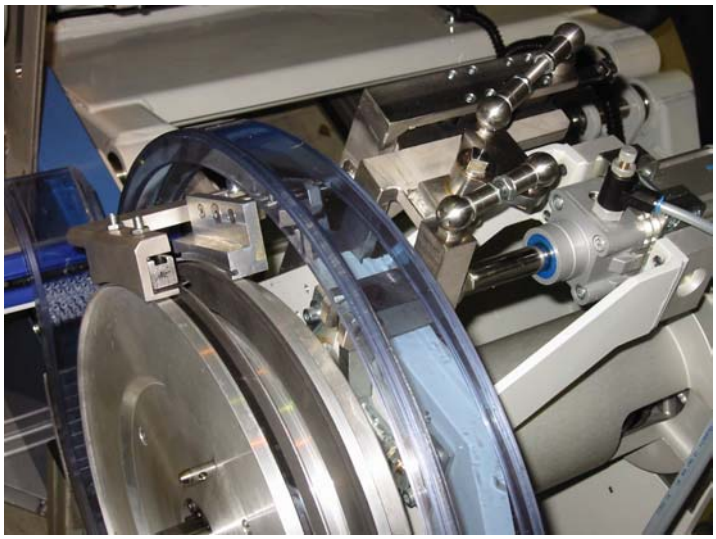

Figure 54. Improved gripping and cutting mechanism

The trials were run during December 2001. On the pay-off side 50 km standard spools were used and on the take-up side Sonoco-Crellin's 250 km reels. The test speed was 2,100 m/min. The trial was started by fixing the fiber spool on payoff and empty spools to both take-ups. Then the fiber was threaded at slow speed to the take-up after which the speed was ramped up to 2,100 m/min. Right after the machines reached the set speed the transfer was activated

manually. After transfer the speed was ramped down to 20 m/min to save the fiber. After this all information like visual observations, dancer swing values and pass or fail was recorded. Then the fiber was scraped from stopped take-up spool, blade area was cleaned and fork movement checked. After this the spool was put back and machine ramped again to set speed for next transfer. As a result of these trials the next phase started, which was field tests with improved design in real production environment.

Field tests with improved design

The new mechanism was upgraded first to three of the 10 machines used with original design. This was done to minimize the possible modification costs. After setting-up the machines the reliability data was collected as before. The upgrade included both the new cutting and gripping mechanism and the new auxiliary blade needed to prevent in-side-end whipping. These trials were done starting July 2002. The result is again the overall reliability of the transfer mechanism and whipping protection.

To confirm the promising results from the first customer the performance of the transfer was further evaluated at another fiber plant. A new machine with the latest transfer mechanism design was built and the performance tested together with a fiber manufacturer. The trials begun in July 2003 and they lasted two months. The ultimate goal for these trials were to confirm the performance in state of the art production conditions and continue development for the higher speeds, which are required in the future with combined process. Prior and after these trials a test series simulating production conditions and to study potential for higher speeds was run.

This test was conducted to evaluate the potential of the transfer design for the higher speeds in the future applications like on-line proof testing or high speed draw process with large performs. The trial was run in controlled conditions during December 2002 and further trials at speed 3,500 m/min in December 2003.

The test set up is in Figure 55. The setup was quite similar to the earlier trials, but the layout was designed to simulate one known production environment. The tests included three different parts.

The first was transfer test at speeds 1,500 m/min, 1,800 m/min, 2,000 m/min and 2,400 m/min. 15 transfers total at each speed were run. Additionally 30 transfers at speed 3,500 m/min were run later. The transfer command was given 5 – 10 seconds after the desired transfer speed was achieved. After the transfer at least one full layer was run to see the winding quality.

The second was fiber break test at speeds 1,500 m/min, 1,800 m/min, 2,100 m/min and 2,400 m/min. 5 fiber breaks at each speed were done. The fiber breaks were done after rewinding 25 – 30 km fiber on to the reel. The fiber breaks were done by operator cutting

the fiber between the pay-off pulleys and the take-up dancer pulleys. The efficiency of whipping protection was inspected visually.

The third was speed variation test at 1,500 m/min and 2,100 m/min. 5 test runs were run at each speed. The program of the pay-off was modified that it was ramping ±5 m/s of the test speed at acceleration of 0.2 m/s^2. The transfers were done after rewinding 25 – 30 km fiber on to the reel. Last wound reel of the each test speed was saved for analyzing the winding quality.

Figure 55. Test set up for high-speed transfer trial

5 RESULTS

5.1 Tension Behavior Results

This section presents the results of the various trials to investigate the tension behavior of the fiber. The results are presented in graphs and tables. The error margins of the results are presented in the tables and graphs. The maximum errors are combinations of the measurement sensor errors and recorder errors.

5.1.1 Draw Tension Data

Draw tension was measured to find the relationship between line speed and draw tension before capstan. The measurements were carried out at various speeds in several draws. The Figure 56 shows the result, where the measurement values are averaged over 1 second. The curve is extrapolated down to 0 m/min using Power function. The formula is shown in the graph. The accuracy of the averaged values is roughly ± 0.01 N, which is the output accuracy of the control system.

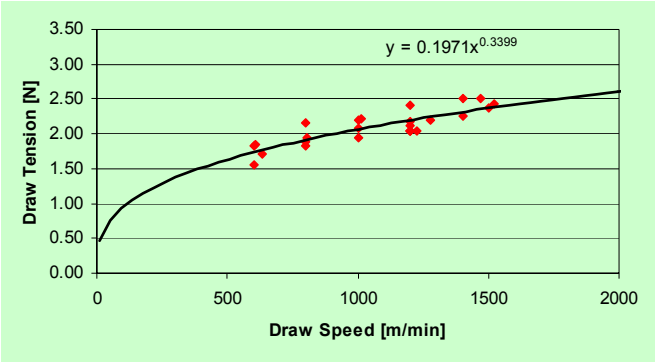

Figure 56. Draw tension as function of line speed

It should be noted that the draw tension is strongly dependent on the die design. By changing the die geometry the draw tension may be lower or higher and still the fiber diameter remains the same. The dies used this time were optimized for production speeds 1,000 - 1,200 m/min, but 1,500 m/min is possible in controlled conditions.

Table 17. Tension measurement results from draw tower measurement

	Speed [m/min]		
Draw Tension	600	900	1200
Average [N]	1.73	1.99	2.19
Minimum [N]	1.72	1.95	2.17
Maximum [N]	1.75	2.03	2.22
Max. var. ± [N]	0.016	0.039	0.021
Std. deviation [N]	0.007	0.016	0.009

The following graph in Figure 57 illustrates the measured tension data to be used in simulation model. The data was recorded at 1,200 m/min. The measurement result is not analysed more in this study, but it will be used as it is as input. The average tensions, tension variations and standard deviations are shown in Table 17.

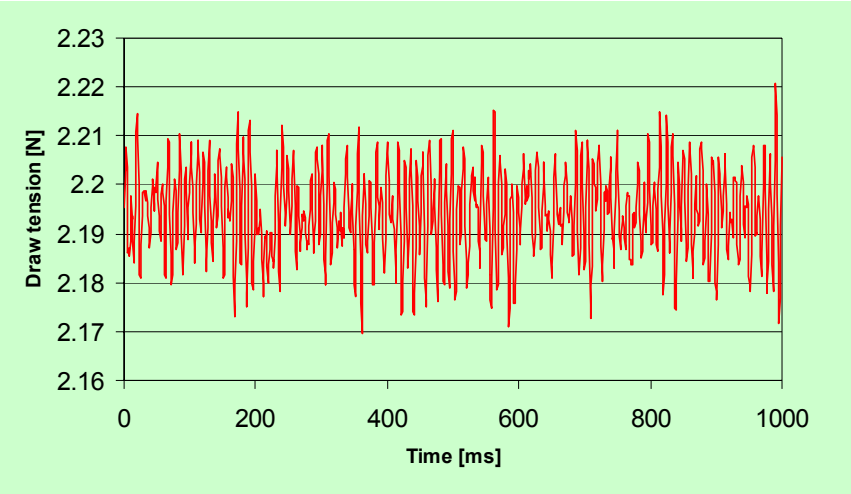

Figure 57. Data from fiber draw tower

5.1.2 Proof Tension Measurement results

Linear bearing model

As described in earlier chapters, the trials started with a measurement method, where the capstan was assembled on linear bearings and the fiber tension was measured indirectly with a sensor between machine frame and the capstan. The first trial was a simple test to verify the potential of this kind of measurement. The Figure 58 illustrates the results of the trial.

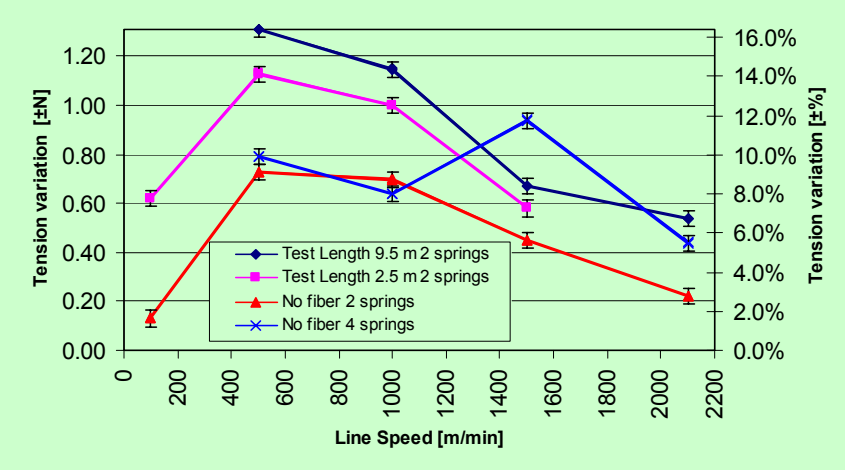

Figure 58. Measurement method test results

The Figure 58 and Table 18 show that the sensor signal was measurable, but the tension variation according to these

measurements was too high. The limit for the tension variation was ± 5%. The results from the runs without fiber, however, indicated that the greater part of the variation was sensor vibration rather than real fiber tension variation. The maximum measurement error is dominated by the resolution of the used recorder, but includes the sensor and amplifier errors as well.

Table 18. Measurement method test results

	Test Length 9.5 m 2 springs		Test Length 2.5 m 2 springs		No fiber 2 springs		No fiber 4 springs	
Speed [m/min]	Tension Variation [±N]	Tension Variation [±%]	Tension Variation [±N]	Tension Variation [±%]	Tension Variation [±N]	Tension Variation [±%]	Tension Variation [±N]	Tension Variation [±%]
100	- ± -	- ± -	0.62 ± 0.03	7.8% ± 0.4%	0.13 ± 0.03	1.6% ± 0.4%	- ± -	- ± -
500	1.31 ± 0.03	16.4% ± 0.4%	1.13 ± 0.03	14.1% ± 0.4%	0.73 ± 0.03	9.1% ± 0.4%	0.79 ± 0.03	9.9% ± 0.4%
1000	1.15 ± 0.03	14.4% ± 0.4%	1.00 ± 0.03	12.5% ± 0.4%	0.70 ± 0.03	8.8% ± 0.4%	0.64 ± 0.03	8.0% ± 0.4%
1500	0.67 ± 0.03	8.4% ± 0.4%	0.58 ± 0.03	7.3% ± 0.4%	0.45 ± 0.03	5.6% ± 0.4%	0.94 ± 0.03	11.8% ± 0.4%
2100	0.54 ± 0.03	6.8% ± 0.4%	- ± -	- ± -	0.22 ± 0.03	2.8% ± 0.4%	0.44 ± 0.03	5.5% ± 0.4%

The Figure 59 shows the results of the next test, which was a comparison with two different measurement methods performed during the same run at different speeds. The same results are presented in Table 19. The error margins for the results were the same as in the previous trial ± 0.03 N or ± 0.4%.

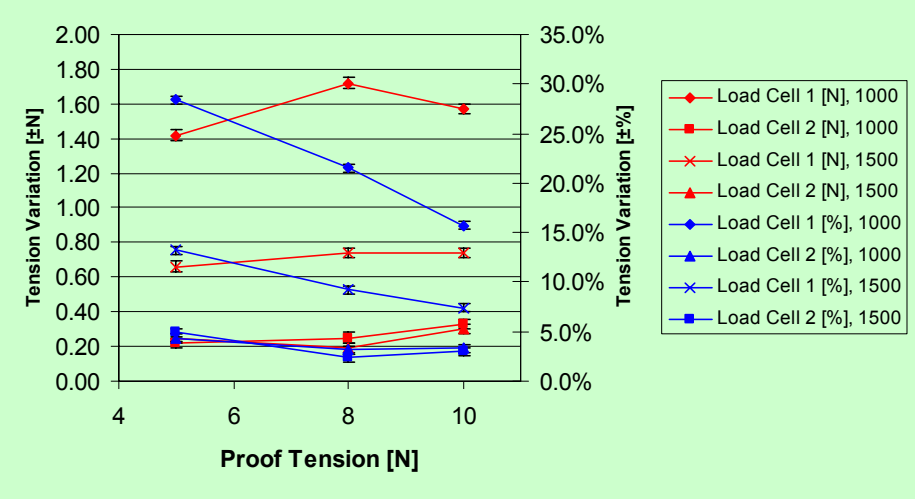

Figure 59. Results for linear bearing effect

The results show that this new method for measuring tension does not cause too high additional variation in fiber tension. There is, however, greater variation in the signal (load cell 1), but this is only a measurement error caused by vibration of the capstan unit. Since the error is not detectable in the tension of the fiber, the signal could be suitably filtered for the needs of the control system.

Table 19. Results for linear bearing effect

		Measurements accuracy = ± 0.03 N or ± 0.4%			
Line speed	Proof tension	Load Cell 1 [N], Variation (±N)	Load Cell 1 [%], Variation (±%)	Load Cell 2 [N], Variation (±N)	Load Cell 2 [%], Variation (±%)
1000	5	1.42	28.4%	0.22	4.4%
1000	8	1.72	21.5%	0.25	3.1%
1000	10	1.57	15.7%	0.33	3.3%
Line speed	Proof tension	Load Cell 1 [N], Variation (±N)	Load Cell 1 [%], Variation (±%)	Load Cell 2 [N], Variation (±N)	Load Cell 2 [%], Variation (±%)
1500	5	0.66	13.2%	0.25	4.9%
1500	8	0.74	9.3%	0.19	2.4%
1500	10	0.74	7.4%	0.30	3.0%

Pivoting joint model

After finalizing the trials with linear bearing system, a new prototype based on pivoting joint design was designed and built. Before these trials some preliminary trials were run to find best possible mounting type for the sensor. Several different rubber dampers were tested between capstan and the sensor, but it was found out that depending on the rubber type the signal was more or less non-linear as function of the line speed. The conclusion was that the signal was the best without dampers and after that the trials begun with fixed mounting.

The trial was run in similar way than with the linear bearing system earlier. The results of the test series are in Figure 60 and Figure 61.

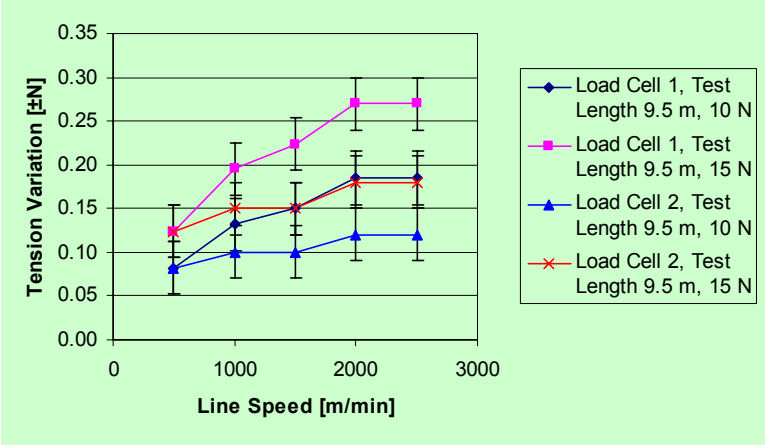

Figure 60. Pivoting joint system results in Newton

The results indicate that the variation in both cases is now below the limit ± 5%. The conventional method to measure the tension with a wheel gave better result, but pivoting joint design eliminated the majority of the vibration seen with linear bearing system. The results shown above were promising, but the test length was long compared to the needed test length in combined process. After accepting the measurement principle a test series with short test length was run. This time only the signal from new sensor was measured at different line speeds. The results are reported in Figure 62.

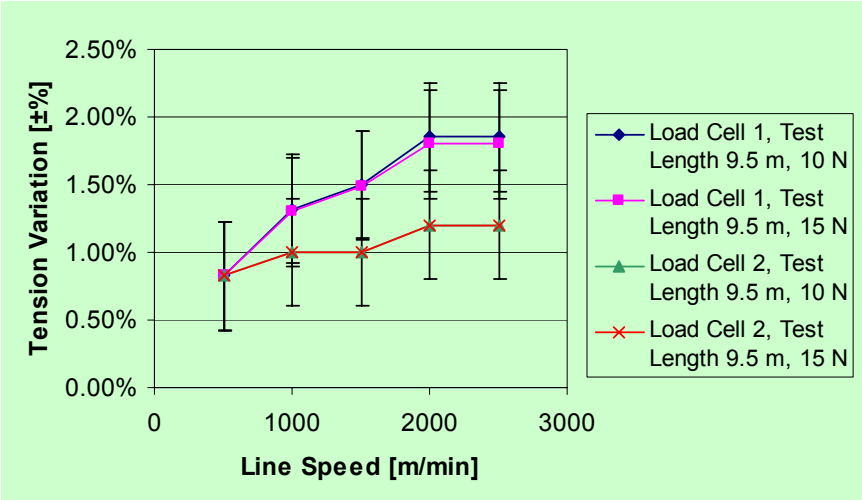

Figure 61. Pivoting joint system results in percentage

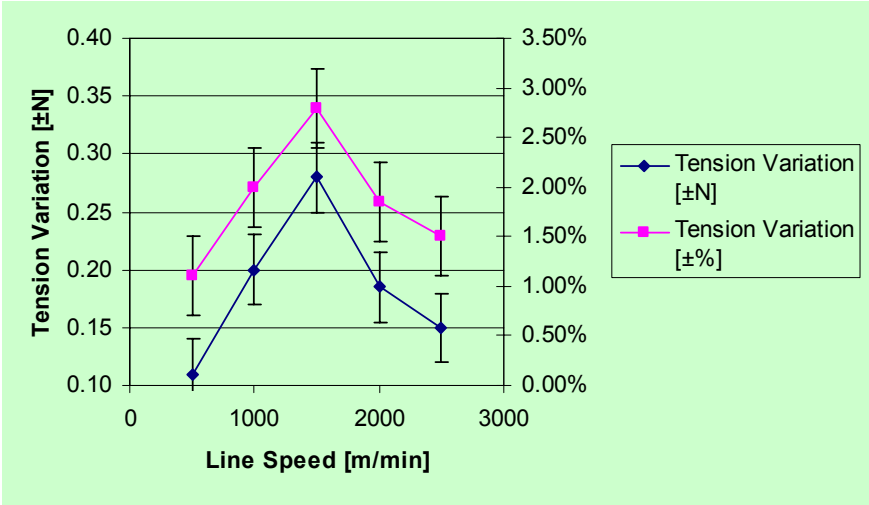

Figure 62. Tension variation with short test length

It can be seen that the variation was increasing first as function of the speed, but came down again at higher speeds. The variation was, however, clearly below the specification and therefore the phenomenon was not studied further.

5.1.3 Process Elements Affecting Tension

Turning wheel test result

This trial was realized to investigate the turning wheel effect on the fiber tension. This was then compared to the theoretical model, which was adjusted according to this experiment. The test set-up was explained earlier. Table 20 shows the results in numerical format and the Figure 63 has the same graphically.

Table 20. Results from wheel tests

Experimental test results Tension level changes as function of speed in OFC 53						
Speed [m/min]	Winding Tension [N] (40g)	Winding Tension [N] (50g)	Unwinding Tension [N]			
0	0.40	0.50	0.80			
500	0.42	0.51	0.82			
1000	0.44	0.54	0.87	Error margin for tension mesurement (5 wheels) = ± 0.01 N		
1500	0.47	0.58	0.91	Error margin for 1 wheel tension = ± 0.002 N		
2000	0.53	0.60	0.94	Error margin for 1 wheel torque = ± 0.0002 Nm		
2500	0.57	0.66	0.98			
3000	0.62	0.72	1.04			
Tension level increase caused by wheels						
Speed [m/min]	Winding Tension [N] (40g)	Winding Tension [N] (50g)	Unwinding Tension [N]	Average tension of 5 wheels [N]	Average tension of 1 wheel [N]	Torque/ of 1 wheel [Nm]
0	0.00	0.00	0.00	0.00	0.000	0.0000
500	0.02	0.01	0.01	0.02	0.003	0.0003
1000	0.04	0.04	0.06	0.05	0.010	0.0009
1500	0.07	0.08	0.11	0.09	0.017	0.0016
2000	0.13	0.10	0.14	0.12	0.025	0.0022
2500	0.17	0.16	0.18	0.17	0.034	0.0031
3000	0.22	0.22	0.24	0.23	0.045	0.0041

The same test result is applicable for dancer wheel, which is the same design. The turning wheel before entry capstan was not tested at this time, but the air resistance factor and bearing factors were estimated based on these results. The behavior follows the same principle, but higher bearing friction and air resistance were assumed, since the wheel diameter and bearing diameter are bigger.

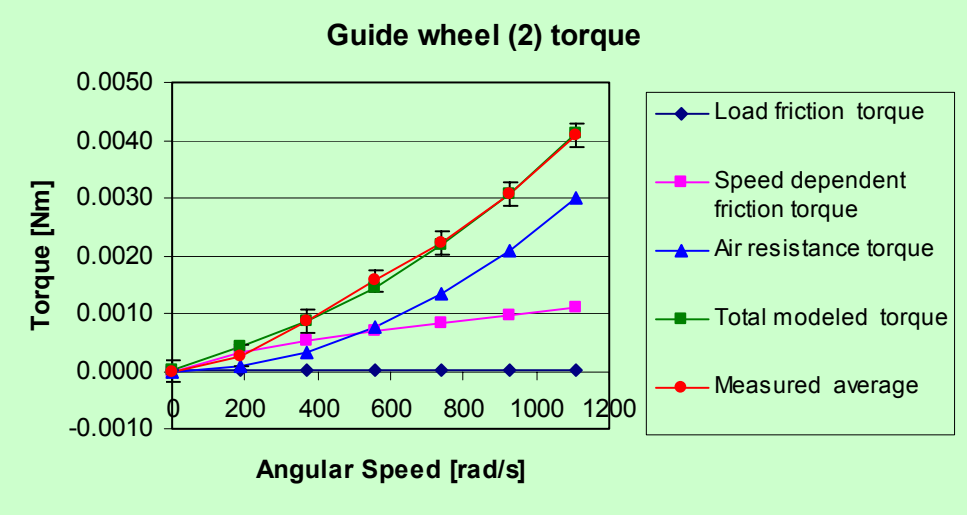

Figure 63. Results from wheel tests

The graph shows that there is a good match between model and practise. The graph shows the torque needed to rotate the wheel at different speeds. The graph shows also the modelled air resistance and bearing friction torques.

Capstan test result

Capstan was tested also separately. The torques needed to rotate the capstan at different speeds were measured. Using the information gathered from this trial the capstan model was adjusted. The test

results from the torque measurements are in Table 21 and the comparison of the model and experiments can be seen in Figure 64.

Table 21. Results from capstan torque test

Speed [m/min]	Measurement accuracy ± 1.0% or ± 0.025 Nm			
	Capstan 1 [%]	Capstan 2 [%]	Average [%]	Average [Nm]
1	4.0	3.0	3.5	0.09
5	4.0	3.0	3.5	0.09
50	6.0	5.0	5.5	0.13
150	9.0	7.0	8.0	0.20
300	10.0	9.0	9.5	0.23
600	11.0	12.0	11.5	0.28
900	11.0	13.0	12.0	0.29
1200	11.0	17.0	14.0	0.34
1500	12.0	19.0	15.5	0.38
1800	16.0	20.0	18.0	0.44
2100	20.0	21.0	20.5	0.50
2400	21.0	22.0	21.5	0.53
2700	23.0	27.0	25.0	0.61
3000	24.0	-	24.0	0.59
3200	26.5	-	26.5	0.65

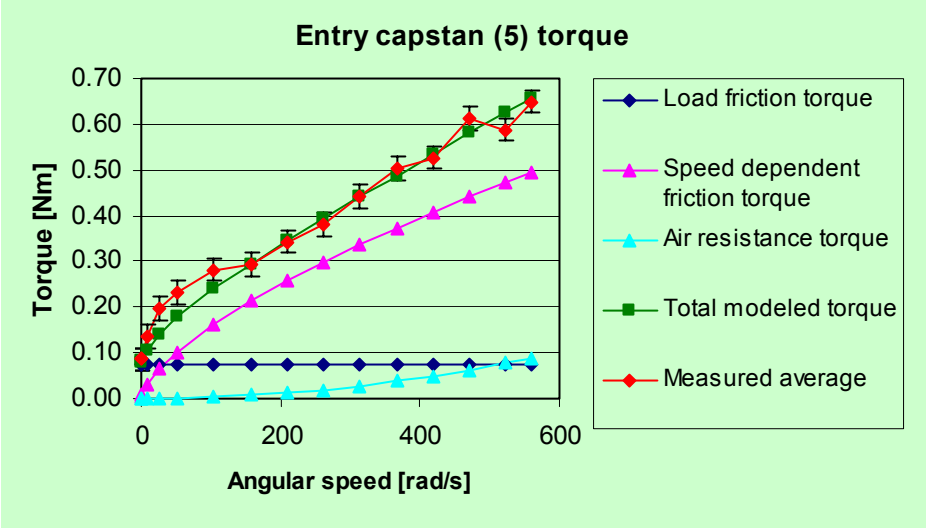

Figure 64. Results from capstan measurements and simulation

The graph shows quite good match between model and practice at higher speeds, but the behavior at low speed was slightly different. The air resistance was modeled separately again, but speed dependent torque and load friction torque include both bearing friction and belt friction. This may cause the difference at low speeds, since only the bearing model was used and the belt behavior was neglected.

Take-up test result

The take-up was tested in similar way than the capstan. The torque needed to rotate the selected reel was measured and it was compared to the measurements without reel. By doing this it was possible to evaluate accurately the air resistance torque the spool creates. Then the model was adjusted again according to the measured results. The

Table 22 includes the measured data and the Figure 65 the comparison of the model and test results.

Table 22. Results from take-up torque measurement

Speed bit	rpm	Angular speed	Measurement accuracy ± 1.0% or ± 0.025 Nm			
			M%	M [Nm]	M%	M [Nm]
32767	6000	rad/s	50km spool	2.45	No spool	2.45
10	1.83	0.19	2.5%	0.06	2.5%	0.06
100	18.31	1.92	2.5%	0.06	2.0%	0.05
500	91.56	9.59	3.5%	0.09	3.0%	0.07
1000	183.11	19.18	4.0%	0.10	4.0%	0.10
5000	915.56	95.88	6.5%	0.16	5.5%	0.13
10000	1831.11	191.75	8.5%	0.21	6.0%	0.15
15000	2746.67	287.63	10.0%	0.25	7.0%	0.17
20000	3662.22	383.51	15.0%	0.37	8.0%	0.20
25000	4577.78	479.38	19.0%	0.47	10.0%	0.25
30000	5493.33	575.26	26.0%	0.64	12.0%	0.29

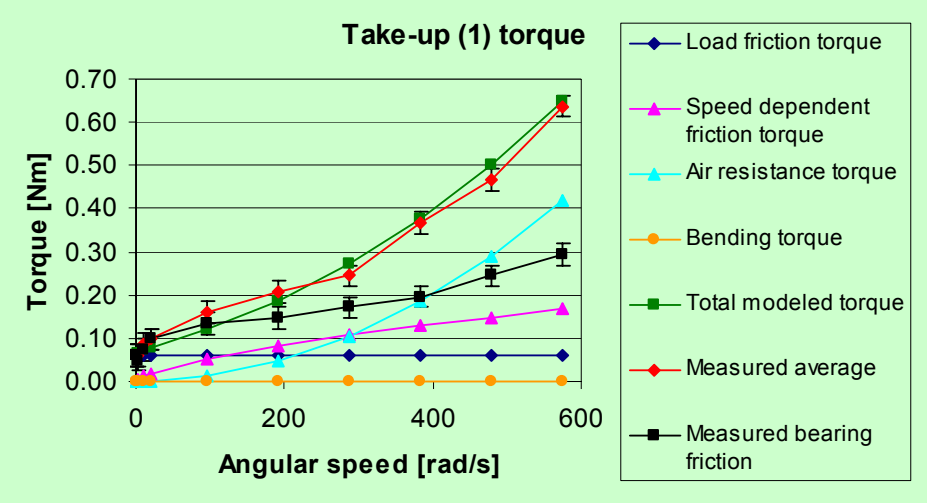

Figure 65. Results from take-up measurement and simulation

It must be remembered that the air friction torque is depending on the used spool. Now a standard 50 km spool was used. There are several manufacturers of such spools and the design is almost identical. Therefore the result is comparable to 50 km spools when the design is similar, but other size of spools needs to be tested in similar way. The air resistance is caused by the ribs typically used outside the flanges to make them more rigid. The effect of the air resistance can be minimized, if the flanges are covered completely by friction flanges of the machine. In this case the flanges were only partially covered.

Dancer test result

The behavior of the dancer in turning point was tested and compared to the calculated results. The mathematics behind the calculations was presented earlier. The Figure 66 shows the calculated dancer position and fiber tension as function of time when the direction change is performed. The example is a case where there is a bump on

the flange and dancer position changes causing additional tension to the fiber. The model takes in to account dancer position, bearing friction, past tension values, air resistance and inertia.

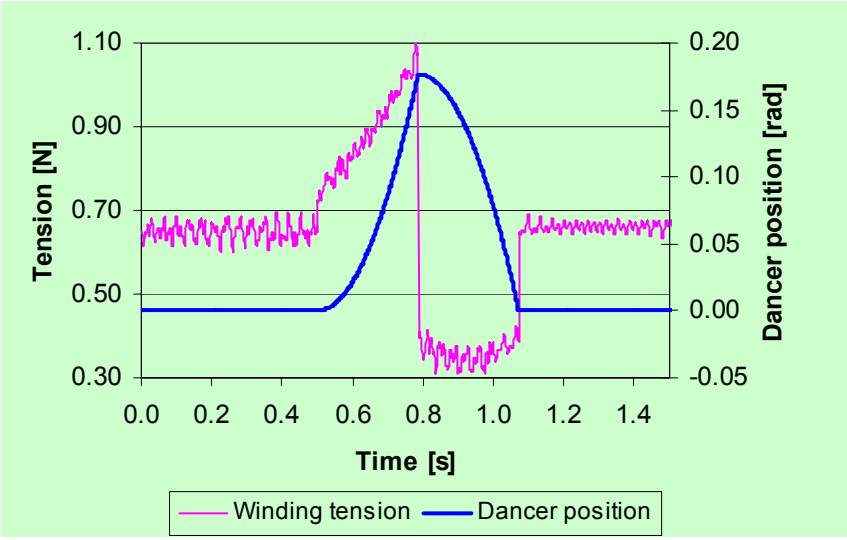

Figure 66. Calculated fiber tension and dancer position in turning

The following graph in Figure 67 shows a real time measurement of the dancer movement and winding tension. A calculated curve is added for comparison.

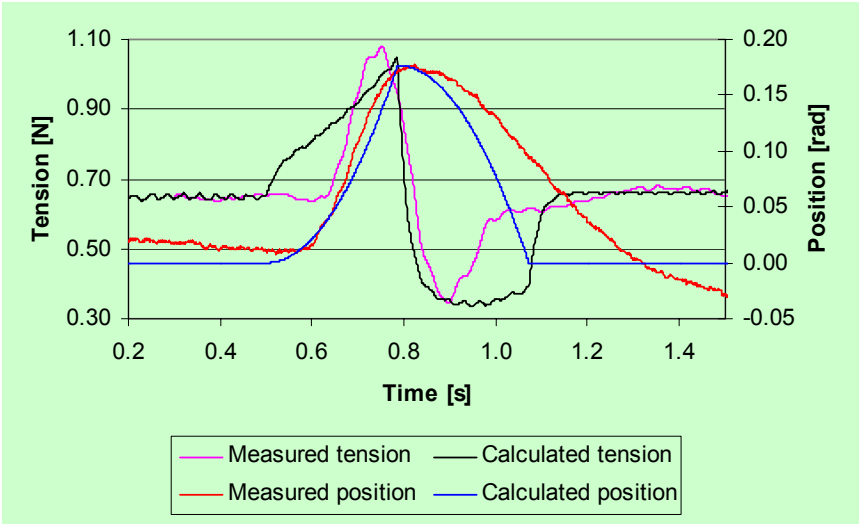

Figure 67. Dancer behavior and winding tension in turning point at 1,000 m/min

The measured signals, especially tension signal, had higher frequency noise and also lower frequency sine form. Neither the high frequency phenomena nor the sine form were investigated at this time, since they were not related to the traversing turning point. Therefore these disturbances were filtered from the data afterwards by using recursive digital low pass filter. The same was done to dancer position signal and also for the calculated tension to get good comparison.

Some clear differences between the measured and calculated curves can be seen. The measured dancer position curve follows the calculated pretty well when the fiber enters the bump. After the turning point the dancer approaches the home position slower than predicted with the calculation. The measured tension curve has clearly sharper form than the calculated. The difference between calculation and the real life is the machine control algorithms. The model takes into account only the mechanical phenomena like inertia, bearing friction and air resistance. The machine, however, starts to adjust the rotating speed of the take-up according to the changes in dancer position. The control uses normal PID algorithm, where only P and I terms are used.

These trials were run at lower speeds at 100 – 1,000 m/min and still at 1,000 m/min it is seen that the speed correction starts to correct the rotating speed and the dancer position recovers slower from the bump. In real life PID algorithm must be used or the dancer starts to oscillate at certain speeds. It is concluded that the model is accurate enough and can be used to predict the maximum and minimum tensions and dancer positions, which were quite near of the measured.

5.1.4 Complete Tension Simulation Results

Using the information collected in the previous tests the tension behavior in entire on-line proof testing process was modelled. The created program uses the general models described earlier. It can be used to model different post draw processes as well with minor modifications.

Time domain result

As a result of simulation the fiber tension in all free fiber spans is solved. The tension variations travelling both directions from take-up to coater and from coater to take-up are calculated. The final result is given by using superposition principle. The sampling rate for the analysis is now 1 kHz. The Appendix 8 shows the summarized results when the tension behavior is calculated from take-up to draw coater.

Using the same principle and the equations shown in theory section the Appendix 9 summarizes the vibrations travelling from coater to take-up. Finally the tension disturbances travelling both directions are combined. This is done by superposition principle. The results are shown numerically and graphically in Appendix 10.

Fourier analysis

The same data was then possible to present in frequency domain using Fourier transform. Fast disturbances were of special interest. Therefore the frequency range 0 Hz – 1,000 Hz was selected for Fast Fourier transform. Fast Fourier Transform was possible when the number of samples was suitable and this time it was selected to be 1,024 samples, which corresponds to slightly more than one second

with the sampling rate used. The Appendix 11 shows the amplitude of the each disturbance as function of the frequency.

As expected the frequencies of the rotating elements where disturbances were caused by dislocating the mass centre can be seen. The frequency 75.5 Hz corresponds to take-up rotating speed, approx 84 Hz to entry and exit capstans, approx 177 Hz to guide wheel and dancer wheel and 106 Hz to turning wheel. The noise seen in addition to the maximum peaks mentioned above come from the actual draw tension measurement data.

Stress analysis

As mentioned earlier, ultimately the stress caused to the glass fiber throughout the entire process was of interest. Using tension information calculated with simulation program the maximum stress level of the fiber in each fiber span can be calculated. Additionally the stress when the fiber is subjected to bending in process elements needs to be calculated. To be able to do that the contact length that the fiber has against each element needs to be determined more accurately and also the free span lengths. Schematic view of the process parameters is in Figure 68.

It is important that all the different parameters can be selected freely for calculation. This is possible with the model generated for stress analysis purposes. An example of the parameters is shown Table 23. As a result of analysis the maximum stress the fiber is subjected when it passes each of the process elements or when in a free span was found. These results are shown in Figure 69. The same results are plotted as function of the line length in the Figure 70.

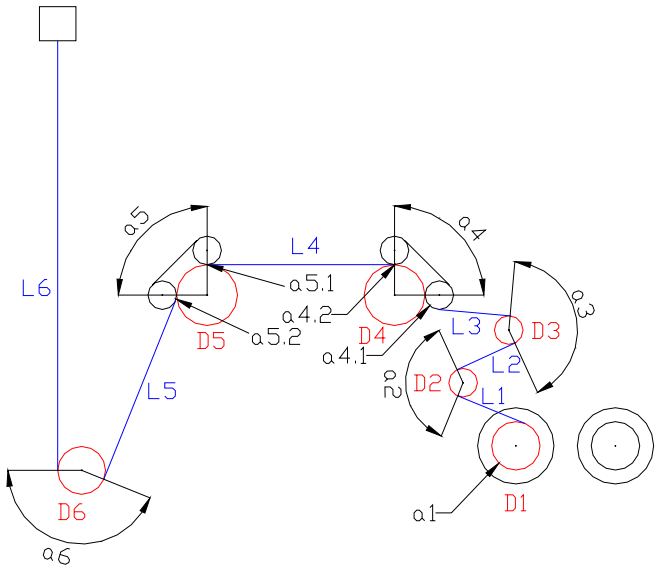

Figure 68. Schematic view of on-line proof testing

Table 23. Parameters for stress analysis

Fiber span Symb.	Free span length L_s [m]	Process element		Bending angle a [deg]
		Name	Symb.	
L1	0.20	Take-up	D1	360.0
L2	0.20	Guide wheel	D2	130.0
L3	0.30	Dancer wheel	D3	150.0
L4	1.00	Belt pulley 2	D4.1	80.0
L5	0.60	Exit capstan	D4	90.0
L6	1.35	Belt pulley 1	D4.2	0.0
		Belt pulley 2	D5.1	0.0
		Entry capstan	D5	90.0
		Belt pulley 1	D5.2	10.0
		Turning wheel	D6	160

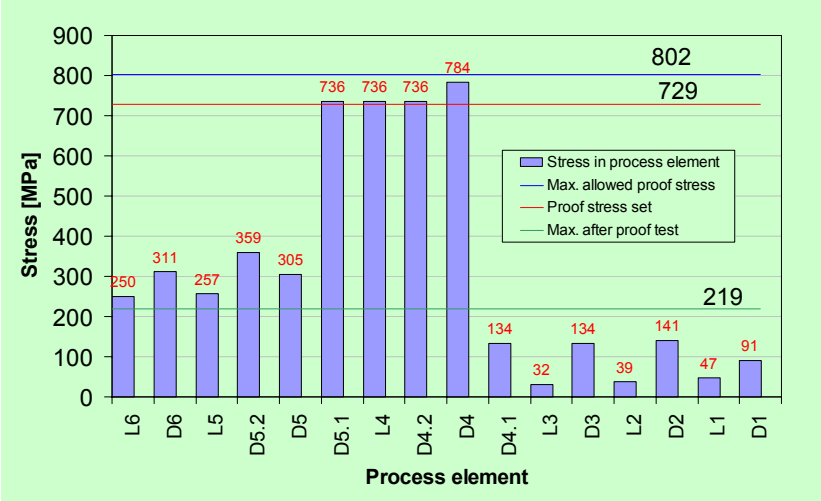

Figure 69. Maximum stress in different process phases

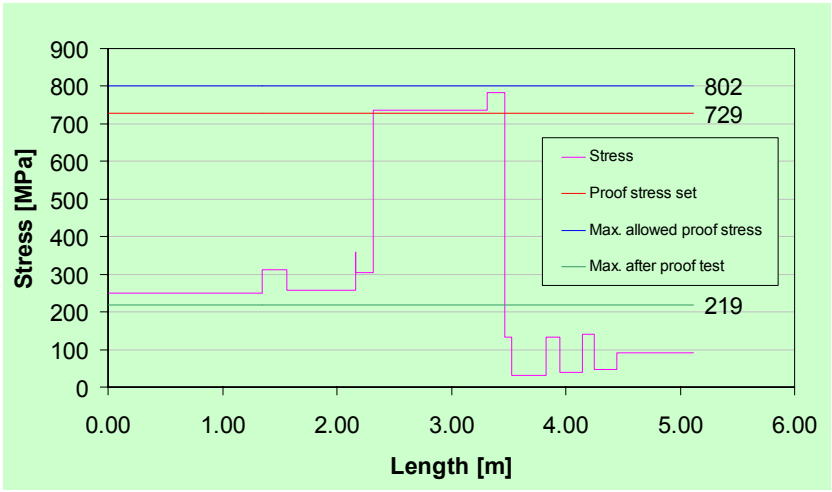

Figure 70. Fiber stress as function of the line length

5.2 Break Recovery Reliability

The following section presents the results about the break recovery trials. Many of the results presented are not based on excessive number of trials, but the purpose has been to select the right

solution for further trials. The confidence intervals presented in the following graphs are based on the sample size at 95% confidence level (CRS 2004). The same principle applies for the following chapter 5.3 discussing about winding quality results.

5.2.1 Tube System Results

The first trial focused on the right material selection for the channel needed to guide fiber after fiber break between the entry capstan and exit capstan.

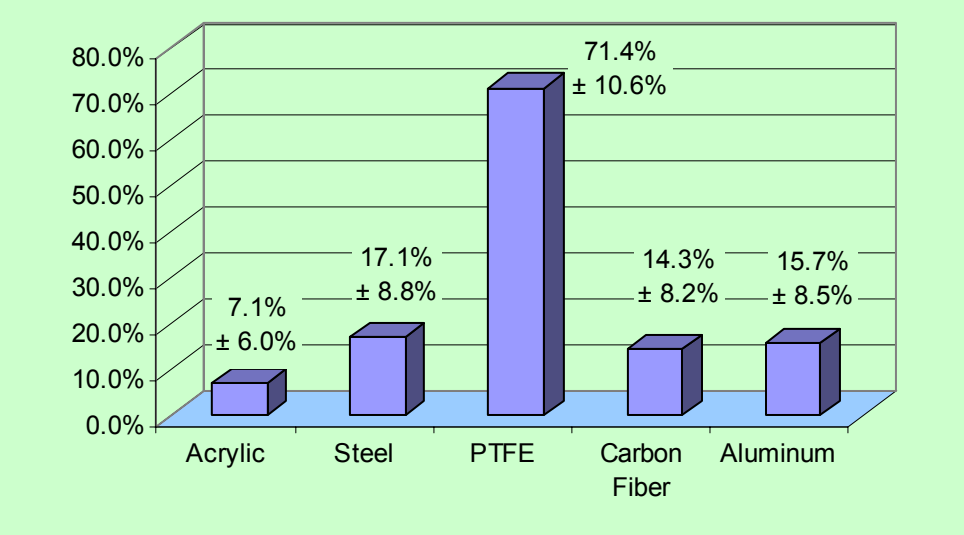

Figure 71. Success rate with different tube materials

As is clearly seen in Figure 71, PTFE ("Teflon") was the best material; all the other materials induce reduction to the break recovery probability. This is caused by several different phenomena. First, Teflon is a quite effective insulator, and therefore it easily creates a strong surface electricity field around it. This field had the same polarity as the fiber. When the surface voltage of Teflon was measured, the values ranged from +5 kV to +20 kV and varied excessively depending on the point of measurement on the tube. The same polarity helped conveying the fiber compared to the other materials. Second, the friction coefficient between the fiber and Teflon is extremely low, and therefore friction force breaks least compared to other materials. Third, the so-called "rubber band effect" at the proof test region interferes with the threading event, but the above mentioned two first phenomena worked in favor of the Teflon.

As a result of this first test Teflon was selected to be used in further testing. The second test series focused on removing the negative effect of static electricity on conveying the fiber in the tube.

The results are in the Figure 72. Six different speeds between 200 – 1,500 m/min were used. The results may look a bit confusing in the beginning, since it seems that normal static elimination did not

work. The result without static elimination was well in line with the earlier result with Teflon tube. The static bars alone, however, couldn't improve the success rate, since they discharged only the fiber. The potential difference was then bigger and caused the fiber to stick in to the tube. The challenge with Teflon is to really be able to control static. The best result was achieved with special tube structure, where around the inner Teflon tube there is ionized pressurized air. On the Teflon tube there where small 1 mm holes through which the air was guided in the tube. This seemed to stabilize the static of the tube also and together with the static elimination on payoff and capstan the best results were achieved.

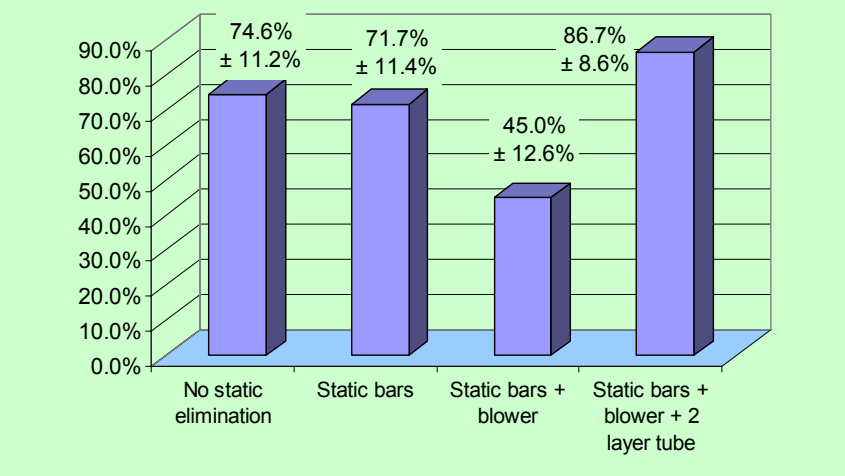

Figure 72. Effect of static elimination on success rate

After finding the most promising tube configuration with proper static elimination that structure was tested in more details. In the Figure 73 are the results of the next setup. Two different pressures were used in the tube at different line speeds. It can immediately be seen that there is no clear pattern or indication that the speed has an effect on the success rate at speed range 250 m/min – 2,500 m/min.

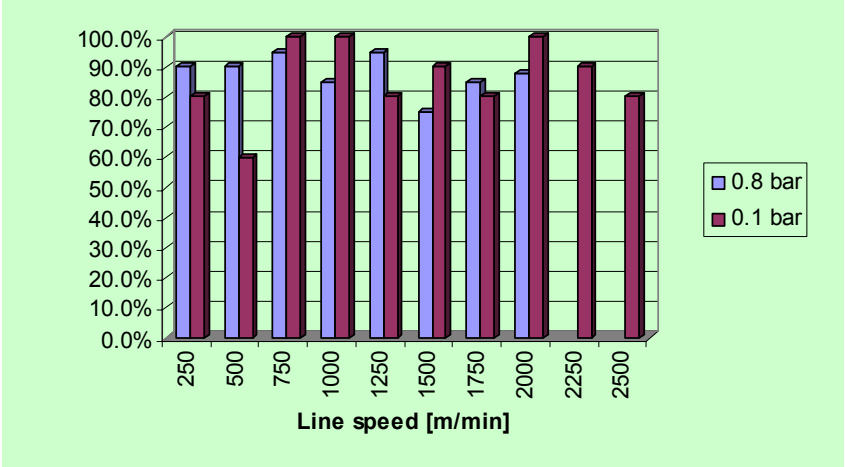

Figure 73. Success rate at different speeds and tube pressures

The Figure 74 summarizes the break recovery success rate result for both setups. The conclusion was that the effect of the pressure was negligible. Enough pressure to have a positive airflow through the tube is only needed. That was enough to stabilize the static of the Teflon tube, but not enough to remove static completely. The result was better than with only simple Teflon tube, since it was repeated several times.

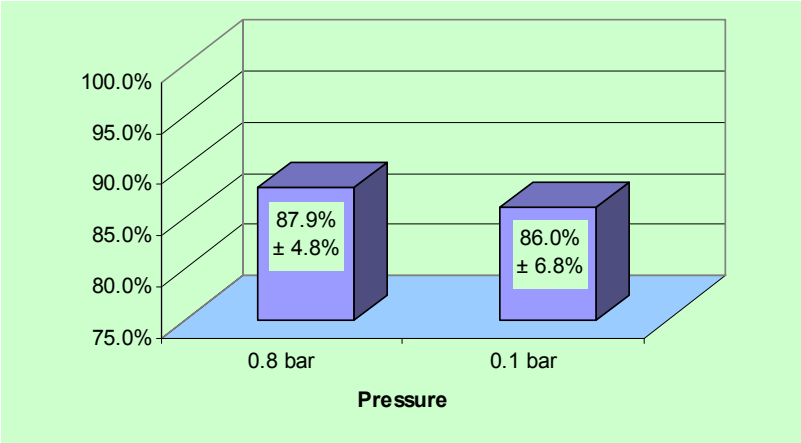

Figure 74. Tube pressure effect on success rate

5.2.2 Belt System Results

The other alternative for break recovery was tested after tube system, since the result was not satisfactory. The prototype of belt system was tested without a tube-guide, which will further improve the design later. The belt system was assembled between entry and exit capstans. The break recovery success rate was tested similarly to the tube system at different line speeds. The Figure 75 summarizes the success rates at different speeds.

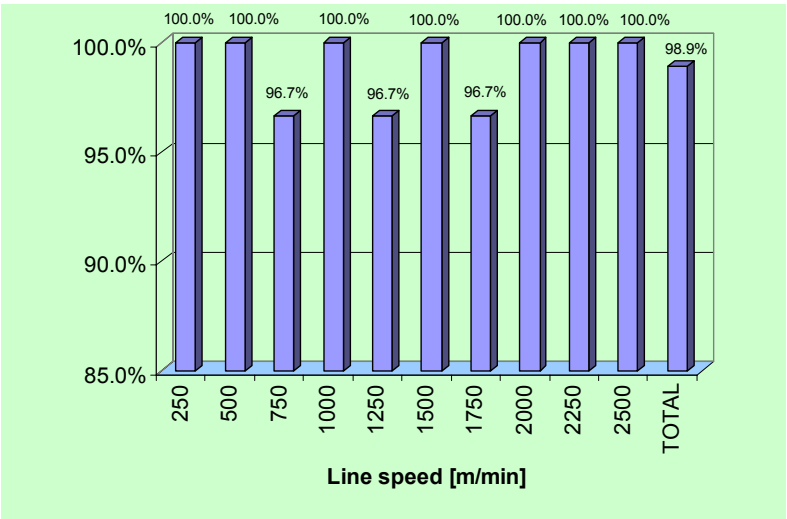

Figure 75. Break recovery success rate with belt system

The success rate was 98.9%, which shows clear improvement compared to the tube system. Only 3 breaks out of 285 failed. All the failures looked similar and happened at different speeds. The fiber slipped out from the side and the fiber went only partially between the belts. Belts managed to catch the fiber, but the fiber end did not go through exit capstan cleanly. All these 3 were considered as failures. It was also noticed in several runs that there were a small loose loop forming after entry capstan just after the belts caught the fiber end. This happened because the fiber end hit first the belt and its speed slowed before belts started to pull the fiber. Introducing the walls on the side of the belts can help with this phenomenon.

Comparison of tube and belt system results is presented in the Figure 76. The result is very convincing in favor of the belt system, which was selected to be the construction for future break recovery system needed in continuous combined fiber draw and proof testing processes.

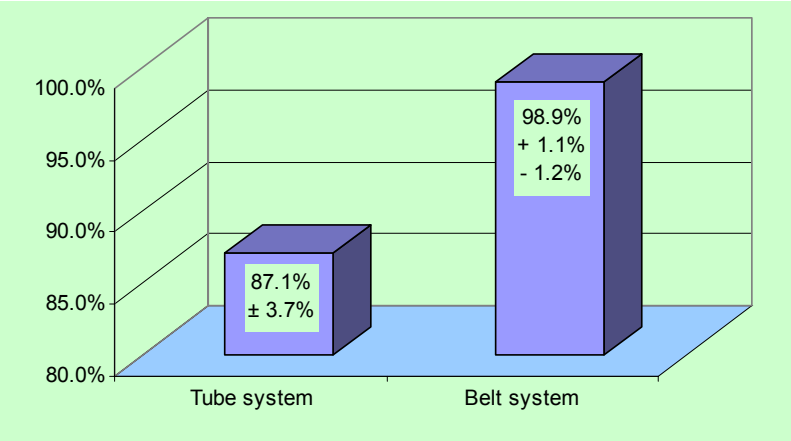

Figure 76. Success rate of tube system and belt system

The success rate of the tube system includes all tests run with the 2-layer tube, where the inner tube is made of Teflon. The Table 24 shows a summary of tube system and belt system runs and results.

Table 24. Summary of tube system and belt system trials

	Tube system	Belt system
Breaks	317	285
Success	276	282
Failures	41	3
Success%	87.1% ± 3.7%	98.9% + 1.1% -1.2%

5.3 Winding Quality

5.3.1 Winding Control Algorithm Test Results

Trials with existing system

First the cause of the attenuation steps was investigated. See Figure 77 for a step in OTDR measurement graph. Appendix 12 illustrates what is happening during typical step formation with a difficult "sticky fiber". In this picture evenly alternating blue and white curves are the fine tune values. The white curve is the inner flange fine tune and the blue curve is the outer flange fine tune. When the curves go up the traverse is spreading and vice versa. The white vertical line marks the length where a step has occurred (distance 15,700 meters from the start of the run). The step occurred at the inner flange. The gray rapidly alternating curve indicates the dancer position in the inner turning point (when the value is high there is a gap and when it is low there is a bump). The light blue curve is the same for outer flange. Notice that the traverse is at its widest and the gap has just been filled. The yellow curve is the fiber length and the red curve the traversing speed.

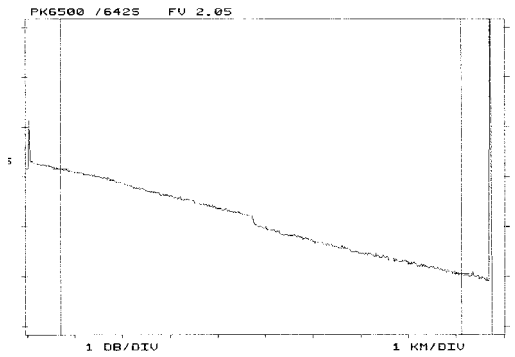

Figure 77. Attenuation step in an OTDR curve

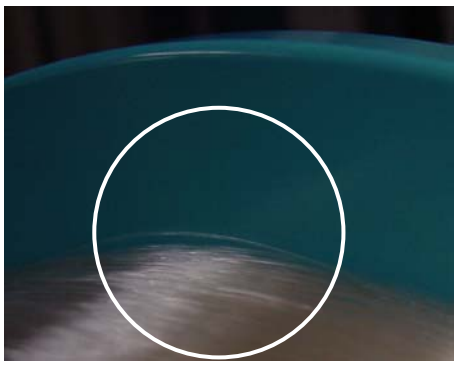

Figure 78. Loose loop on the reel

Several spools where the step had found in OTDR-measurement were then paid off. Figure 78 shows how the loose loop looks on the reel when the layers above it have been removed. The fiber length wound on to the spool had also an effect on step occurrence. The steps begun to occur after 10 km of fiber had been wound. The greatest risk to see a step is between 15 and 23 km (or approx. 48 km when 50 km spools are used) when there is enough fiber already wound on the reel to cause gaps and lumps and there is still plenty of fiber left to be wound to the reel that will press these fallen loops and cause a step. The last kilometer of fiber does not cause steps because there is not enough fiber to be wound to cause enough pressure to press the loose loop of fiber and cause a step. The widening of the reel is at its greatest also at this point, since the pressure against the flange is high enough. This means that the gaps are forming constantly near flange and winding algorithm needs to fill them.

The trial to investigate the efficiency of the original winding algorithm was carried out in normal production gathering the rewinding percent information during long period. The reported failure percent from that test period was nearly 30%, which is rather high in modern production environment. The fiber was, however, more difficult than normally and without turning correction algorithm the operators needed to adjust turning points manually.

Results with modified algorithm

Appendix 13 illustrates the behavior of the winding after software modifications. The smooth white and red curves are now the fine tunes; white is the inner. The two other curves just below the fine tunes are the dancer positions in turning point. This graph shows that the new algorithm works well keeping the dancer movement at minimum during turning. At this time the efficiency to reduce the steps was confirmed first by recording limited amount of runs in laboratory conditions. The total number of recordings was 151, of which only 2 failed. This gave very low failure percentage 1.3% compared to the original 30%. The testing continued at fiber plant using the same methods than in first trial series. The reported failure percent from the production was 4% in this second trial period.

Finally the results about winding algorithm development are summarized in Figure 79. It is concluded that the algorithm was successfully improved, although there is room for improvement, since the rewinding percent with difficult fiber was still 4%.

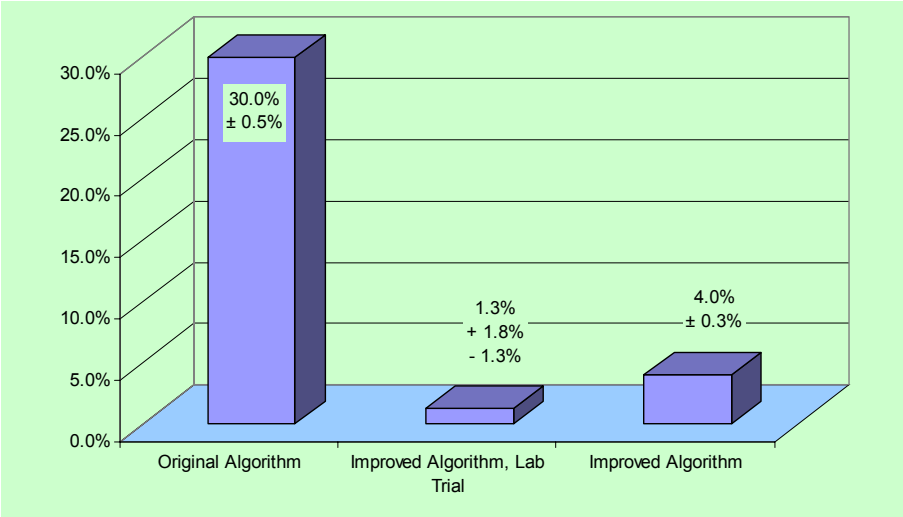

Figure 79. Summary of winding algorithm trials

5.3.2 Whipping Guard Testing Result

These trials were run to find an efficient solution to prevent whipping damages the fiber tail could do to the take-up reel after fiber break or planned transfer. The trials started with a known principle, called “spiral”, which was improved when the trial

proceeded. A new whipping guard was designed and built based on the initial trials. This new guard was called “round”. Also this one was improved while tests proceeded. The result of the whipping prevention reliability with different evolution models is shown in Table 25 and Figure 80.

The first column shows the result when the fiber is broken after entry capstan (normal fiber break). In this case the take-up has time to decelerate and whipping protection is easy with both guard types. All the other columns show the results when the fiber is broken nearer take-up and as is seen now the protection is more difficult.

Table 25. Whipping guard reliability results

	Long fiber tail	Spiral: Proto	Spiral: Improved	Round: Proto	Round: Improved
Runs	21	28	64	35	80
Passed	21	19	54	30	76
Pass%	100.0% + 0.0% - 4.3%	67.9% ± 17.3%	84.4% ± 9.0%	85.7% ± 11.5%	95.0% ± 4.8%

The best result achieved was 95% protection reliability. All the 4 failures with the best guard seemed to be such where the fiber tail came out from the guard before the take-up stopped. In these cases the tail had hit to the take-up structures and then back to the spool surface. The performance can be further improved by small design changes. The guard should be wider and also the edges should be higher to prevent the fiber tail coming out from the guard, when it is rotating inside.

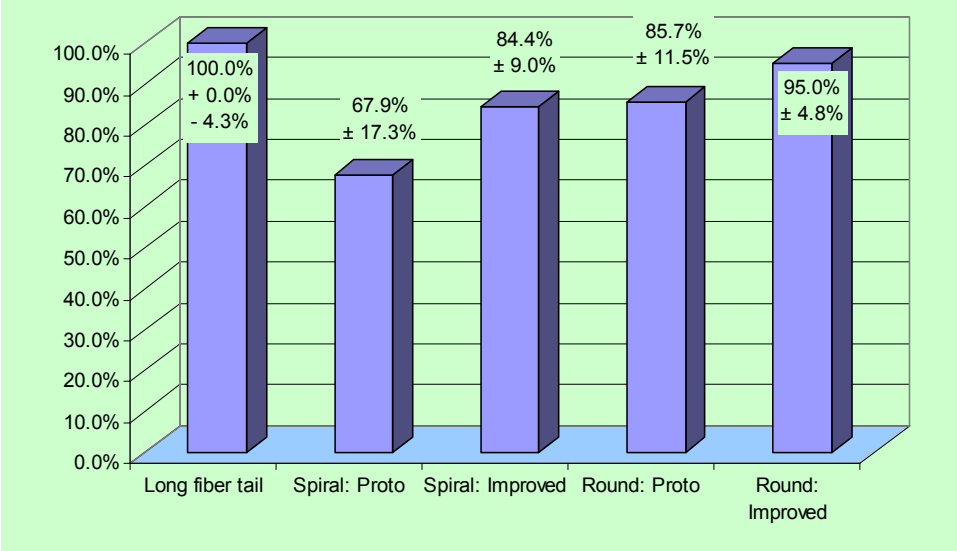

Figure 80. Whipping guard trial results

5.3.3 In-Side End Whipping Investigation Results

The visual inspection of the in-side-end whipping did not give the desired result. It was not possible to find the reason for the in-side-end getting loose during the run. The in-side-end whipping was

repeated constantly with one of the machines available at that time. A high-speed camera was then used to record the trials.

The results are still shots from the longer series of photographs. Four runs were photographed and recorded, where the in-side-end got loose causing whipping. One of them is presented in Appendixes 14 to 18, which clearly show the reason for the whipping.

Appendix 14 shows four frames from the shot. There the short fiber tail is seen for the first time, which is sticking out from between the gripping flanges. The same tail is shown in Figure 81 as well. The flanges and the fiber tail rotate here counter clockwise.

The Appendix 15 shows the fiber tail coming again from right side, the 3rd and the 4th frame. Before that it can already be seen in the 1st and 2nd frame that the fiber has got loose. The 5th frame shows how the fiber tail hits to the cutting blade construction, which swings the tail backwards.

The next Appendix 16 shows the same again later in the same shot. The fiber is even looser now in the frames 1 to 4. The 5th frame shows the fiber tail again moving towards the blade construction.

Finally in the Appendix 17 and Appendix 18 it is found what is creating the loose loop seen above. The fiber is broken, because the short fiber tail has hit back from the blade construction damaging the fiber. The figures show how the broken fiber hits to the blade construction similarly to the short tail. This creates severe whipping, which in production conditions may destroy the whole fiber package very quickly.

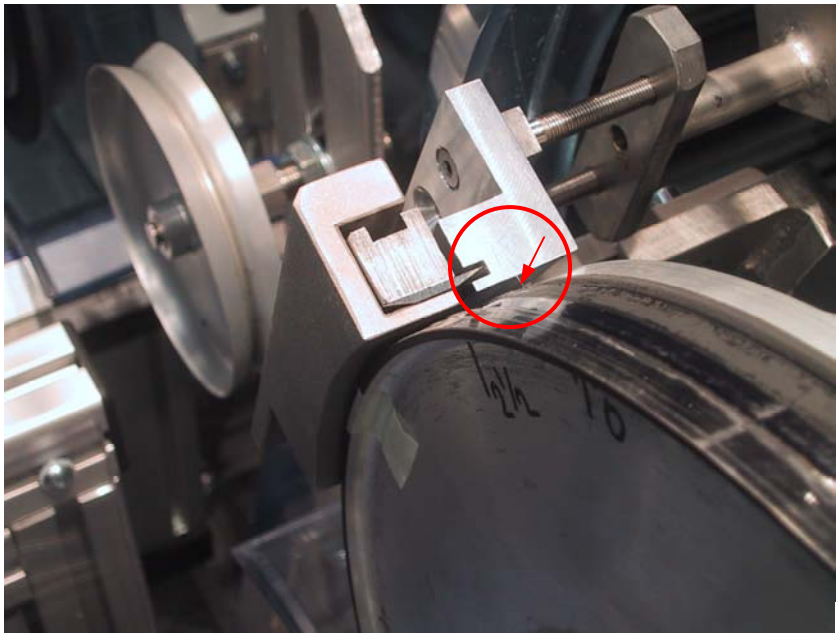

Figure 81. Still photo showing fiber tail hitting the blade construction.

Depending on the machine individual the tail length can slightly differ. Also depending on the alignments and initial parameters the tail often bends under the wound fiber on scrap flange, when it cannot cause the in-side-end whipping. Normally when the whipping has occurred in production it is not possible to find the fiber tail anymore, since it has been destroyed with the rest of the fiber. These are the reasons why it was so difficult to find the reason for in-side-end whipping without high-speed photographing.

5.3.4 Auxiliary Blade Test Results

After finding the reason for in-side-end whipping a prototype was designed and built to prevent this from happen. The suggested solution was an auxiliary blade to cut the short fiber tail as explained earlier. Table 26 summarizes the trials and results with and without the auxiliary blade.

Table 26. Summary of auxiliary blade trials

	With Blade	Without Blade
Runs	20	20
Whipping breaks	0	11
Coating damages	0	9
Pass	20	0
Pass% (margin ~4.4%)	100%	0%
Whipping break%	0%	55%
Coating damage%	0%	45%

The same results are presented graphically in Figure 82. The auxiliary blade removed the problem completely according to these trials. This was confirmed later as feedback from customer running production with this new blade.

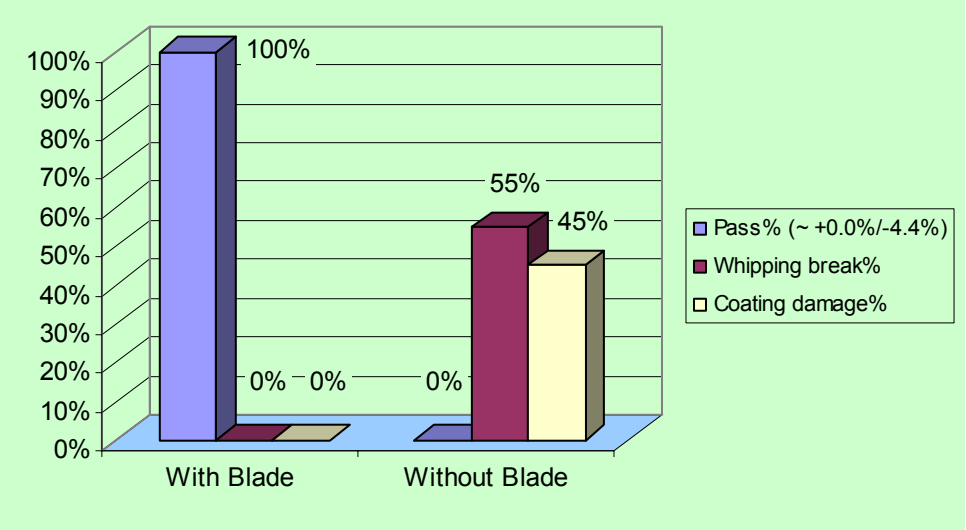

Figure 82. Auxiliary blade trial results

5.3.5 Transfer Reliability of the Original Design

The reliability of the original cutting and gripping design was tried in production conditions. The results were recorded in production tracking system. The weekly failure percent is presented in Figure 83.

The big variation between weeks can at least partly be explained by the differences between machine individuals. This was clearly the case on week 9, when one problematic machine caused big failure percent when the production rate was low. It is not, however, the only explanation, but also the skills of the operators may have something to do with variation between test weeks.

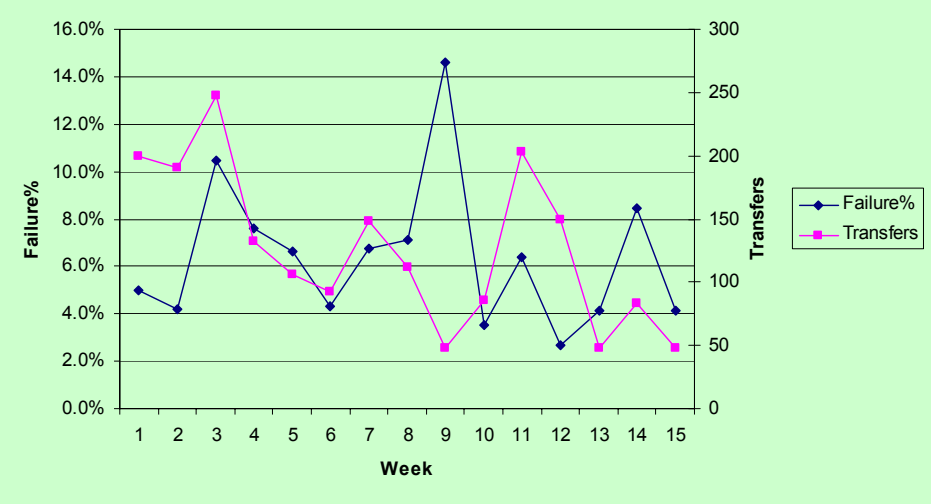

Figure 83. Weekly transfer failure percent

The Figure 84 shows the differences between the seven machine individuals used in this trial and the total failure percent, which was 6.4%. Transfer reliability was then 93.6%.

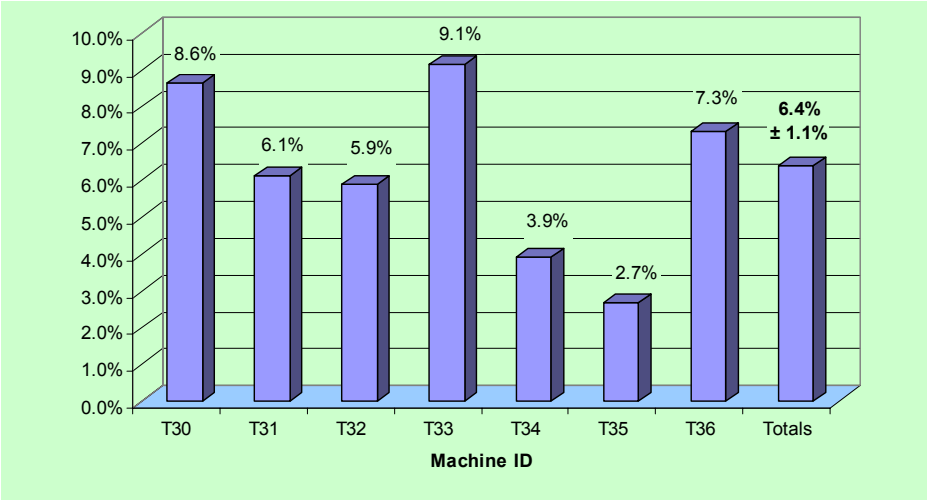

Figure 84. Transfer failure percent per machine

The Figure 85 shows the total number of transfers and the number of transfers with each machine. The runs were not quite equally distributed. All the machines had anyway a significant number of transfers run.

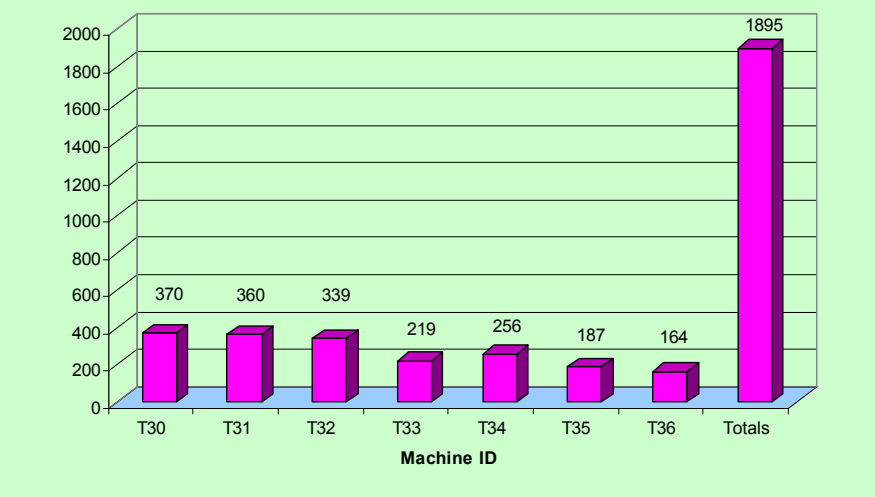

Figure 85. Number of transfers with each machine

5.3.6 Transfer Reliability of the Improved Design

Laboratory tests result with improved design

Based on the data collected from the tests with original cutting and gripping design the construction was improved and in many parts redesigned. The new improved mechanism was first tested in laboratory conditions. It should be noted that these trials were run before developing the auxiliary blade explained earlier and also before the optimized whipping guard was developed and tested. The Table 27 summarizes the results of this trial.

Table 27. Summary of laboratory trials with improved design

	Right to Left	Left to Right	Total
Transfers	227	197	424
Transfer breaks (cutting and gripping)	0	0	0
Transfer whipping (full side)	2	1	3
Fiber mess (full side)	2	4	6
Transfer reliability	100.0% + 0.0% - 1.3%	100.0% + 0.0% - 1.4%	100.0% + 0.0% - 1.0%
Whipping reliability	98.2 ± 1.7%	97.5% ± 2.2%	97.9% ± 1.4%

The same results are shown graphically in Figure 86. The transfer reliability result indicates clear improvement, but there is still room for improvement. The whipping problems here were mainly related to the guard alignment and design, since the runs were short. The fiber was not inspected for the coating damages, which means that there may have been the in-side-end whipping cases, which were missed.

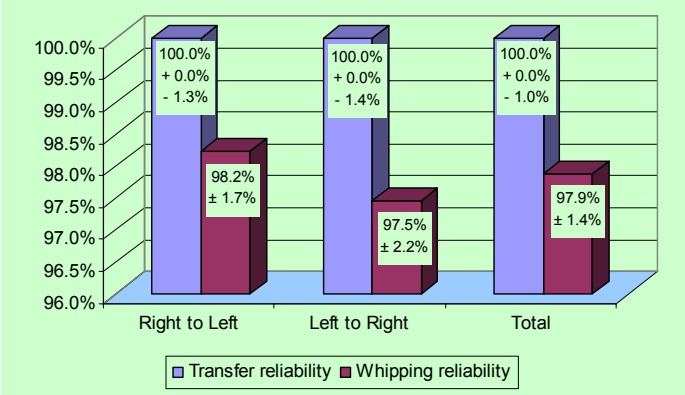

Figure 86. Test results with improved design in lab conditions

Field Test Results with Improved Design

After successful lab trials the same mechanism was used in the same machines in production as earlier. Additionally the new system was tested in another production environment to get more feedback and from different kind of perspective. These are trials one and three in Table 28. Trial two is the runs in controlled environment simulating the production at the speeds beyond the capability of existing production draw towers.

Table 28. Summary of results with improved design

	Trial one 1500 m/min	**Trial two** 1500-3500 m/min	**Trial three** 1500 m/min	**Total**
Transfers	108	90	31	229
Transfer breaks	0	0	0	0
Whipping	0	0	0	0
Over-all reliability	100.0% + 0.0% - 1.9%	100.0% + 0.0% - 2.1%	100.0% + 0.0% - 3.5%	100.0% + 0.0% - 1.3%

These trials were run with the latest mechanisms, auxiliary blade design and whipping guards. The transfer reliability and whipping reliability was not separated, but only over-all reliability was recorded. The results are presented graphically in Figure 87.

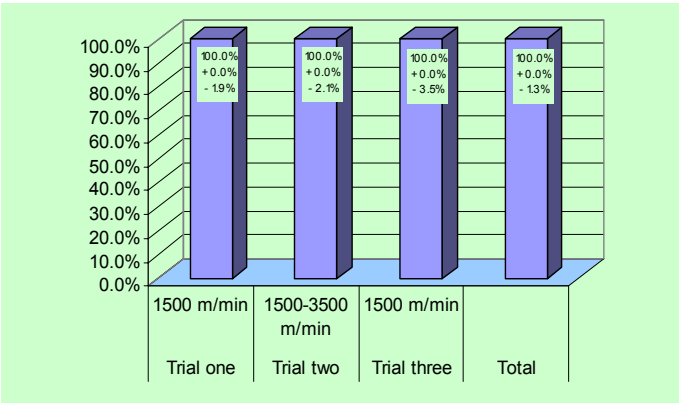

Figure 87. The over-all reliability percent with improved design

The trial two included also break tests and speed variation tests. The fiber breaks were done after rewinding 25 – 30 km fiber on to the reel. The fiber breaks were done by operator cutting the fiber between the pay-off pulleys and the take-up dancer pulleys. The left take-up spool started to whip during the first acceleration to 2,400 m/min, but the reason was that operator didn't clean the scarp flanges properly, but fiber from previous run was found, which caused the whipping. This was not considered to be a failure. When machine was cleaned no such problems occurred. Fiber break test results are in Table 29 having success rate 100% with confidence interval + 0.0%/- 4.4%.

Table 29. Fiber break test results

Speed 1500 m/min Successful (YES/NO)		**Speed 1800 m/min** Successful (YES/NO)		**Speed 2100 m/min** Successful (YES/NO)		**Speed 2400 m/min** Successful (YES/NO)	
1	YES	1	YES	1	YES	1	YES
2	YES	2	YES	2	YES	2	YES
3	YES	3	YES	3	YES	3	YES
4	YES	4	YES	4	YES	4	YES
5	YES	5	YES	5	YES	5	YES

After completing the regular transfer trials and break tests the performance of the transfer was investigated when the fiber speed was varying. The program of the payoff was modified to ramp ± 5 m/s of the test speed at acceleration of 0.2 m/s^2. The reel transfers were done after rewinding 25 – 30 km fiber to the reel. Speed variation test results are in Table 30 showing success rate 100% with confidence interval + 0.0%/- 6.2%.

Table 30. Transfer results at varying speeds.

Speed 1500 m/min Successful (YES/NO)		**Speed 2100 m/min** Successful (YES/NO)	
1	YES	1	YES
2	YES	2	YES
3	YES	3	YES
4	YES	4	YES
5	YES	5	YES

It is concluded that the transfer reliability of the improved design is at satisfactory level at the existing production speeds. The design also shows clear potential for the future high speeds, but to fully confirm this, more high-speed trials in production environment are necessary, as soon as the production speeds reach higher levels.

6 DISCUSSION

As was stated in the introduction, the optical fiber industry is in transition phase. Now in this new situation, when there are still too many manufacturers and the fiber prices are down, probably permanently, the future survivors have started to think about the ways to cut the costs, but at the same time increase the productivity. One answer to this is the combined processes. The important aspect is the upgrade ability, because of excess manufacturing capacity and limited investment possibility.

It's concluded that the continuous combined draw and proof testing process is possible to realize mechanically as described in this work. The solutions to mechanical fiber handling at high speed and to all main challenges were presented. The mechanical behavior and reliability of the fiber in combined process were clarified theoretically and by experiments. This included the solution for break recovery and its reliability, transfer reliability and whipping protection principles. Also the winding process was discussed and solution for high speed fiber winding presented. It is shown that it is possible to achieve high reliabilities with the solutions presented, which is essential, before combined draw and proof testing can even be considered in mass production. To get reliable results many of the trials were performed in production conditions over long period of time.

In this work the focus was on the combined fiber draw and proof testing processes. There are always standards related to industrial manufacturing and especially this is true in case of proof testing. The standards were studied carefully and no limitations were found to combine proof testing to draw. The standards are naturally based on the theoretical research, but very often they follow several years behind the newest theoretical findings. There was a change in the standards about ten years ago. Before that, the dwell time was specified to be 1 s and that was the only concern. In machinery point of view that was inconvenient, since it limited the speed of the proof testing machines or otherwise the test length would not be practical. The situation changed with the new standards, where the dwell time is not specified clearly anymore, but only required it to be long enough. The thinking was that the unload time is more important, since if it is too long it may cause fiber weakening and affect reliability of the fiber. This is where the standards are now 2004.

In this work a literature research about unload time, two-region crack growth, dwell time effect on lifetime, coating effect and effect of the water on the strength was carried out. It is concluded that the unload time is important when speaking about the fiber reliability. The approach has been that the unload time is a machine property by capstan design, where the line speed and the contact length of the belt determines the unload rate. A new approach was suggested where the unload time is a material property, where the fiber is considered to be a spring from which the load is released rapidly after proof capstan. Similarly using this approach it can be seen that

the loading of fiber is the faster the shorter the test length. This would not then be limiting the machine design at all, but the short test length and possibly longer contact lengths in capstans are possible. Literature research also pointed out that when the proof testing cycle was measured with Bragg gratings the loading occurred right after entry capstan and unloading occurred after exit capstan, which supports the new approach well.

As mentioned, the standards are not specifying the dwell time clearly. Theoretically the dwell time has, however, and important role in lifetime prediction of optical fiber. The finding here is that the shorter dwell time is possible to compensate by using higher proof stress and get the same failure probability. This is an important finding, since reliable break recovery system requires shorter test length and therefore shorter dwell time than earlier.

The two-region crack growth theory, which is not introduced in standards, was discussed as well. This theory states that depending on the unload rate the crack growth may happen in two region, where the slopes are different. If the unload rate is low enough, the crack first grows following region II slope, but eventually starts to follow the slope of the region I effecting on the strength of the fiber. The important notion is that if the unload rate is high enough the strength decrease during unloading shouldn't happen.

The effect of the coating was also studied. The standards recognize that the coating carries a part of the load, but the share is calculated simply by using the ratio of the cross sectional areas and Young's modulus. When the coating effect have been studied it has been found that at high load rates the coating may carry a substantially higher part of the load, which must be taken into a consideration at short test length. This may then also require elevated proof tension.

An important finding was the effect of the water on the strength of the fiber. In fact this may be the biggest obstacle in front of combined draw and proof testing. The theory suggests that the strength of the fiber is significantly higher just after draw than approx. 1 hour later. For the practical reasons the proof testing is nowadays always done more than 1 hour after fiber draw. This is not the case in on-line proof testing where the time between draw and proof testing is less than 1 s. Some preliminary solutions to overcome this problem were suggested, but this is definitely a field where further studies and investigations are needed.

One important part of this thesis was creating general models for critical process elements. The target was to keep the models as simple as possible and include only the basic phenomena. Eventually what happened was that the models may include some negligible terms, like e.g. fiber bending torque, which is small compared to many other terms. To prove that the independent process elements work when joined together, they were programmed in a complete simulation model for combined draw and proof testing process. All critical process elements were also tested and the parameters found were used as inputs in the program. By combining purely theoretical

mathematical models and empirical test results it is possible to predict the tension behavior accurately through whole process. The principle of process elements makes it possible to combine different processes easily and without any special software, but normal office or laboratory softwares are suitable, if the computer has enough capacity.

The tests that were carried out for modeling purpose included; a turning wheel test, a capstan test, a take-up test and a dancer test. As was found in results section a good match between model and reality was found. Turning wheel torque could be modeled very accurately and at low error margins. Take-up torque and capstan torque tests showed small difference between modeled curves and measured curves. Both the measured curves gave higher torque than model suggested at low speeds. The difference was outside of the measurement error, which indicates that there was some non-linearity in the servo drive's torque behavior.

Some clear differences between the measured and calculated dancer curves could be seen. The measured dancer position curve followed the calculated curve when the fiber enters the bump. After the turning point the dancer approached the home position slower than predicted with the calculation. The measured tension curve had clearly sharper form than the calculated. The difference between calculation and the real life was the machine control algorithms. The model takes into account only the mechanical phenomena like inertia, bearing friction and air resistance. The machine, however, starts to adjust the rotating speed of the take-up according to the changes in dancer position. In real life PID algorithm must be used or the dancer starts to oscillate at certain speeds. It is concluded that the model is accurate enough and can be used to predict the maximum and minimum tensions and dancer positions, which were quite near of the measured.

In addition to the process element trials, some critical components of a combined process were tested thoroughly. These included proof tension measurement, break recovery reliability and winding quality trials. It was found out that a pivoting joint type of proof tension measurement gave good results. The error margins in these trials were quite high, but even the highest and lowest end were inside the specification. Break recovery trials gave a clear total result where, the belt system was the best. In some trials the error margins were quite big compared to the actual measured value. This indicates that the sample size of those trials was too small. This was found out afterwards, when further testing was not possible anymore.

Winding trials included algorithm testing, whipping protection and transfer reliability. The winding algorithm and transfer reliability were mostly tested in production, where the number of samples was statistically high enough. As result of these trials a new algorithm and a transfer mechanism were developed. The whipping protection trials were run in laboratory conditions and the number of trials remained relatively low. Therefore the error margins in these trials were also quite high and the result is not indisputable.

The future work will include more experimental testing with a second prototype, which will combine the critical components into one machine. The overall reliability depends on how well these critical components are integrated to each other.

7 SUMMARY

The use of optical telecommunication fiber has steadily increased over the past two decades. The driving force has been the data transfer capacity. The fiber manufacturing has traditionally had three different process phases: Preform Manufacturing, Fiber Draw and Proof Testing. Proof testing does not add any value to the fiber, but it must be done for quality assurance. Combining draw process and proof testing would create saving potential. The nature of proof test is that the fiber breaks randomly on a weak spot. If proof test is combined to the fiber draw the ultimate goal is to be able to catch the fiber end after the break and to be able to thread it through proof test zone all the way to the take-up spool.

Fiber manufacturing processes were described more detailed. The finished preform is drawn to optical fiber in a drawing tower. The preform turns to fiber in a furnace at high temperature. Typically the preform diameter is 60-100 mm and length 1.5 – 3.0 m, but on-going development focuses on diameters around 150 mm. The bare glass is coated with two UV-acrylate coatings. One drawing nowadays produces 200-1,000 km fiber from one preform, but on-going development targets lengths even over 3,000 km from one preform. The height of the tower is usually between 20 and 30 m depending on the desired drawing speed.

Nowadays there are still two different methods in use for creating the proof tension. First is a braked-capstan type. The desired tension on the fiber is caused by two capstans, which have a small speed difference. The second is a dead-weight type, where the load is applied by using an additional dead-weight pulley between capstans. The fiber is tested over its entire length. The typical testing speed is between 1,200 and 2,100 m/min.

There have been significant developments in the general understanding of fiber reliability, and especially the role of proof testing, over the last two decades. The latest theory and standards, which the industry follows, highlight the following aspects: A). The dwell time of the proof testing cycle has minor effect on the final minimum strength of proof tested fiber. B). There is always a decrease in strength during the proof testing cycle; load, dwell and unload, in a non-ideal environment. C). The operation of the proof tester must be designed to minimize the decrease in strength. D). Since a decrease in strength does in fact occur, it must be monitored and reported.

The dwell time does, however, cause crack growth. Therefore a higher initial strength is needed to survive a longer dwell time. Longer dwell time, does not produce stronger fiber, but affects the

lifetime prediction. Failures during unloading are of special interest because the strength at failure is at that point below the proof stress.

The approach has been that the unload time is a machine property by capstan design, where the line speed and the contact length of the belt determine the unload rate. A new approach was suggested where the unload time is a material property, where the fiber is considered to be a spring from which the load is released rapidly after proof capstan.

The two-region crack growth theory, which is not introduced in standards, was discussed as well. This theory states that depending on the unload rate the crack growth may happen in two regions, where the slopes are different.

The effect of the coating was also studied. The standards recognize that the coating carries a part of the load, but the share is calculated simply by using the ratio of the cross sectional areas and Young's modulus. When the coating effect have been studied it has been found that at high load rates the coating may carry a substantially higher part of the load, which must be taken into a consideration at short test length. This may then also require elevated proof tension.

An important finding was the effect of the water on the strength of the fiber. The theory suggests that the strength of the fiber is significantly higher just after draw than approx. 1 hour later. For practical reasons the proof testing is nowadays always done more than 1 hour after fiber draw. This is not the case in on-line proof testing where the time between draw and proof testing is less than 1 s.

An approach for modeling tension behavior in combined draw and proof testing process mathematically was introduced. The models are general and can be used to model all fiber finishing processes. The problem of modeling whole fiber finishing processes is solved by the assumption that the processes can be divided into several primitive elements. During the process, these elements may then dynamically interact with each other. The possible outputs of the aggregate models are tension levels and the tension variation of the fiber, the velocity variations of the rollers and the position changes of the dancers. The modeling of free fiber between elements is based on the observation that the tension in a fiber span depends on its past value, the tension in the next span, and the velocity difference between the two ends of the free span.

A universal simulating tool was generated to predict the tension behavior of the fiber. The created program uses the general models described. As a result of the simulation the fiber tension in all free fiber spans is solved. The same is possible to present in frequency domain using Fourier transform. Using tension information calculated with simulation program the maximum stress level of the fiber in each fiber span can be calculated. Additionally the stress when the fiber is subjected to bending in process elements is calculated.

It was important to make necessary experiments to verify the theory. First draw tension experiment was carried out. Draw tension was measured to find the relationship between line speed and draw tension before capstan. The measurements were carried out at various speeds in several draws. The measurement result was not analysed more in this study, but it was used as it was as input for the simulation.

The second part was the comparison of the conventional proof tension measurement and the new method needed for the combined processes. The sensor signal of the new linear bearing system was measurable, but the tension variation according to these measurements was too high. After finalizing the trials with linear bearing system, a new prototype based on pivoting joint design was tested. The results indicated that the variation was now below the limit ±5%. The conventional method to measure the tension with a wheel gave better result, but pivoting joint design eliminated the majority of the vibration seen with linear bearing system.

After this the effect of the different process elements; turning wheel, capstan, take-up and dancer movement were evaluated. These trials were realized to investigate the effect of the process element on the fiber tension. These were then compared to the theoretical models, which were adjusted according to these experiments. The result shows that there is a good match with turning wheel model and practise. There was quite good match between capstan model and practice at higher speeds, but the behavior at low speed was slightly different. The same was true with take-up as well. Dancer model took in to account dancer position, bearing friction, past tension values, air resistance and inertia. Some clear differences between the measured and calculated curves could be seen. The measured dancer position curve followed the calculated pretty well when the fiber entered the bump. After the turning point the dancer approached the home position slower than predicted with the model. The measured tension curve had clearly sharper form than the calculated.

Two different methods to survive proof testing break were introduced and tested. The first method uses tubes between capstans to guide the fiber end. The second is a combination of tubes and belt conveying system.

The first trial focused on the right material selection for the channel needed to guide fiber after fiber break between the entry capstan and exit capstan. PTFE was the best material. The second test series focused on removing the negative effect of static electricity on conveying the fiber in the tube. The best result was achieved with special tube structure, where around the inner PTFE tube there was ionized pressurized air.

The other alternative for break recovery was tested after tube system, since the result was not satisfactory. The prototype of belt system was tested without tube-guide, which will further improve the design later. The belt system was assembled between entry and exit capstans. The break recovery success rate was tested similarly to

the tube system at different line speeds. The success rate showed clear improvement compared to the tube system.

Winding package quality is essential in proof testing machines and in future's high-speed online proof testing machines even more challenging. The trial to investigate the efficiency of the original winding algorithm was carried out in normal production gathering the rewinding percent information during long period. The reported failure percent from that test period was nearly 30%, which is rather high in modern production environment. The efficiency of the improved algorithm to reduce the steps was confirmed first by recording limited amount of runs in laboratory conditions. This gave very low failure percentage 1.3% compared to the original 30%. The testing continued at fiber plant using the same methods than in first trial series. The reported failure percent from the production was 4% in this second trial period.

The take-up needs to be equipped with means to prevent whipping. Several trials focused on preventing whipping phenomenon; the whipping guard trials, trials to investigate the in-side-end whipping and testing for invented auxiliary blade.

The first test series were focused on the proper whipping guard design. A prototype (called "spiral"), suitable for 25 km or 50 km standard delivery spools, was manufactured and tested. As the trials proceeded it became clear that the spiral design did not have optimal performance. A new prototype (called "round") was designed and manufactured based on the "spiral" trial results. The best result achieved was 95% protection reliability. The performance can be further improved by small design changes.

Trials to investigate in-side-end whipping were carried out, since occasionally it was a problem with existing gripping and cutting design of the dual take-up. These whippings occurred typically after several tens of kilometers were run after the transfer. As it turned out a high-speed camera was needed to find the cause to this whipping phenomenon. Four runs were photographed and recorded, where the in-side-end got loose causing whipping. There the short fiber tail was seen for the first time, which was sticking out from between the gripping flanges and hitting on to the transfer mechanism causing eventually fiber break.

After finding the reason for in-side-end whipping a prototype was designed and built to prevent this from happen. The suggested solution was an auxiliary blade to cut the short fiber tail. The auxiliary blade removed the problem completely according to these trials. This was confirmed later as feedback from customer running production with this new blade.

The transfer reliability was tested with a separate take-up module. The same principle only slightly modified is used in online proof testing module needed for combined continuous process.

The first test period was realized at customer's fiber plant, where normal production speed was 1,500 m/min. After this first test period the design was improved to achieve higher reliability. The new design was tested first in laboratory, after which the same was repeated at the same factory as before and additionally also in another fiber factory. All these tests were carried out at lower speeds than needed for online proof tester eventually. To simulate this requirement an additional test series was run at high speeds in laboratory conditions for future need.

The result was that the transfer reliability of the improved design is at satisfactory level at the existing production speeds. The design also shows clear potential for the future high speeds, but to fully confirm this, more high-speed trials in production environment are necessary as soon as the production speeds reach higher levels.

REFERENCES

Apone, S. Chiaro, L. and Grego, G. 1995. Viscoelastic Properties of Optical Fibers Coating. PITVII. p. 331 – 339.

Baker, L. K. 1999. Mechanical Reliability Modeling of Optical fibers. In: Wire & Cable Technology International. November 1999. p. 40 – 41.

Baker, L. K. Bhatia, V. Glaesemann, G. S. Marro, A. A. and Mansfield, C. Fiber Bragg Gratings for Stress Fiels Characterization inside a Connector. In: SPIE Conference proceedings on Optical Fiber Reliability and Testing. Boston, MA. SPIE Vol. 3848. September 1999. p. 207 – 211.

Bouten, P.C.P. 1987. Lifetime of Pristine Optical Fibres. Eindhoven: TU Eindhoven. 140 p.

Bracewell, R. 1999. The Fourier Transform and Its Applications, 3rd. ed. New York: McGraw-Hill, 1999. 640 p.

Cain, M. B. Kannabiran, R. and Squires, E. M. 1991. Optical Fiber Fabling. United States patent 5,046,815. US patent & trademark office. 8 p.

Capouilliet, S. Smith, J. A. Walter, D. J. Glaesemann, G. S. Kohnke, G. E. and Irion, R. D. A Fiber Bragg Grating Measurement System for Monitoring Optical Fiber Strain. In: International Wire & Cable Symposium proceedings 2001 (50: Orlando, FL 12 - 15.2001). p. 240-248.

Castilone, R. J. Mechanical Reliability: Applied Stress Design Guidelines. WP5053. Corning, NY. Corning Inc. Issued February 1999. 4 p.

Conte, S. D. and de Boor, C. 1980. Elementary Numerical Analysis (3rd ed.), McGraw-Hill.

Corning. 2004. Corning® SMF-28e® Optical Fiber Product Information. PI1344. Corning, NY. Corning Inc. Issued February 2004. 4 p.

CRS Creative Research Systems. 2004. The Survey System/Research Aids: Sample Size Calculator. www.surveysystem.com\sscalc.htm. 26 April 2004. 4 p.

CRU Group. 2003a. Optical Fibre & Fibre Optic Cable Monitor. January 2003. CRU International Ltd. 12 p.

CRU Group. 2003b. Optical Fibre & Fibre Optic Cable Monitor. July 2003. CRU International Ltd. 12 p.

CRU Group. 2003c. Worldwide Telecom Cables Six-monthly Market Report. July 2003. London: CRU International Ltd. 105 p.

DSM Desotech. 2001a. DeSolite® Optical Fiber Coatings. DeSolite® 3471-1-129. Optical Fiber Primary Coating. Data sheet. Issue date 07/2001. 5p.

DSM Desotech. 2001b. DeSolite® Optical Fiber Coatings. DeSolite® 3471-2-136. Optical Fiber Secondary Coating. Data sheet. Issue date 07/2001. 5p.

Fuller, E. R. Wiederholm, S. M. Ritter, J. E. Oates, P. B. Proof Testing of Ceramics, Part 2: Theory. Journal of Material Science 15 (1980). P. 2282-2295.

Glaesemann, G. S. 1991. The Effect of Proof Testing on the Minimum Strength of Optical Fiber. In: International Wire & Cable Symposium proceedings 1991 (40: New Jersey, 18-21.11.1991). p. 582-586.

Glaesemann, G. S. 1997. Designing for the Mechanical Reliability of Optical Fiber and Components. Educational short cources lecture material. In: International Wire & Cable Symposium 1997 (46: Philadelphia PA, November 1997).

Glaesemann, G. S. 1995. In: Proceedings of Optical Network Engineering and Integrity. SPIE Vol. 2611. Ed. Yuce, H. Paul, D. and Greenwell, R.A. Boston: SPIE. p. 38.

Glaesemann, G. S. 1999. Advancements in Mechanical Strength and reliability of Optical Fibers. In: Proceedings of the SPIE Critical Reviews Vol. CR 73. Reliability of Optical Fibers and Optical Fiber Systems. (Boston MA, 20-21 September 1999). 23 p.

Glaesemann, G. S. Castilone, R. J. The Mechanical Reliability of Corning® Optical Fiber in Bending. WP3690. Corning, NY. Corning Inc. Issued September 2002. 4 p.

Glaesemann, G. S. and Helfinstine, J. D. 1993. Benign and Adverse Environments. In: Proceedings to Fiber Optics Reliability and Testing. SPIE Vol. 2072. Ed. Paul, D. and Yuce, H. Boston: SPIE. p. 95.

Griffioen, W. 1994. Optical Fiber Mechanical Reliability. Eindhoven: Eindhoven University of Technology. 210 p. ISBN 90-386-0494-7.

Hanson, T. A. and Glaesemann, G. S. 1997. Incorporating Multi-region Crack Growth into Mechanical Reliability Predictions for Optical Fibers. Journal of Material Science 32 (1997). Chapman & Hall p. 5305-5311.

Harris, T.A. 1984. Rolling Bearing Analysis. 2nd ed. New York: John Wiley & Sons. 565 p. ISBN 0-471-79979-3.

IEC International Standard. 2001. Optical Fibres – Measurement Methods and Test Procedures - Fibre Proof Test, IEC 60793-1-30. 1st Ed. Geneva, Switzerland: International Electrotechnical Commission. 21 p.

IEC International Standard. 2002. Optical Fibres – Power Law Theory, IEC TR 62048. International Electrotechnical Commission. 68 p.

ITU-T Recommendation. 2002. Definitions and Test Methods for Linear, Deterministic Attributes of Single-mode Fibre and Cable, G.650.1. Geneva, Switzerland. International Telecommunication Union. Telecommunication Standardization Sector. 60 p.

Jacobs, J. M. Suggested Guidelines for the Handling of Optical Fiber. WP3627. Corning, NY. Corning Inc. Issued December 2001. 7 p.

Kapron, F. P. 1999. The Influence of Prooftest Dwelltime on Fiber Reliability. In: International Wire & Cable Symposium proceedings 1999 (48: Atlantic City, NJ 15 – 18.11.1999). p. 55-60.

Karppo, J. S. 1974. Puolauslaitteen jaon automaattinen säätö. Kuulutusjulkaisu 47976. Finland: Patentti- ja rekisterihallitus. 7 p.

KMI Research. 2003. Trends in Fiber Production and Equipment for Preform and Draw-tower Production Processes. Providence, RI. 23 p.

Kouzmina, I. Chien, C-K. Bell, P. and Fewkes, E. Corning® CPC® Protective Coating An Overview. WP3703. Corning, NY. Corning Inc. Issued July 2003. 5 p.

Lawn, B. R. 1993. In. Fracture of Brittle Solids. 2nd Ed. Cambridge University Press.

Lin, K. C. Campbell, M. K. 1994. A Computer-based Analysis Program for Multi-span Web Transport Systems WTS 6.0; User's guide. Oklahoma: Web Handling Research Center. 102 p.

Lipponen, M. 2001. Optisen kuidun vetoprosessiin yhdistetyn lujuustestilaitteen kehittäminen. Master's Thesis, Faculty of Machine Building. University of Oulu. 75 p.

Lipponen, M. and Turunen, H. K. 2002. Investigation of Possibilities for the Proof Testing of Optical Fiber Immediately after Draw. In: International Wire & Cable Symposium proceedings 2002 (51: Orlando, FL 18 - 21.11.2002). p. 357 – 361.

Mack, R. Market update; Fiberoptic Cable. In: Optical Fiber Conference 2003 (19th annual executive briefing & breakfast 25.3.2003) Atlanta, GA: KMI Research. 10 p.

Mattila, T. 1997.Reliable High-Speed Proof Testing of Optical Fiber. In: Interwire 97 (67th annual WAI convention, April 5-11, 1997). Boston: WAI. p. 166 – 172.

Mrotek, J, Matthewson, M. and Kurkjian, 2001. C. Diffusion of Moisture Through Optical Fiber Coatings. In: Journal of Lightwave Technology. 19 Vol. 7. p. 988 – 993.

Overton, B. and Orcel, G. 1995. The Effects of Coating Characteristics on the Determination of the Dynamic Fatigue Parameters for Optical Fibers. PITVII. p. 341–350.

Reeve, M. H. and Cassidy, S. A. 1987. Optical Fibre Transmission Line. United States patent 4,691,896. US patent & trademark office. 11 p.

Reid, K. N Shelton, J. J. Shin, K-H. 1989. Distributed Control of Tension in a Web Handling System. Oklahoma: Web Handling Research Center (Project Report 04/89). 34 p.

Shelton, J .J. 1994. Sensing of Web Tension by Means of Roller Reaction Forces. Oklahoma: Web Handling Research Center (Project Report May 1994). 34 p.

TIA/EIA Standard. 1999. FOTP-31 Proof Testing Optical Fibers by Tension, TIA/EIA-455-31C. Arlington, VA: Telecommunications Industry Association, Standards and Technology Department. 17 p.

Turunen, H. K. 1997a. Tension Behavior of Optical Fiber in Finishing Processes. In: Interwire 97 (67th annual WAI convention, April 5-11, 1997). Boston: WAI. 12 p.

Turunen, H. K. 1997b. Mechanical Behavior of Optical Fiber in Finishing Processes. Licentiate's thesis. Espoo: Helsinki University of Technology. 104 p.

Turunen, H. K. 1998. The Effects of Winding Parameters on Optical Attenuation Measured from Wound Fiber. In: Euro Cable proceedings (Communication Cables and Related Technologies) 1998. IOS Press. 7 p.

Turunen, H. K. Mattila, T. and Sinkko, J. 2000. Combined Optical Fiber Draw Process and Proof Testing: A Unique Method to Increase Productivity. In: International Fiber & Cable Symposium proceedings 2000 (49: Atlantic City, NJ 13 - 16.11.2003). p. 449 - 454.

Turunen, H. K. and Mäkelä, K. 2002a. Rasitusmenetelmä ja laitteisto optisille kuiduille. Patenttijulkaisu FI 108754 B. Finland: Patentti- ja rekisterihallitus. 14 p.

Turunen, H. K. and Mäkelä, K. 2002b. Proof Testing Method and Apparatus For Optical Fibers. International patent application WO 02/35210 A1. 16 p.

Turunen, H. K. and Mäkelä, K. 2003. Proof Testing Method and Apparatus for Optical Fibers. United States patent application 200301677855. US patent&trademark office. 13 p.

Wells, J. P. Aidan, P. J. and Beverley, A. P. 2000. Optical Fibre Assemblies and Duct Therefor. United States patent 6,022,620. US patent & trademark office. 10 p.

The profitability analysis is started by calculating the fiber yield and profit of manufacturing equipment investment based on existing technology. To simplify the calculation only one draw line is used in this exercise. The specifications in the example presented in Table 31 represent state of the art fiber manufacturing equipment commercially available to any manufacturers. The result is approx. 220 thousand fiber-km and profit 500 kEUR.

The Table 32 presents similar calculation for the future equipment with combined continuous fiber draw and proof testing process. When the fiber yield and profit of the state of the art system and future system are compared, it is seen a clear difference in favour of the combined draw and proof testing processes. Using all the same assumptions, but the latter having combined processes, the yield is approx. 340 thousand fiber-km and profit 760 kEUR. This calculation suggests thus more than 50% improvement in fiber yield and profitability.

Table 31. Profitability of state of the art fiber manufacturing equipment

FIBER DRAW (ONE PREFORM)		INTERMEDIATE SPOOL HANDLING		PROOF TESTING	
Draw speed [m/min]	1,500	Spool unloading [min]	1	Proof testing speed [m/min]	2,100
Preform size [km]	1,000	Measurements [min]	5	Payoff spool loading [min]	1
Draw setup time [min]	60	Spool transfer to post draw area [min]	5	Therading from payoff to take-up [min]	5
Take-up spool size [km]	250	**Total intermediate handling time [min]**	**44**	Take-up spool size [km]	50
Take-up start scrap [m]	10			Take-up spool change [min]	1
Transfer reliability	99%	**REWINDING**		Winding quality	99%
Scrap in failured transfer [km]	10	Rewinding speed [m/min]	1,000	Scrap per proof tested spool [m]	10
Extra work time in failure [min]	15	Payoff spool loading [min]	1	Proof break rate [1/1000 km]	10
Winding quality	99%	Therading from payoff to take-up [min]	5	Proof break scrap [m]	50
Whipping protection reliability	99%	Scrap per rewound spool [m]	10	Whipping protection reliability	99%
Scrap in whipping [km]	10	Rewound draw spools (quality+whipping)	0.1	Scrap in whipping [km]	2
Transfers per preform	3	Rewound draw length [km]	20	Payoff spools	4.04
Spools per preform	4.04	Rewound proof test spools (Quality+whipping	0.4	Proof breaks	10
Total draw time [min]	**727**	Rewound proof tested length [km]	10	Take-up spools	30.2
Total draw scrap [m]	**670**	**Total rewinding time [min]**	**33**	**Total proof testing time [min]**	**531**
		Total rewinding scrap [m]	**5**	**Total proof testing scrap [m]**	**1,002**
FINAL SPOOL HANDLING		**TOTALS FOR ONE PREFORM**			
Quality mesurements [min]	5	**Total processing time [min]**	**1,637**		
Spool handling [min]	5	**Total labour cost [EUR]**	**546**		
Total final handling time [min]	**302**	**Total scrap length [m]**	**1,677**		
		Scrap cost [EUR]	**25**		
GENERAL ECONOMICS		**Preform yield [km]**	**998**		
Hours per shift [h]	8				
Shifts per day	3	**FIBER YIELD**			
Work days per year	250	**Fiber yield per man-day [km]**	**878**		
Labour cost [EUR/h]	20	**Fiber yield per man-year [km]**	**219,435**		
Fiber price [EUR/km]	15				
SM%	15%	**PROFITABILITY**			
Machine cost [EUR]	1,700,000	**Profit per day [EUR]**	**1,975**		
		Profit per year [EUR]	**493,730**		

To know all the aspects of equipment investment the pay back time of different alternatives needs to be evaluated. To be able to do that, the cost of investment needs to be estimated. The problem is simplified by assuming that no new buildings are needed and that the infrastructure and utilities are available. The cost now includes thus only the machine cost and installation and start-up costs.

The pay back time for different investment alternatives is shown in the Figure 88, which clearly points out the attractiveness of this concept even in the current world of over capacity. Right now when the capacity is not a problem an upgrade is an attractive alternative. With relatively small investment it is possible to increase the

profitability. In the future when the capacity is fully utilized it is more beneficial to invest a combined continuous draw and proof testing process. The graph shows the needed investment for all three possibilities; new standard equipment, new combined process and upgraded equipment. The profit is calculated for all these alternatives as well. Upgraded process gives the investment money back as soon as 2.23 years, which is an attractive result now when the existing capacity is not fully utilized. When new capacity is needed combined process pays back in 2.88 years compared to 3.44 years with standard equipment.

Table 32. Profitability of future's fiber manufacturing equipment

FIBER DRAW (ONE PREFORM)		REWINDING		TOTALS FOR ONE PREFORM	
Draw speed [m/min]	1,500	Rewinding speed [m/min]	1,000	**Total processing time [min]**	**1,058**
Preform size [km]	1,000	Payoff spool loading [min]	1	**Total labour cost [EUR]**	**353**
Draw setup time [min]	60	Therading from payoff to take-up [min]	5	**Total scrap length [m]**	**5,065**
Take-up spool size [km]	50	Scrap per rewound spool [m]	10	**Scrap cost [EUR]**	**76**
Take-up start scrap [m]	10	Rewound draw spools (quality+whippin	0.60	**Preform yield [km]**	**995**
Transfer reliability	99%	Rewound draw length [km]	20		
Scrap in failured transfer [km]	10	**Total rewinding time [min]**	**24**	FIBER YIELD	
Extra work time in transfer failure [min]	15	**Total rewinding scrap [m]**	**6**	**Fiber yield per man-day [km]**	**1,356**
Winding quality	99%			**Fiber yield per man-year [km]**	**338,951**
Whipping protection reliability	99%	FINAL SPOOL HANDLING			
Scrap in whipping [km]	2	Quality mesurements [min]	5	PROFITABILITY	
Proof break rate [1/1000 km]	10	Spool handling [min]	5	**Profit per day [EUR]**	**3,051**
Break recovery reliability	99%	**Total final handling time [min]**	**302**	**Profit per year [EUR]**	**762,641**
Scrap in failured recovery [km]	10				
Extra work time in recovery failure [min	15	GENERAL ECONOMICS			
Proof break scrap (15 s) [m]	375	Hours per shift [h]	8		
Proof breaks	10	Shifts per day	3		
Transfers per preform	28.9	Work days per year	250		
Spools per preform	30.20	Labour cost [EUR/h]	20		
Total draw time [min]	**733**	Fiber price [EUR/km]	15		
Total draw scrap [m]	**5059**	SM%	15%		
		Machine cost [EUR]	2,200,000		

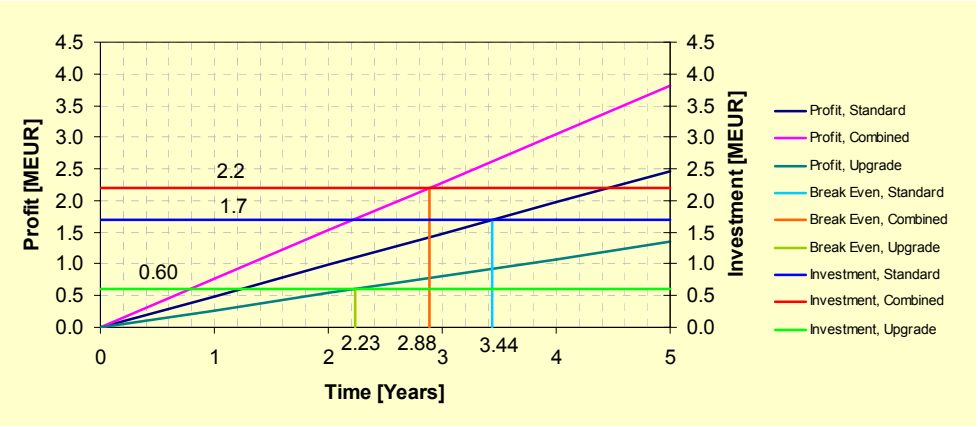

Figure 88. Break even for investment

It's estimated that the amount of fiber installed worldwide will increase from 55 million fiber-km in 2003 to 73 million fiber-km in 2008 (Table 33). This level of growth will not be enough to change the situation of excess fiber-manufacturing capacity, which has affected the world since 2001. Estimated worldwide capacity was approx. 100 million fiber-km in 2003. This means there is likely to be significant excess capacity and continued competition on the basis of price and fiber performance features among the fiber suppliers.

Table 33. Single-mode and multimode cabled-fiber demand by region, 2002-2008

Region	2002	2003	2004	2005	2006	2007	2008
North America	12,275	11,583	12,570	13,619	14,755	16,081	17,480
Western Europe	7,587	7,790	8,345	9,060	9,865	11,075	12,053
Eastern Europe	1,852	1,659	1,834	2,180	2,443	2,631	2,839
Asia-Pacific	31,390	30,915	30,253	31,141	32,316	33,966	35,483
Emerging Markets	3,080	3,262	3,406	3,604	3,908	4,262	4,635
TOTAL	**56,184**	**55,209**	**56,408**	**59,604**	**63,287**	**68,015**	**72,490**

The mix of fiber types in the market is changing as well. One significant change is a reduction in the amount of non-zero dispersion-shifted fiber (NZDSF) or G.655 fiber installed worldwide. In the years of peak demand, about 2000, NZDSF was 15% to 20% of total fiber demand. This has dropped to levels of 5-10%, and shows no potential for a major ramp-up in volume. In the peak years, NZDSF was manufactured at rates of about 15 million fiber-km per year, and this has fallen below 5 million fiber-km in 2002 and 2003.

The situation of low-water-peak fiber (LWPF), however, is markedly different. LWPF was introduced in 1998. Today the suppliers have almost entirely eliminated any price premium for LWPF. The outlook for the next five years is for LWPF to ramp up from a level of about 20% to more than 80% of all single-mode fiber. Fiber demand by type is in Table 34.

Table 34. Cabled-fiber demand by type, 2002-2008

Fiber Type	2002	2003	2004	2005	2006	2007	2008
NZDSF	2,498	2,000	2,000	2,200	2,500	3,000	3,500
CSMF	47,354	38,668	31,619	26,024	16,373	11,046	9,565
LWPF	3,583	11,595	19,606	27,934	40,668	49,877	54,961
MMF	2,749	2,946	3,183	3,446	3,746	4,092	4,464

The over 20-year history of fiber prices is one of consistent price decreases due to process improvements, higher volumes, and other phenomena when new technology is introduced. This trend of falling prices has been interrupted twice since 1990 by fiber shortages. During these two-to-three years shortage intervals, fiber prices remained stable.

The most recent shortage ended in 2001, and prices have fallen sharply. In some quarters and in some regions, fiber prices dropped 10% per quarter. Single-mode fiber prices are now below $0.02 per meter, or $20.00 per km worldwide, and below $0.015 per meter or $15.00 per km in some regions.

Although manufacturing costs are not public information, prices below $15.00 per km are considered to be approaching or even lower than the minimum cost structure of some manufacturers. As a result of this price pressure, some manufacturers have abandoned fiber production, or have pursued cost-cutting strategies, such as drawing fiber from purchased performs or trying to increase the overall efficiency.

LWPF prices have dropped and presently are at parity with CSMF. Although the LWPF suppliers initially had hoped to capture a price premium relative to CSMF, competitive and market factors have led them to lower prices along with those of CSMF. The estimated price trend is in Table 35.

Table 35. Single-mode fiber price comparisons, 1999 – 2008, $/km

S-M Fiber Type	1999	2000	2001	2002	2003	2004	2005	2006	2007	2008
NZDSF	120	106	80	64	57	45	44	42	40	40
CSMF	35	37	35	23	18	15	15	14	13	13
LWPF	49	41	39	23	18	15	15	14	13	13

Recently published information for year 2004 indicates even lower fiber prices than forecasted. In some regions the price can be as low as $12.00 per km.

APPENDIX 3. User Inputs for Simulation Model

GENERAL			
Line speed	v_{set}	[m/min]	3000
Fiber diameter	d_f	[m]	0.000245
Cladding diameter	d_c	[m]	0.000125
Dencity of silica	ρ_c	[kg/m^3]	2200
Dencity of acrylate	ρ_f	[kg/m^3]	1129
Young's modulus of glass	E	[GPa]	73.2
Proof tension set	F_{pset}	[N]	8.95
Draw tension set	F_{dset}	[N]	3.00
Winding tension set	F_w	[N]	0.50
Ramp time	Δt	[s]	20
Initial time	t_i	s	0.000
Machine status *)	q	-	0
Non-linearity constant	α	-	6
DANCER WHEEL (3)			
Diameter	D_3	[m]	0.090
Mass	m_3	[kg]	0.190
Bearing speed coefficient	K_{b3}	[Nms$^{2/3}$]	0.0000101400
Bearing load coefficient	K_{bl3}	[Nm]	0.0000367771
Fiber bending coefficient	M_{W3}	[Nm]	0.0000000000
Air resistance coefficient	K_{a3}	[Nms^2]	0.0000000024
Mass center x	x_{c3}	[m]	0.00010
Mass center y	y_{c3}	[m]	0.00000
Start angle	ϕ_3	[rad]	0.00000
ENTRY CAPSTAN (5)			
Diameter	D_5	[m]	0.191
Mass	m_5	[kg]	1.000
Bearing speed coefficient	K_{b5}	[Nms]	0.0072917080
Bearing load coefficient	K_{bl5}	[Nm]	0.0883309466
Fiber bending coefficient	M_{W5}	[Nm]	0.0000000000
Air resistance coefficient	K_{a5}	[Nms^2]	0.0000002831
Mass center x	x_{c5}	[m]	0.00010
Mass center y	y_{c5}	[m]	0.00000
Belt pulley 1 diameter	D_{51}	[m]	0.090
Belt pulley 2 diameter	D_{52}	[m]	0.090

TAKE-UP (1)			
Flange diameter	D_1	[m]	0.235
Barrel diameter	d_1	[m]	0.158
Top of flange width	W_{t1}	[m]	0.202
Barrel width	W_{b1}	[m]	0.169
Flange angle	β	[deg]	66.80
Package clearance	h	[m]	0.012
Empty reel mass	m_r	[kg]	0.700
Laying factor (0.7865…0.9082)	K_L	-	0.846148923
Bearing speed coefficient	K_{b1}	[Nms$^{2/3}$]	0.0024305693
Bearing load coefficient	K_{bl1}	[Nm]	0.0603232588
Fiber bending coefficient	M_{W1}	[Nm]	0.0000000000
Air resistance coefficient	K_{a1}	[Nms^2]	0.0000012653
Mass center x	x_{c1}	[m]	0.00010
Mass center y	y_{c1}	[m]	0.00000
Start angle	ϕ_1	[rad]	0.00000
DANCER PIVOT ARM			
Mass of dancer wheel	m_3	[kg]	0.190
Bearing coefficient	K_{bp}	[Nms]	0.0500000000
Diameter of sylinder piston	d_s	[m]	0.015
Sylinder distance to pivot joint	l_E	[m]	0.061
Distance of output fiber	l_o	[m]	0.155
Distance of input fiber	l_i	[m]	0.245
Number of dancer loops	j	-	2
Air resistance coefficient	K_{ap}	[Nms^2]	0.0100000000
TURNING WHEEL (6)			
Diameter	D_6	[m]	0.150
Mass	m_6	[kg]	0.200
Bearing speed coefficient	K_{b6}	[Nms$^{2/3}$]	0.0000101400
Bearing load coefficient	K_{bl6}	[Nm]	0.0000490040
Fiber bending coefficient	M_{W6}	[Nm]	0.0000000000
Air resistance coefficient	K_{a6}	[Nms^2]	0.0000000113
Mass center x	x_{c6}	[m]	0.00010
Mass center y	y_{c6}	[m]	0.00000
Start angle	ϕ_6	[rad]	0.00000

GUIDE WHEEL (2)			
Diameter	D_2	[m]	0.090
Mass	m_2	[kg]	0.040
Bearing speed coefficient	K_{b2}	[Nms$^{2/3}$]	0.0000101400
Bearing load coefficient	K_{bl2}	[Nm]	0.0000077425
Fiber bending coefficient	M_{W2}	[Nm]	0.0000000000
Air resistance coefficient	K_{a2}	[Nms^2]	0.0000000024
Mass center x	x_{c2}	[m]	0.00100
Mass center y	y_{c2}	[m]	0.00000
Start angle	ϕ_2	[rad]	0.00000
EXIT CAPSTAN (4)			
Diameter	D_4	[m]	0.191
Mass	m_4	[kg]	1.000
Bearing speed coefficient	K_{b4}	[Nms]	0.0072917080
Bearing load coefficient	K_{bl4}	[Nm]	0.0680806876
Fiber bending coefficient	M_{W4}	[Nm]	0.0000000000
Air resistance coefficient	K_{a4}	[Nms^2]	0.0000002831
Mass center x	x_{c4}	[m]	0.00010
Mass center y	y_{c4}	[m]	0.00000
Start angle	ϕ_4	[rad]	0.00000
Belt pulley 1 diameter	D_{41}	[m]	0.090
Belt pulley 2 diameter	D_{42}	[m]	0.090

Return to Main Menu

APPENDIX 4. Intermediate Outputs of Simulation Model

TAKE-UP (1)			
Actual diameter	D_a	[m]	0.211
Surface width	W_s	[m]	0.192
Volume of fiber	V_{tot}	[m^3]	0.003
Length of fiber	L	[m]	49872
Actual rotating radius	r_{act1}	[m]	0.106
Rotating speed	n_1	[1/min]	4530.6
Rotating speed	n_{s1}	[1/s]	75.5
Total mass	m_{t1}	[kg]	3.983
Inertia	J_1	[kgm^2]	0.03553
Angular acceleration	$q\alpha_1$	[rad/s^2]	0.0
Torque (t=0)	M_1	[Nm]	0.55
Angular speed (t=0)	ω_1	[rad/s]	474.2
Tension (t=0)	F1	[N]	0.50
Surface speed (t=0)	v	[m/min]	3001.7

EXIT CAPSTAN (4)			
Actual rotating radius	r_{act4}	[m]	0.096
Rotating speed	n_4	[1/min]	5052.0
Rotating speed	n_{s4}	[1/s]	84.2
Total mass	m_{t4}	[kg]	1.000
Inertia	J_4	[kgm^2]	0.00456
Angular acceleration	$q\alpha_4$	[rad/s^2]	0.0
Torque (t=0)	M_4	[Nm]	1.45
Angular speed (t=0)	ω_4	[rad/s]	528.8
Tension (t=0)	F4	[N]	8.95
Surface speed (t=0)	v_4	[m/min]	3029.9

GENERAL			
Mass of fiber per meter	m_f	[kg/m]	0.0000658315
Area of fiber cross section	A_f	[m^2]	0.0000000471
Area of fiber glass section	A_c	[m^2]	0.0000000123

GUIDE WHEEL (2)			
Actual rotating radius	r_{act2}	[m]	0.045
Rotating speed	n_2	[1/min]	10615.7
Rotating speed	n_{s2}	[1/s]	176.9
Total mass	m_{t2}	[kg]	0.040
Inertia	J_2	[kgm^2]	0.00004
Angular acceleration	$q\alpha_2$	[rad/s^2]	0.0
Angular speed (t=0)	ω_2	[rad/s]	1111.1
Tension (t=0)	F2	[N]	0.41
Surface speed (t=0)	v_2	[m/min]	3000.0

ENTRY CAPSTAN (5)			
Actual rotating radius	r_{act5}	[m]	0.096
Rotating speed	n_5	[1/min]	5002.2
Rotating speed	n_{s5}	[1/s]	83.4
Total mass	m_{t5}	[kg]	1.000
Inertia	J_5	[kgm^2]	0.00456
Angular acceleration	$q\alpha_5$	[rad/s^2]	0.0
Torque (t=0)	M_5	[Nm]	0.08
Angular speed (t=0)	ω_5	[rad/s]	523.6
Tension (t=0)	F5	[N]	3.07
Surface speed (t=0)	v_5	[m/min]	3000.0

DANCER WHEEL (3)			
Actual rotating radius	r_{act3}	[m]	0.045
Rotating speed	n_3	[1/min]	10610.9
Rotating speed	n_{s3}	[1/s]	176.8
Total mass	m_{t3}	[kg]	0.190
Inertia	J_3	[kgm^2]	0.00019
Angular acceleration	$q\alpha_3$	[rad/s^2]	0.0
Angular speed (t=0)	ω_3	[rad/s]	1110.6
Tension (t=0)	F3	[N]	0.32
Surface speed (t=0)	v_3	[m/min]	2998.6

DANCER PIVOT ARM AT TURNING POINT			
Angular acceleration of arm	$q\alpha$	[rad/s^2]	7.2
Inertia of dancer wheel	J	[kgm^2]	0.00019
Arm angular speed	ω	[rad/s]	0.9
Pressure of dancer sylinder	p	[bar]	0.19
Winding tension change (calc.)	F_{WCh}	±[N]	0.56

TURNING WHEEL (6)			
Actual rotating radius	r_{act6}	[m]	0.075
Rotating speed	n_6	[1/min]	6347.7
Rotating speed	n_{s6}	[1/s]	105.8
Total mass	m_{t6}	[kg]	0.200
Inertia	J_6	[kgm^2]	0.00056
Angular acceleration	$q\alpha_6$	[rad/s^2]	0.0
*) Angular speed (t=0)	ω_5	[rad/s]	664.4
Tension (t=0)	F6	[N]	3.00
Surface speed (t=0)	v_6	[m/min]	2989.8

*) 3rd degree equation for Angular speed 0.000

Calculate Outputs

APPENDIX 5. Estimated Production Data with Original Winding Algorithm

BASIC DATA	
Production speed [m/min]	1,800
TU spool size [km]	25
PO spool size [km]	250
Threading time [min]	5
PO spool change [min]	1
TU spool change [min]	1
Rewinding [%]	30.0%
Measurement end (scrap)/spool [m]	10
Shift [h]	8
Shifts/day [1/day]	2
PAYOFF BATCH CALCULATION	
PO batch length [km]	250
Run time [min]	139
Threading time [min]	50
PO spool change time [min]	1
TU spool change time [min]	10
Payoff batch time [min]	200
PRODUCTIVITY PER DAY	
Max. capasity [km]	1,201
Rewound length [km]	360
Spools proof tested	48
Spools rewound	14
Scrap [m]	624
Actual capasity [km]	840
PROOF TESTED FIBER IN TEST PERIOD	
Number of machines	7
Test period [months]	7
Days/month	21
Test period [days]	147
Proof tested fiber [km]	864,198
Proof tested spools	34,594

APPENDIX 6. Estimated Production Data with Improved Winding Algorithm

BASIC DATA	
Production speed [m/min]	1,800
TU spool size [km]	25
PO spool size [km]	250
Threading time [min]	5
PO spool change [min]	1
TU spool change [min]	1
Rewinding [%]	4.0%
Measurement end (scrap)/spool [m]	10
Shift [h]	8
Shifts/day [1/day]	2
PAYOFF BATCH CALCULATION	
PO batch length [km]	250
Run time [min]	139
Threading time [min]	50
PO spool change time [min]	1
TU spool change time [min]	10
Payoff batch time [min]	200
PRODUCTIVITY PER DAY	
Max. capasity [km]	1,201
Rewound length [km]	48
Spools proof tested	48
Spools rewound	2
Scrap [m]	499
Actual capasity [km]	1,152
PROOF TESTED FIBER IN TEST PERIOD	
Number of machines	7
Test period [months]	2
Days/month	21
Test period [days]	42
Proof tested fiber [km]	338,729
Proof tested spools	13,555

APPENDIX 7. Whipping Guard Designs

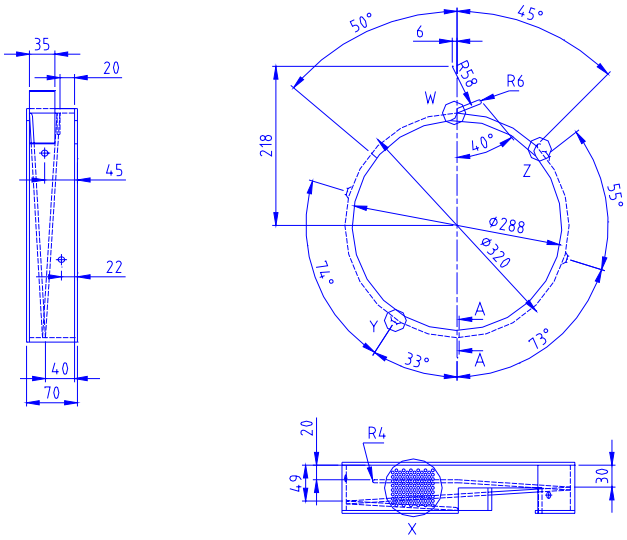

Whipping guard "spiral" design

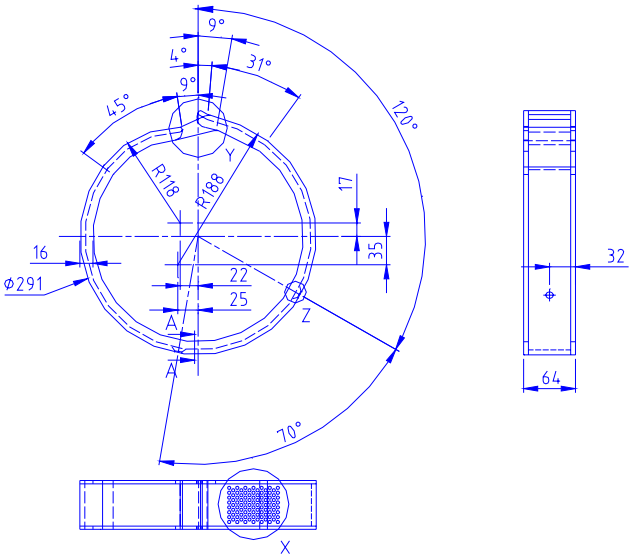

Whipping guard "round" design

APPENDIX 8. Simulated Vibrations from Take-up to Coater

F1	Winding tension	ω_1	Take-up speed
F2	Tension after dancer	ω_2	Guide wheel speed
F3	Tension after exit capstan	ω_3	Dancer wheel speed
F4	Proof testing tension	ω_4	Exit capstan speed
F5	Tension before entry capstan	ω_5	Entry capstan speed
F6	Drawing tension	ω_6	Turning wheel speed

TENSIONS	F1 (N)	F2 (N)	F3 (N)	F4 (N)	F5 (N)	F6 (N)
Variation ± (N)	0.037	0.046	0.049	0.057	0.065	0.066
Average (N)	0.50	0.41	0.32	8.95	3.07	3.00
Max. (N)	0.54	0.45	0.37	9.01	3.14	3.06
Min. (N)	0.46	0.36	0.27	8.89	3.01	2.93

SPEEDS	ω_1 (rad/s)	ω_2 (rad/s)	ω_3 (rad/s)	ω_4 (rad/s)	ω_5 (rad/s)	ω_6 (rad/s)
Variation ± (rad/s)	0.000	0.046	0.056	0.000	0.000	0.048
Average (rad/s)	474.20	1111.11	1110.61	528.78	523.56	664.39
Max. (rad/s)	474.20	1111.16	1110.66	528.78	523.56	664.44
Min. (rad/s)	474.20	1111.07	1110.55	528.78	523.56	664.34

APPENDIX 9. Simulated Vibrations from Coater to Take-up

F1	Winding tension	ω_1	Take-up speed
F2	Tension after dancer	ω_2	Guide wheel speed
F3	Tension after exit capstan	ω_3	Dancer wheel speed
F4	Proof testing tension	ω_4	Exit capstan speed
F5	Tension before entry capstan	ω_5	Entry capstan speed
F6	Drawing tension	ω_6	Turning wheel speed

TENSIONS	F6 (N)	F5 (N)	F4 (N)	F3 (N)	F2 (N)	F1 (N)
Variation ± (N)	0.025	0.027	0.029	0.035	0.036	0.042
Average (N)	3.00	3.08	8.95	0.32	0.41	0.50
Max. (N)	3.02	3.10	8.98	0.35	0.45	0.55
Min. (N)	2.97	3.05	8.92	0.28	0.37	0.46

SPEEDS	ω_6 (rad/s)	ω_5 (rad/s)	ω_4 (rad/s)	ω_3 (rad/s)	ω_2 (rad/s)	ω_1 (rad/s)
Variation ± (rad/s)	0.048	0.000	0.000	0.056	0.046	0.000
Average (rad/s)	664.39	523.56	528.78	1110.61	1111.11	474.20
Max. (rad/s)	664.44	523.56	528.78	1110.66	1111.16	474.20
Min. (rad/s)	664.34	523.56	528.78	1110.55	1111.07	474.20

APPENDIX 10. Time Domain Tension Results

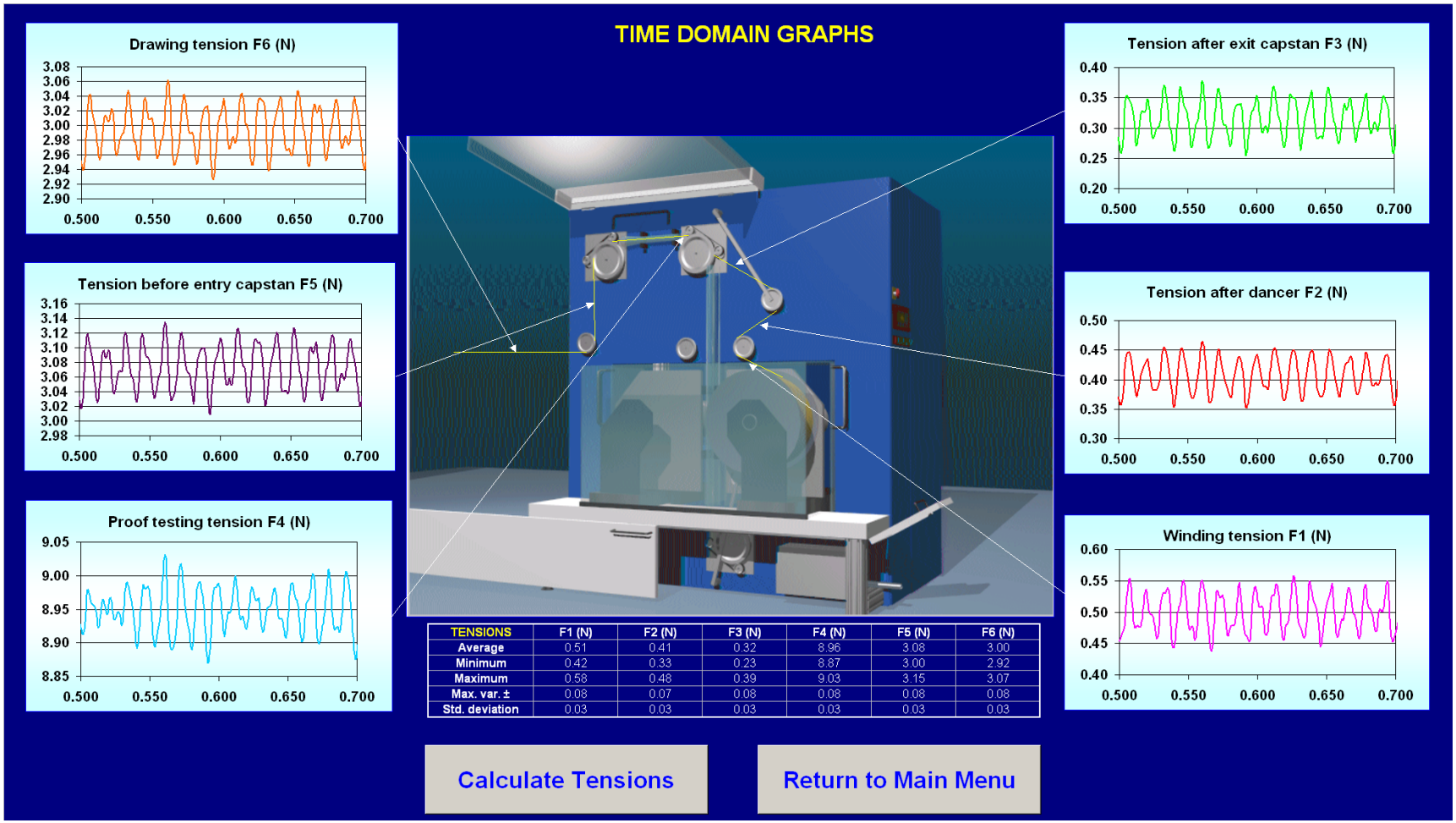

F1	Winding tension
F2	Tension after dancer
F3	Tension after exit capstan
F4	Proof testing tension
F5	Tension before entry capstan
F6	Drawing tension

TENSIONS	F1 (N)	F2 (N)	F3 (N)	F4 (N)	F5 (N)	F6 (N)
Average	0.51	0.41	0.32	8.96	3.08	3.00
Minimum	0.42	0.33	0.23	8.87	3.00	2.92
Maximum	0.58	0.48	0.39	9.03	3.15	3.07
Max. var. ±	0.079	0.074	0.078	0.081	0.076	0.077
Std. deviation	0.031	0.030	0.031	0.031	0.031	0.031

APPENDIX 11. Frequency Domain Results

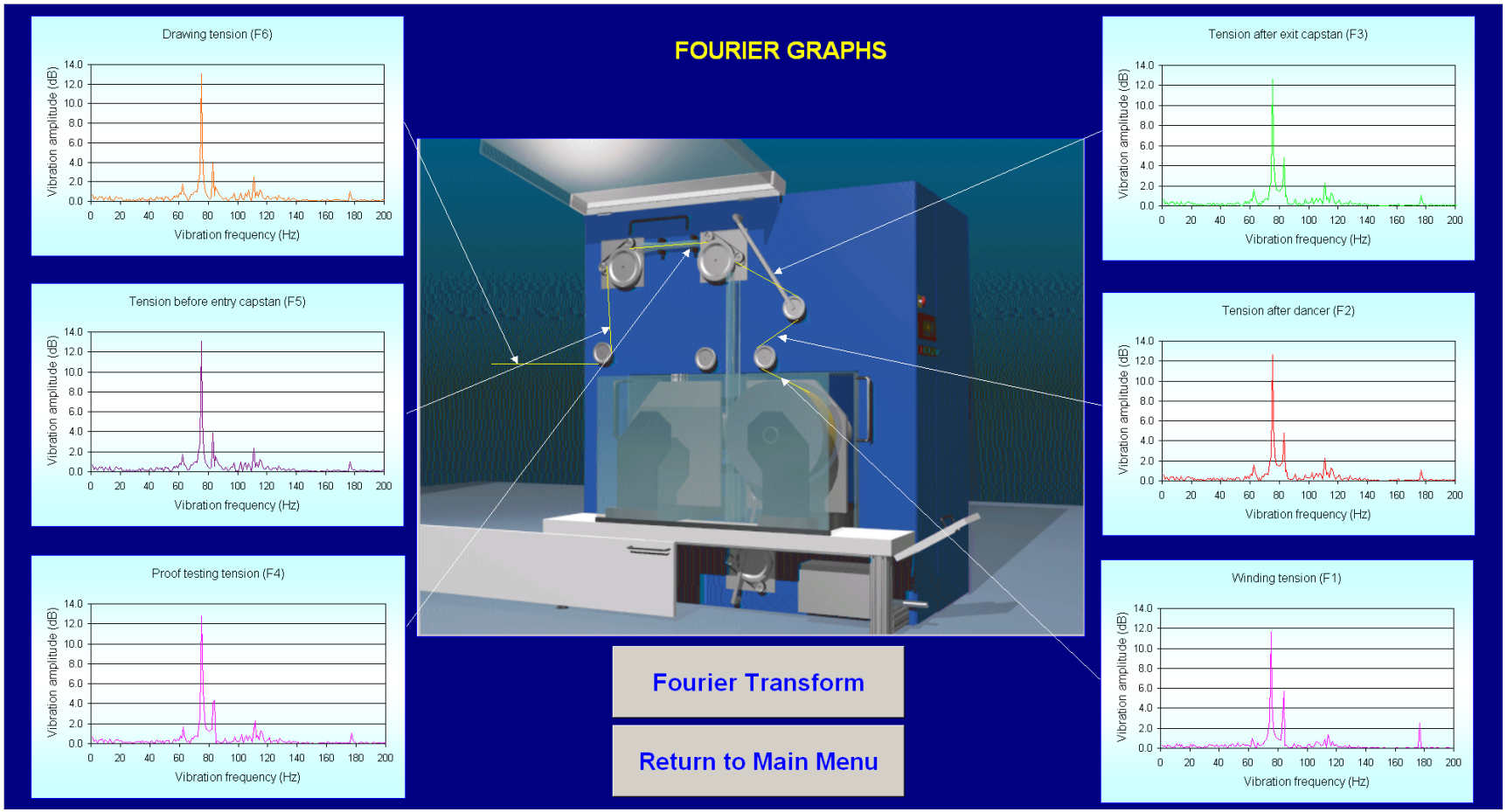

APPENDIX 12. Measured Signals during Turning Point with Original Algorithm

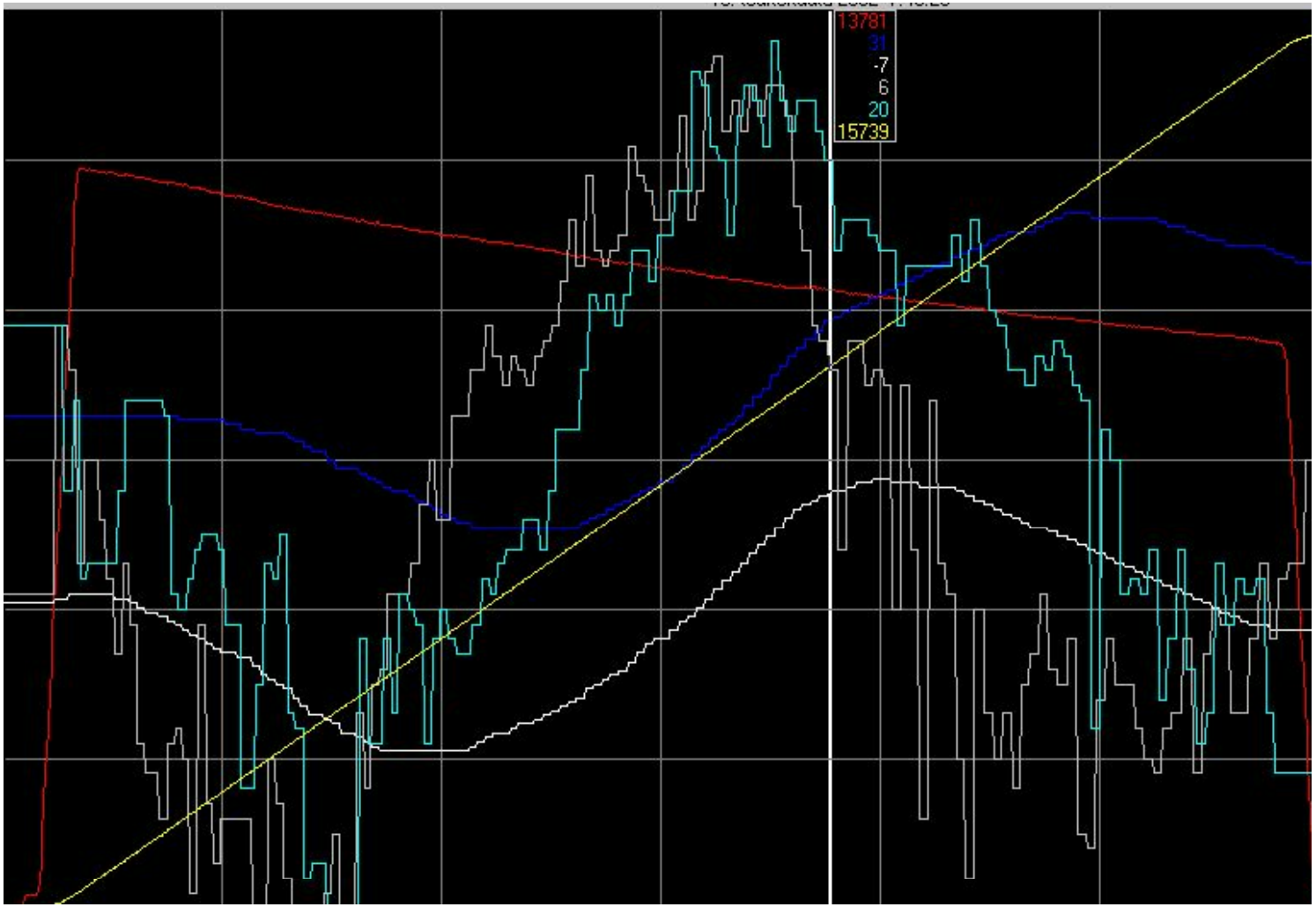

APPENDIX 13. Measured Signals with Improved Algorithm

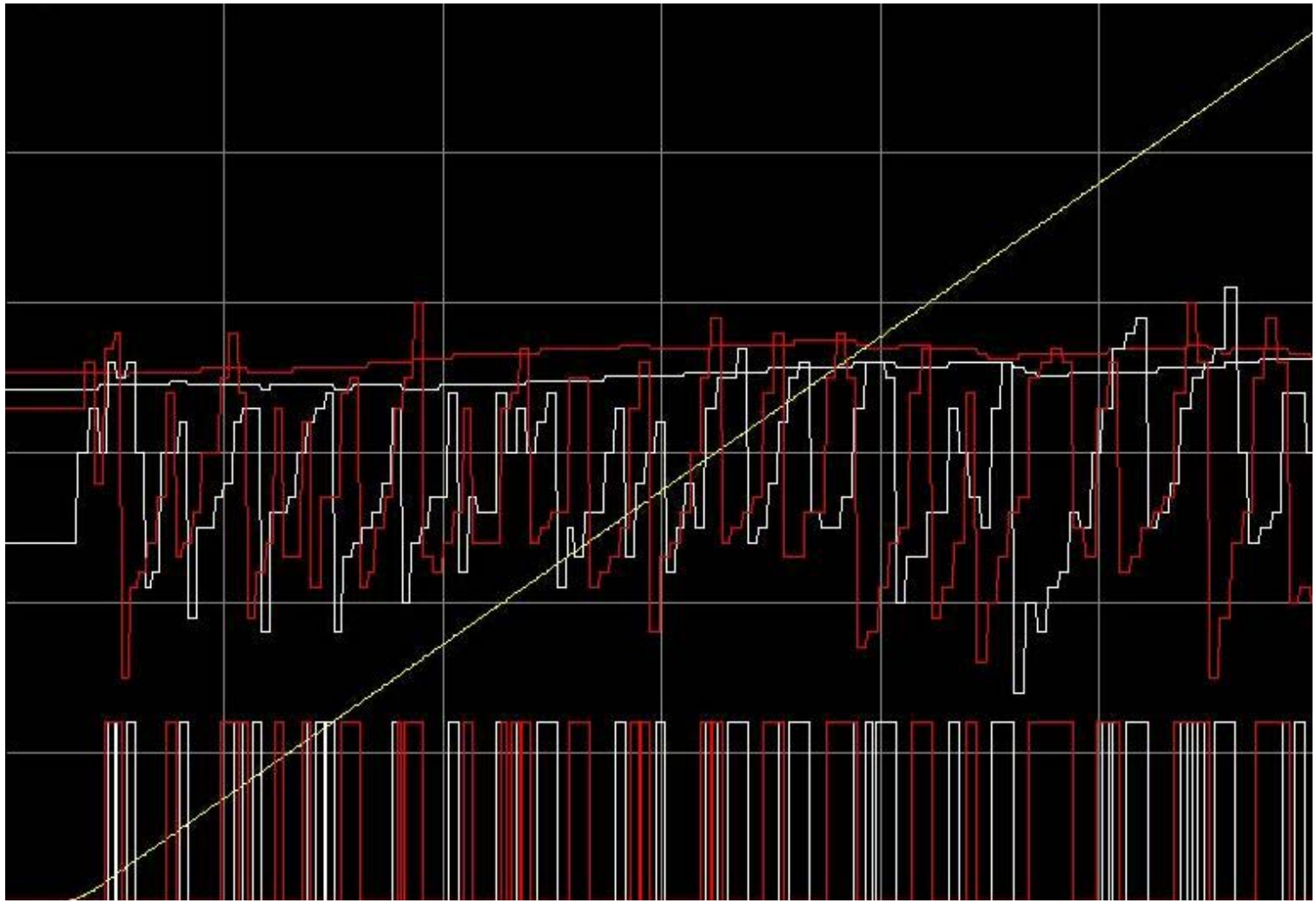

APPENDIX 14. Run 3: Frames 46-49 Showing Short Fiber Tail

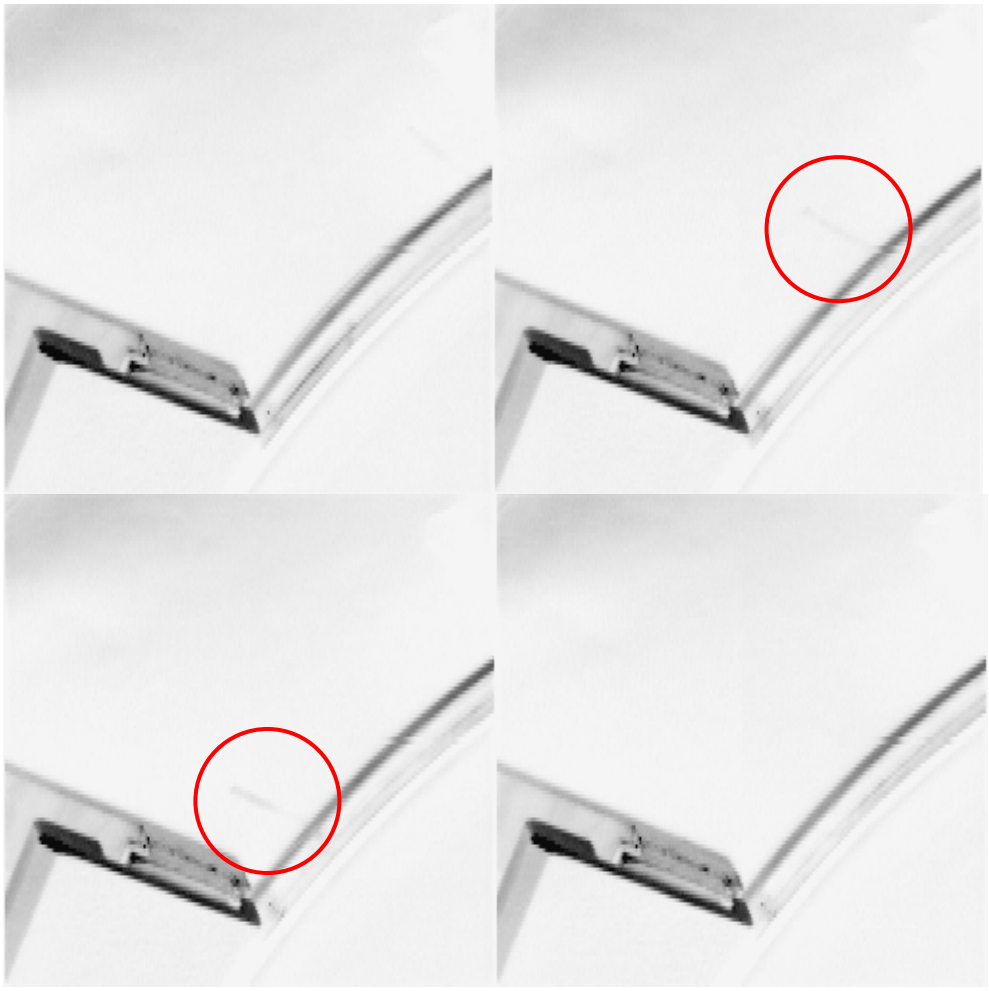

APPENDIX 15. Run 3: Frames 110-115 Showing the Loose Fiber and Fiber Tail Hitting Blade Construction

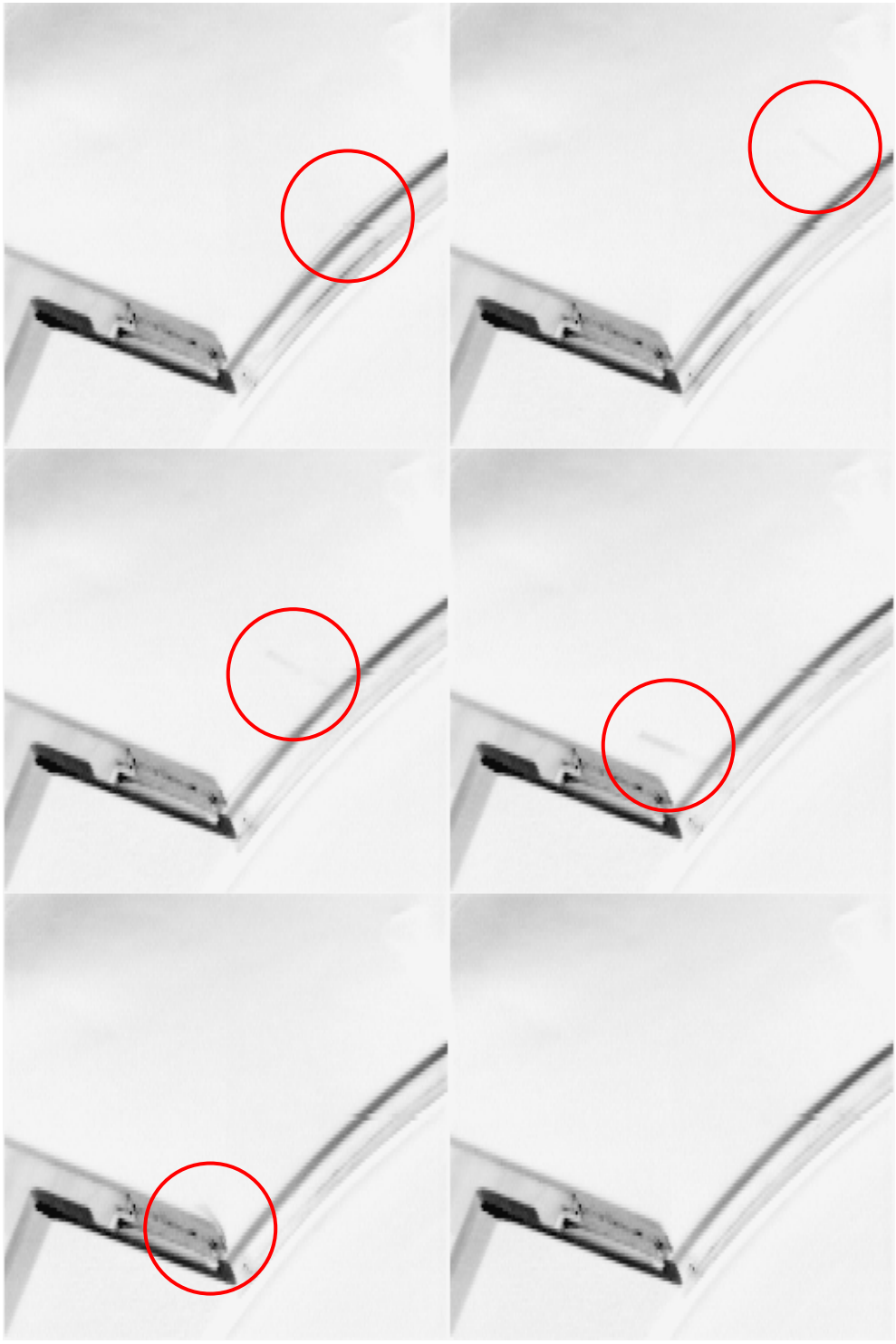

APPENDIX 16. Run 3: Frames 174-179 Showing That Fiber Is Looser

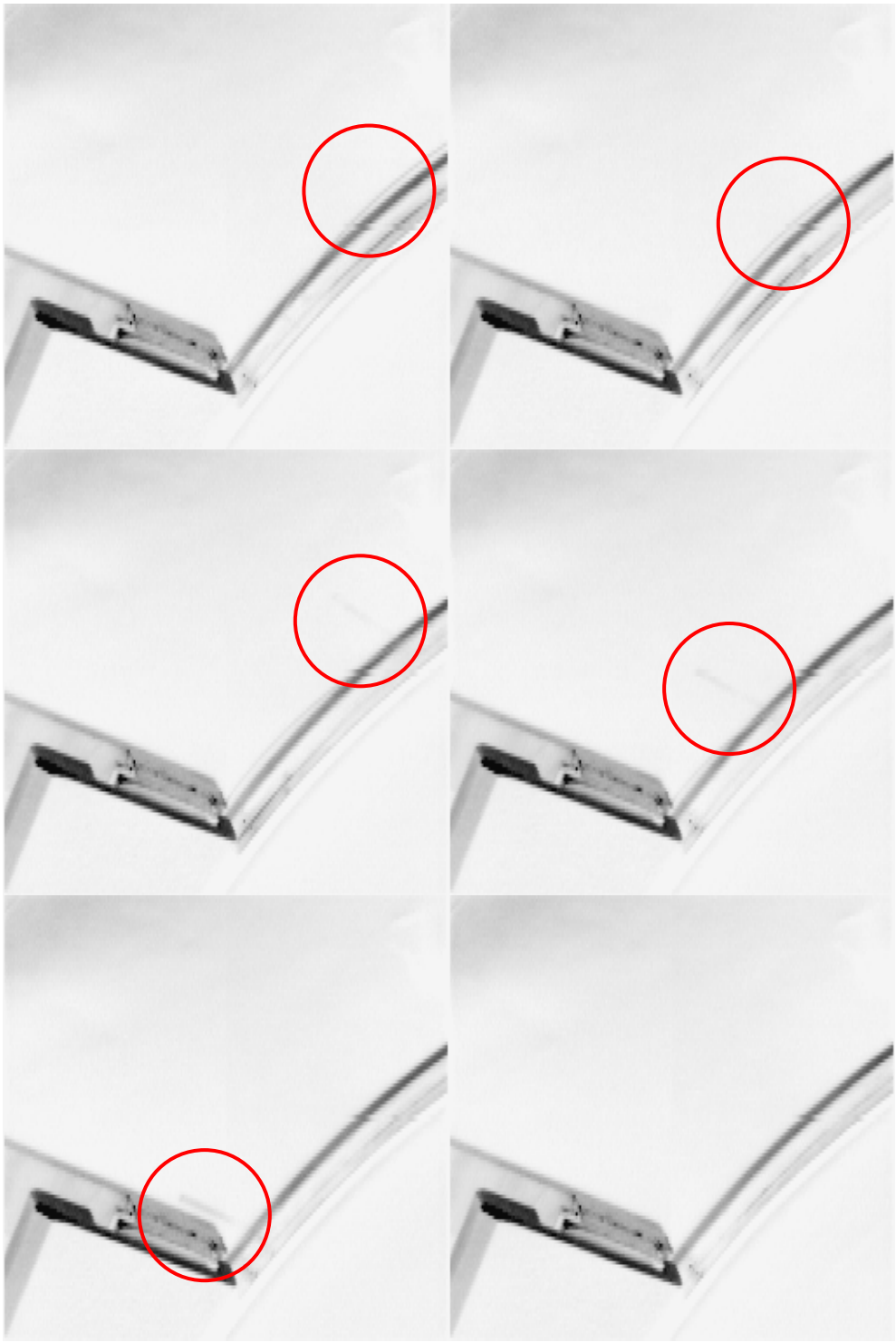

APPENDIX 17. Run 3: Frames 279 – 284 Showing Broken Fiber

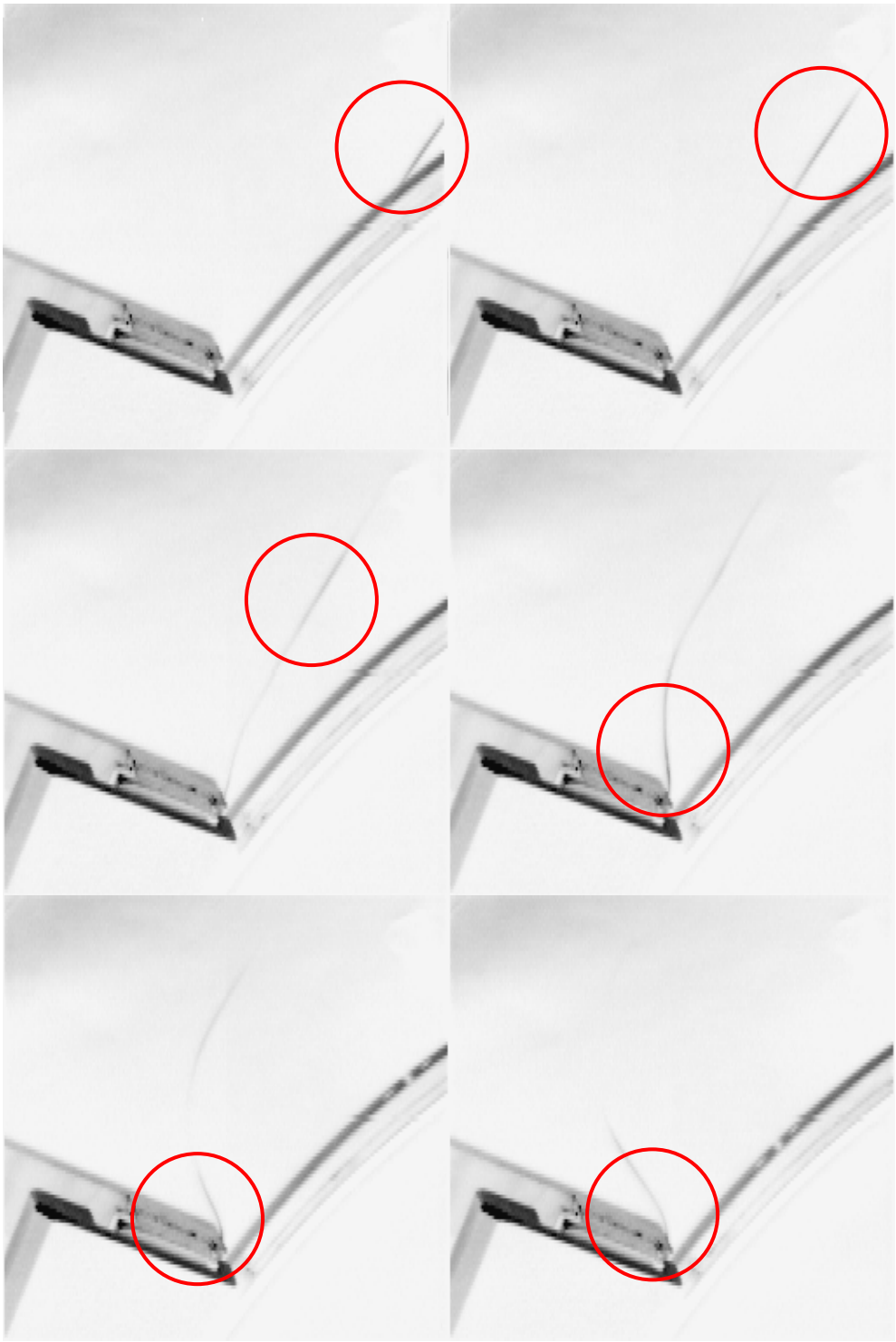

APPENDIX 18. Run 3: Frames 285 – 288 Showing the Broken Fiber

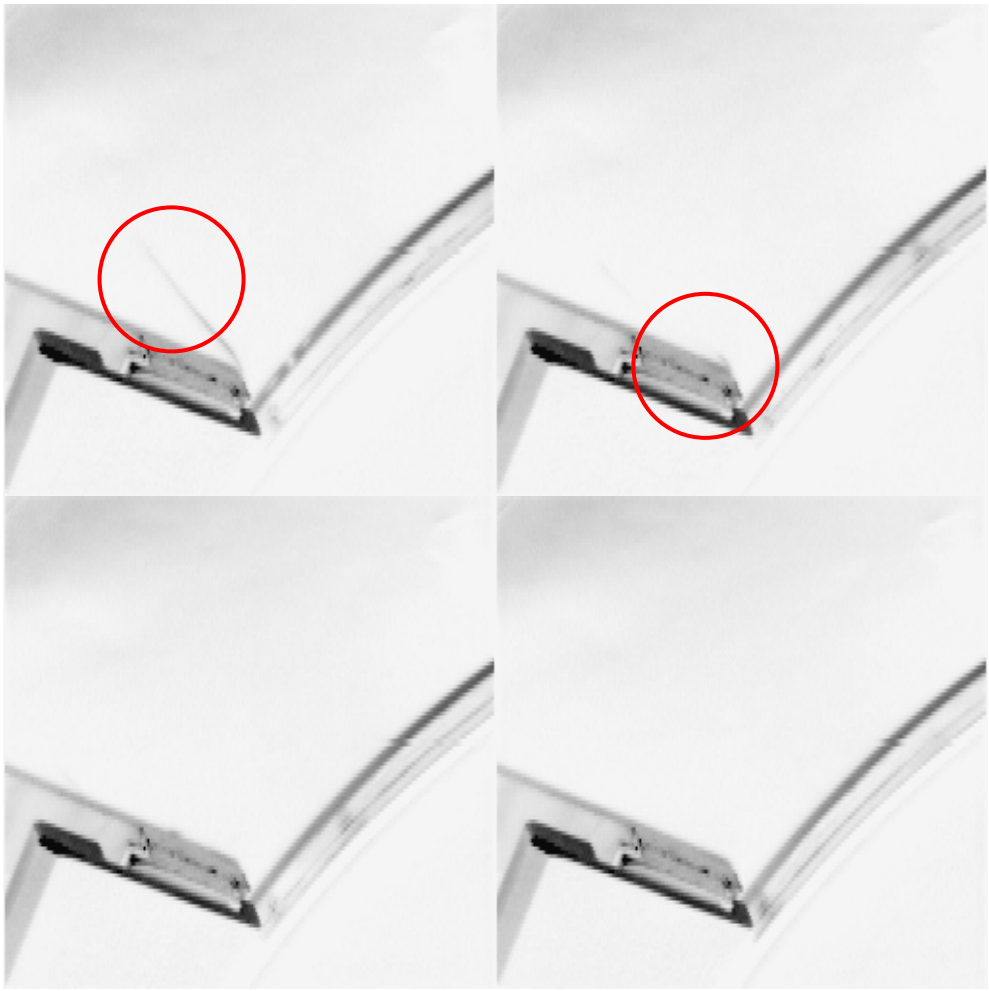

APPENDIX 19. Test Equipment Specifications

Tension Sensor RFS® 150	
Manufacturer	Honigmann
Rated measuring range	0 - 10 N
Rated output	1.5 mV/V
Rated output tolerance	<± 0.2%
Excitation voltage max.	12 V
Reference excitation voltage	10 V
Isolation resistance	> 10 GΩ
Rated temperature range	+5 to +50 °C

FA-30 Strain Gauge Amplifier	
Manufacturer	IEC OY
Power supply	110/220 V ± 15%, 50/60 Hz
Input signal range	adjustable 0.3 - 24 mV
Output	0 - 10 V, 5 mA max.
Accuracy	CMRR 110 dB
Non-linearity	< 0.01%
Temperature coefficient for span	<± 110 ppm
Temperature drift for zero point	<± 0.2 µV/°C
Ambient temperature range	0 to +50 °C

Fluke Scopemeter 123	
Bandwidth	20 MHz
Max. real time sample rate	25 MS/s
Max. equivalent time sample rate	1.25 GS/s
Display	102 mm monochrome LCD
Max. record length	512 min/max points per input
Number of inputs	2
Number of digitizers	2
Input sensitivity	5 mV/div. … 500 V/div.
Glitch capture	40 ns
Time base range in Scope mode	20 ns/div … 1 min/div.
Trigger types	Connect-and-View™, Free run, Single Shot, Edge, Video
Scope Measurements	26 automatic measurements
Dual input Trend Plot	Yes
Memory for screens and set-ups	Fluke 123: 10
True RMS multimeter	5000 counts, Volts, Amps, Ohms, Continuity, Diode, Temp
Safety certified (EN61010-1)	600 V CAT III (instrument and included accessories)
PC and Printer interface	Using optional Optically Isolated RS-232 adapter / cable

OFC 35 Proof Testing and Rewinding System	
Standard	
Manufacturer	Nextrom
Speed, max.	2,100 m/min
Motor RPM max.	4,500
Ramp time, min.	20 s
Fast stop	0.5 - 5.0 s
Payoff and winding tension	0.20 - 1.00 N
Proof testing tension	5 - 20 N (variation <± 3%)
Length measurement accuracy	0.05% >
Control system	PLC Allen-Bradley SLC 500
Load cells	Tension Sensor RFS® 150
Load cell amplifiers	FA-30 Strain Gauge Amplifier
Dancer position sensors	924AB3XM-L2P
Payoff	
Reel weight, max.	25 kg
Flange diameter, max.	550 mm
Barrel diameter, min.	150 mm
Width, max.	500 mm
Take-up	
Reel weight, max.	7 kg
Flange diameter, max.	350 mm
Barrel diameter, min.	150 mm
Width, max.	250 mm
High Speed Option	
Speed, max.	2,700 m/min
Motor (Omron) RPM max.	6,000

DFT 55 Dual Fiber Take-up	
Manufacturer	Nextrom
Speed, max.	2,700 m/min
Motor RPM max.	4,500
Ramp time, min.	30 s
Fast stop	0.5 - 5.0 s
Payoff and winding tension	0.20 - 1.00 N
Change-over sequence	< 15 s
Control system	PLC Allen-Bradley SLC 500
Load cells	Tension Sensor RFS® 150
Load cell amplifiers	FA-30 Strain Gauge Amplifier
Dancer position sensor	924AB3XM-L2P
Spool spec.	
Reel weight, max.	25 kg
Flange diameter, max.	550 mm
Barrel diameter, min.	150 mm
Width, max.	500 mm

OFC 53 Advanced Coloring System	
Manufacturer	Nextrom
Speed, max.	3,000 m/min
Motor RPM max.	6,000
Ramp time, min.	30 s
Fast stop	0.5 - 3.0 s
Payoff and winding tension	0.20 - 1.00 N
Attenuation increase, max.	0.01 dB/km
Length measurement accuracy	0.05% >
Control system	PLC Allen-Bradley SLC 500
Load cells	Tension Sensor RFS® 150
Load cell amplifiers	FA-30 Strain Gauge Amplifier
Dancer position sensors	924AB3XM-L2P
Payoff	
Reel weight, max.	25 kg
Flange diameter, max.	450 mm
Barrel diameter, min.	150 mm
Width, max.	450 mm
Take-up	
Reel weight, max.	7 kg
Flange diameter, max.	350 mm
Barrel diameter, min.	150 mm
Width, max.	200 mm

FTC Draw Capstan	
Manufacturer	Nextrom
Speed, max.	2,700 m/min
Motor RPM max.	4,500
Pulling force, max.	6 N
Load cells	Tension Sensor RFS® 150
Load cell amplifiers	FA-30 Strain Gauge Amplifier

Proximity sensor 924AB3XM-L2P	
Manufacturer	Honeywell
Sensing range	2 - 5 mm
Supply voltage	13.5 - 30 VDC
Sensitivity	2.66 V/mm
Linearity	± 0.25 VDC
Output voltage	0.2 - 10 V
Linear zone	1 - 9 V
Response time	1 V/ms
Temperature drift	2 mV/°C/mm

SLC 500 Programmable Controller	
Manufacturer	Allen-Bradley
Processor type	SLC 5/05
Typical scan time	0.9 ms/K
Max. I/O capacity	4096 discrete inputs and outputs

ControlLogix 1756 Programmable Controller	
Manufacturer	Allen-Bradley
Processor type	Logix5555, 1756-L55
Typical scan time	0.08 ms/K
Max. I/O capacity	128,000 discrete inputs and outputs

535QD Z-Folded Load cell	
Manufacturer	DS Europe
Rated measuring range	0 - 60 N
Rated output	2 mV/V
Rated output tolerance	<± 0.023%
Excitation voltage max.	20 V
Reference excitation voltage	10 V
Isolation resistance	> 5 GΩ
Rated temperature range	-10 to +40 °C

Fiber Spools	Sonoco-Crellin Art. Nr. 9835	Sonoco-Crellin Art. Nr. 9901	Sonoco-Crellin Art. Nr. 9820
Fiber length	25 km	50 km	250 km
Flange diameter	235 mm	265 mm	410 mm
Barrel diameter (with foam)	158.4 mm	180 mm	316 mm
Width (overall)	108 mm	176.5 mm	391 mm

Omron 6000 RPM Servomotors and Drives		
Servo-motor Type R88M-W	1K560	3K060
Servo-driver Type R88D-WT	15HF	30HF
Rated output	1,500 W	3,000 W
Rated torque	2.45 Nm	4.90 Nm
Max. momentary torque	11.0 Nm	21.5 Nm
Rated speed/Max. speed	6000 r/min	6000 r/min
Rated current	4.1 A(rms)	8.1 A(rms)
Rotor inertia	2.47 kgm2 x 10^{-4}	7.00 kgm^2 x 10^{-4}
Power rate	24.5 kW/s	34.3 kW/s

Aerostat® XC™ Air Blower	
Manufacturer	Simco
Discharge Time	< 2 s at 300 mm
Size (W x H x D)	390 mm x 110 mm x 210 mm
Weight	7.9 kg
Power Requirements	220-230 VAC, 50 Hz 0.3 Amp (heater off) 1.8 Amp (heater on)
Air Volume Output	70 CFM at low fan speed, 95 CFM at medium fan speed, 120 CFM at high fan speed
Operating Temperature	0 - 50 °C
Heated Air Temperature	6 °C at low fan speed, 5 °C at medium fan speed, 4 °C at high fan speed

StatAttack DC Ionizing Bar	
Manufacturer	AEA Technology
Length	250 or 500 mm
Width	36.5 mm
Depth	25 mm
Optimum operating distance	25 - 45 mm
Power supply/controller	7220
Input	115/230V, 50/60 Hz
Output	±ve = 7kV max., 8 W

High Speed Camera: Trustivapaa Oy	
Camera Model	2001
Camera memory size	256Mb
Interface type	ISA (330h)
I/O port address	330h
Software version	HiSIS2000 Application Ver. 1.32

OTDR	
Manufacturer	Photon Kinetics
Model	PK6500/642S FV 2.05
Fiber type	Single mode
Wavelengths	1310 nm, 1550 nm ± 10 nm
Distance range	5,10,20,40,80,160,320 km
Distance resolution	0.1 m
Refractive index range	1.4000 to 1.7000
Horizontal display scales	1.5 to 48 dB full screen
Data storage	3.5 floppy drive

Airpot Actuator	
Manufacturer	Airpot
Model	2K56P
Bore	0.22 in
Piston area	0.038 sq.in
Pressure range	0 to 125 psi
Force output, max.	4.75 lbs
Required pressure differential to actuation	0.05 psi
Leak rate, max.	0.190 (at 65 psi)
Leak rate, max.	0.570 (at 125 psi)
Friction coefficient	0.2
Piston friction as % of load	0.5% - 1.5%
Operating temperature range	-55 to +150 °C

High Speed recorder	
Manufacturer	Hioki
Model	8830
Description	4 Channel Memory recorder
Sample rate (max)	2 µs
Time axis	100 µs/div to 5 s/div
Recording length	20 to 2500 divisions
Input voltage range	100 mV to 500 V full scale
Storage capacity	8 bit x 30 kWord/channel